Dublin City University

School of Chemical Sciences

Development of Low Cost, Low Power Optical Sensing Devices Based on Coupled LEDs for Colorimetric Analysis

Susan Baldwin.

PhD 2005

Development of Low Cost, Low Power Optical Sensing Devices Based on Coupled LEDs for Colorimetric Analysis

By

Susan Baldwin B.Sc. (Hons), AMRSC. Grad MICI

A thesis submitted to Dublin City University in part fulfilment for the degree of

DOCTOR OF PHILOSOPHY

School of Chemical Sciences

June 2005

For Winnie

Declaration:

I hereby certify that this material, which I now submit for assessment on the programme of study leading to the award of Doctor of Philosophy is entirely my own work and has not been taken from the work of others save and to the extent that such work has been cited and acknowledged within the text of my work.

Signed: S. Baldwin

Susan Baldwin

I.D. Number: 51155427

Date: 14th Sept '05

Acknowledgements:

I would like to take this opportunity to thank everybody who has given me support and encouragement throughout my PhD. On a personal note I would like to say a big thank you to my parents who have supported me the whole way through my educational years and I would not be where I am today if it was not for their constant encouragement and help. Thank you also to Ruthie, Winnie, Brenno, Alice, Keeva, Mario and Micka who have had to put up with me through the tough times – I don't know how you have done it!

Thank you to Dermot for all his support over my 3 1/2 years spent at DCU, especially for giving me the opportunity to travel to Japan, Oz and Boston. Thanks to all of the guys in MERL (Boston) where I spent three months working and was so warmly welcomed. What can I say...thanks to all members of the DD group (past and present) it was great working with ye. I would especially like to thank Kimbo for all of his help and patience with me over the years. Thanks to Nigel also for all your help with the CAD drawings!!!

Finally I would like to thank all of the DCU chemistry postgrads whom I had the pleasure of meeting (Eado, Orla, etc …etc…) thank you for all for some of the best nights out.

List of Publications and Presentations

Posters Presentations

2nd annual conference on analytical science

IT Tallaght, Dublin, Ireland, April 2002.

Development of solid-state sensors for ammonia detection in wastewater.

49th Irish universities chemistry research colloquium

Queens University, Belfast, Ireland, June 2002.

Development of a gas phase solid-state ammonia sensor for wastewater analysis,

Environ

NUI Galway, Ireland, January 2003.

Development Of A Method For Online Monitoring Of Ammonia In Water, Susan

Media Lab Europe (MLE) open day

Dublin, Ireland, March 2003.

Sensors for Science Education and Environmental Monitoring.

Analytical Research Forum

University of Central Lancashire, Preston, England, July 2004.

Novel low cost Colorimetric detector based on paired LEDs for the detection of Fe (II).

Oral Presentations

Analytical research forum

Kingston University, Kingston, England, July 2002.

Solid State Optical Sensors for Monitoring Ammonia in Waste Water,

Dublin City University School research day

Dublin, Ireland, March 2003.

All in One Optical Sensor Device Based on a Novel Fused LED Sensor Platform,

3rd international symposium on organic molecular electronics

Kyoto, Japan, May 2004.

Colorimetric Detection of Iron (II) Using Novel Paired Emitter Detector Diode (PEDD) Based Optical System.

56th Irish Universities Chemistry Research Colloquium

University of Limerick, Ireland, June 2004.

Novel Low Cost Optical Sensing Device for the Detection of Fe (II).

Papers

"Novel Fused LEDs devices as optical sensors for colorimetric analysis", King Tong Lau, Susan Baldwin, Roderick L. Shepherd, Paul H. Dietz, William S. Yerazunis, Dermot Diamond, *Talanta*, 2004, **63**, 167.

"Colorimetric detection of Iron (II) Using Novel Paired Emitter Detector Diode (PEDD) based Optical System", Susan Baldwin, King Ton Lau, Roderick L. Shepherd, William S. Yerazunis and Dermot Diamond. Special edition on organic molecular electronics for the 21st Century, IEICE Transactions on Electronics, E87-C, 2004, 2099.

"Light Emitting Diode LED as light detector for measurement of Lead (II) and Cadmium (II)", King Ton Lau, Eimear McHugh, Susan Baldwin and Dermot Diamond. *Submitted for publication, Analyst.*

"A Low-Cost Instrument for Optical Sensing based on Paired Emitter-Detector LEDs", King-Tong Lau, Susan Baldwin, Martina O'Toole, Roderick Shepherd, William J Yerazunis, Shinichi Izuo, Satoshi Ueyama, Dermot Diamond, *submitted for publication, Analyst, ref: B412706D.*

Table of Contents

Abstract

My PhD programme of research with the Adaptive Information Cluster at the National Centre for Sensor Research has focussed on the development of low cost, low powered optical sensing devices. Part of this work was carried out in collaboration with Mitsubishi Electric Research Labs, Boston, USA and was funded by Science Foundation Ireland (SFI).

The optical sensing devices were developed as alternative analytical tools for colorimetric based sensing. The main aim of this work was to design and develop these LED based devices, but some applications were also explored, including the use of the devices for the determination of the pH of a solution and the detection of Fe (II). Transmittance and reflectance based devices were developed and both configurations generated sensitive and reliable data. The circuitry used to operate the devices was simple (no A/D converter required) and inherently digital. All of the devices were operated using a 9 V battery. Overall it can be concluded that all of the LED based optical devices are inexpensive, portable and easy to operate.

List of abbreviations

A/D converter	Analogue to Digital Converter
AdCSV	Adsorptive Cathodic Stripping Voltammetry
Ag^{2+}	Silver
Al^{2+}	Aluminium
B	Boron
BCP	Bromocresol Purple
BTB	Bromothymol Blue
CCD	Charge Couple Device
CdS	Cadmium Sulphide
CO_2	Carbon Dioxide
Cu^{2+}	Copper
EPA	Environmental Agency
Fe^{2+}	Iron
Ga	Gallium
Ge	Germanium
GFAAS	Graphite Furnace Atomic Absorption Spectroscopy
Hg^{2+}	Mercury
HOMO	Highest Occupied Molecular Orbital
ICP-MS	Inductively Coupled Plasma Mass Spectrometry
K^+	Potassium
KNO_3	Potassium nitrate
LC	Liquid Chromatography
LDR	Light Dependant Resistor
LED	Light Emitting Diode
LOD	Limit of Detection
LUMO	Lowest Unoccupied Molecular Orbital
MAC	Maximum Admissible Concentration
MCD	Millicandellas
MERL	Mitsubishi Electric Research Laboratories
N_2	Nitrogen
NH_3	Ammonia

$Ni(NMG)_2$	Nickel Dimethylglyoxime
NY	Nitrazine Yellow
Op amp	Operational Amplifier
OWG	Optical Waveguide
P	Phosphorous
PEDD	Paired Emitter Detector Diode Device
Phen	Phenanthroline
PIC	Programmable Integrated Circuit
PoAnis	Poly (o-methoxyaniline)
PPF	Phenolphthalein Formaldehyde
PPM	Parts Per Million
PTFE	Poly tetrafluoroethylene
PVC	Poly Vinyl Chloride
RB	Rhodamine B
SAMI	Submersible Autonomous Instrument
Si	Silicon
SiO_2	Silicon Dioxide
SLIM	Simple Low Power Inexpensive Microcontroller based spectrometer
TiO_2	Titanium Dioxide
TIR	Total Internal Reflectance
TSA	Toluene Sulfonic Acid
TTP	Tetraphenylporphyrin
UV-Vis	Ultraviolet-visible
Zn^{2+}	Zinc

Extended Abstract

Simple low cost, low powered LED based optical sensing devices have been devised, that have proven to be successful for colorimetric analysis. These devices were based on the use of two LEDs, one which functioned as a light source and the other as a light detector. Chapter 1 provided a comprehensive review on the theory of light absorption, UV-Vis spectroscopy and pH sensing.

In chapter 2 the properties of semiconductors were described. The theory on the doping of a semiconductor was introduced leading on to the formation of a P-N junction and the use of a doped semiconductor material as a diode. The diode could be forward biased (light emitting) or reversed biased (light detecting). The previous use of LEDs as light detectors were described and the method of light detection chosen for use by the optical devices throughout this thesis was described in detail in this chapter. In brief a simple threshold timer circuit was used to measure the photocurrent at the detector LED.

Chapter 3 introduced "the photometer". This is an analytical device in which the LEDs (light emitter and detector) were arranged for transmission-based measurements. The capabilities of the device were demonstrated by its use in the detection of Fe (II). The Fe (II) complexing reagent used in this study was 1,10 phenanthroline. Experiments conducted proved that the device was reasonably resistant to a small change in the distance of the emitter and detector LEDs apart. A LED resetting error of 0.095 % was calculated. The sensitivity of the photometer could be tuned using a simple variable resistor to regulate the emitter

intensity. Within chapter 4 the use of the photometer at two resistances (1 KΩ and 4.6 KΩ) were investigated. At the lower resistance (1 KΩ) a working range of 0.1 – 18 ppm Fe (II) was found while at the higher resistance (4.6 KΩ) a working range of 0.1 – 8ppm Fe (II) was found. The limits of detection found at both resistances were extremely similar, 0.04 ppm and 0.05 ppm at 1 KΩ and 4.6 KΩ respectively. The maximum limit of Fe (II) allowed in drinking water as stated by the EPA is 0.2ppm. The photometer demonstrates that this low cost emitter – detector LED arrangement can be used to make very sensitive analytical measurement capable of detecting sub ppm levels of Fe (II).

Chapter 4 discussed the development of a "reflectometer". This LED based optical device worked in reflection mode. A light emitting and light detecting LED were positioned at a 7.6-degree angle to one another. The light from the emitter was reflected off a mirror and reflected back into the detector. This chapter investigated the use of both a modified and unmodified reflectometer for its use as an analytical measurement tool. The unmodified reflectometer when used to detect a change in the pH (pH 3 – 10) of a 9.26 x 10^{-5} M bromocresol purple (BCP) solution resulted in a 40,000 μs change. When the reflectometer was used to carry out a calibration of a change in the pH of a BCP solution the average (n=3) slope of this device was found to be 20238 μs / pH with an average working range of pH 4.43 –7.1 (RSD = 3.39 %). The pK_a of the solution found using the reflectometer was 5.99 ± 1.64 % and the actual pK_a of BCP quoted in the literature is 6.3. The reflectometer was then modified by attaching a piece of PET coated with a polymer membrane containing the pH indicating dye BCP to the LEDs. The change in colour of the membrane due to a change in the pH of the

solution was measured using the reflectometer. A 10,000 μs change in response was observed with a change in the pH of a bromocresol purple solution from pH 3 – 10. The pK_a found for the BCP solution using the modified reflectometer was 6.27 ± 0.49 % and the response time of the device to a change in pH was found to be less then 1 s.

The third type of LED based optical sensing device developed was a **P**aired **E**mitter **D**etector **D**iode device (PEDD). This device, like that of the reflectometer worked in reflectance mode. The PEDD probe was constructed by fusing two LEDs together. This chapter looked at three different angles of fusion (1) 30-degrees, (2) 45-degrees and (3) 60-degrees and investigated the optimum angle needed to obtain the most sensitive device for the determination of the pH of a solution.

Upon investigation it was concluded that largest change in response with a change in the pH of a BCP solution (from pH 9 - 2) was when using the 45-degree angle. The critical angle for total internal reflection was calculated to be approximately 60 degrees. With the 60-degree angle most of the light was totally internally reflected (as it had the fastest discharge time) and with the 30-degree angle most of the light was lost to the surrounding solution (as it had the longest discharge time).

The initial study carried out using the 45-degree angle involved a simple calibration of a change in the colour intensity (concentration) of a pH indicator dye (rhodamine B) in a pH 9 buffer solution, a linear range of approximately 0.4 – 4.4 μM rhodamine B was observed. The linear range observed when a calibration

was carried out using nitrazine yellow was from approximately 0.4 – 100 μM, when BCP was used the linear range found was from 0.12 – 2 μM.

Following these studies a calibration study was carried out to determine if the PEDD device could detect a change in the pH of a 1.85 μM BCP solution. The plot resulted in a sigmoidal shaped curve with a linear range from pH 4.8 - 7.2. The pK_a of the solution obtained using the device was found to be 6.1, which is very similar to the actual pK_a of the BCP (pK_a 6.3).

A number of different experiments were carried out to determine the proposed mechanism for the device. The experiments found that the presence of a surfactant suppressed the response observed by the device. This demonstrated that the light was being emitted out into the surfactant layer and then into the dye layer before being reflected back to the detector. This concluded that the mechanism most likely for the PEDD device was based on the evanescent wave principle.

We have demonstrated that these LED based sensing devices coupled with measuring the light induced voltage decay time of the detector LED are useful tools for colorimetric based analysis. These devices were fabricated using inexpensive optical and electronic components hence the overall costs of these devices are relatively low. One of the advantages of these devices over conventional colorimeters is that they can be all operated using a standard 9V battery, another advantage is that the platform used has the potential to store and

transmit data. This highlights the possibility of these devices to be used for wireless communication as part of a wireless sensor network.

1. CHEMICAL SENSING & ELECTROMAGNETIC RADIATION/ ABSORPTION

1.1. Introduction

The EPA (Environmental Protection Agency) has the task of monitoring and reporting on the status of the environment in Ireland. This includes the following sectors; air, water, soil, waste, noise and land. In 1971 larger rivers and their tributaries were assessed for the first time. Since then the scope has been extended so that by 1990 virtually all rivers and streams depicted on the Ordinance Survey map have been examined. However, there are many smaller streams present that do not appear on the map and are therefore not tested. The total number of rivers and streams tested is 1072; these are biologically surveyed at some 3,100 locations extending over 13,100 km. For logistical reasons, only a third of the total number of rivers and streams are tested in any one year and therefore it takes three years to complete a full survey e.g. in 2003, 1300 locations and 476 rivers and streams were tested [1]. This results in an average of approximately 3 locations/river/year. The number of sample measurements required depends largely on the location of the river. If the river is located near a factory or farmyard, then the pollutants which enter the river are known as point-source pollutants and these are easily identifiable. Here ideally at least 10 samples should be taken per day at a minimum of 20 sampling points in order to monitor and track the amount of pollutants entering the into the waters. If 20 sampling points are required / point source and there are 1000's of point sources then this would lead to 1000's of sampling points. If the source of pollution comes from distributed sources e.g. run off of nutrients from rivers and lakes and various quality parameters are to be monitored (e.g. dissolved oxygen) then a lot more sample points would be required to find the source of the pollution. Hence there is a huge difference in the sampling requirements and that actually being carried out at present. In order to scale up to this type of sampling, a large number of devices are required that can carry out multiple measurements. These devices must be inexpensive (ownership and purchase) and reliable.

Chemical sensors have previously used in the monitoring of river water/seawater [2, 3]. A chemical sensor is a device that provides information to the user about the chemical nature of its environment [4]. The ideal sensor can be placed in a

sample and will selectively measure the chemical concentration of a specific analyte over time. No sampling, dilution, or reagent addition is required and, ideally, changes in the analyte concentration or activity can be measured and processed in real time [5]. If these sensors can be incorporated into a wireless sensor network, then this opens up a wide range of applications. For example, an array of sensor nodes (sensor, microcontroller and transmitter) may be distributed along a water body such as a stream or lake, with the data from each point being remotely accessible. In one realisation, the data from each individual node is transmitted to the host node via acoustic waves using intermediate nodes as relays [6]. In this case, each node of the sensor network is a data router and contains sensors capable of measuring environmental parameters. Depending on the information required each sensor node can be equipped with different physical/biological/chemical sensors. The advantage of this type of sensing is that it allows for more frequent sampling in more locations than that currently in place, and the sample results are automatically transmitted to the base station (no human interaction is required). Currently a member of staff is required to go out to remote sampling locations, gather water samples, and take them back to the lab to be analysed.

This project focuses on the core of the nodes i.e. the sensor. The sensors need to be inexpensive and of good quality if hundreds of thousands of these will be deployed out in the environment. The focus of this thesis will be colorimetric based optical sensors, as these provide one route to the realisation of low cost chemical sensing technologies. An overview section on research previously carried out on the development and application of optical sensors can be found in the appendix section.

1.2. Electromagnetic Radiation

The radiant energy that is visible to the human eye is called "light" and covers the spectral region from 400 nm to 750 nm. However this is only a small part of the electromagnetic radiation spectrum, which also includes radio waves, microwaves, infrared light on the long wavelength side and also X – rays and γ rays on the short wavelength side (see Figure 1-1) [7]. Different forms of radiation are distinguishable based on their wavelength or frequency region. The UV-Vis region extends over the wavelength range of 200 – 750 nm.

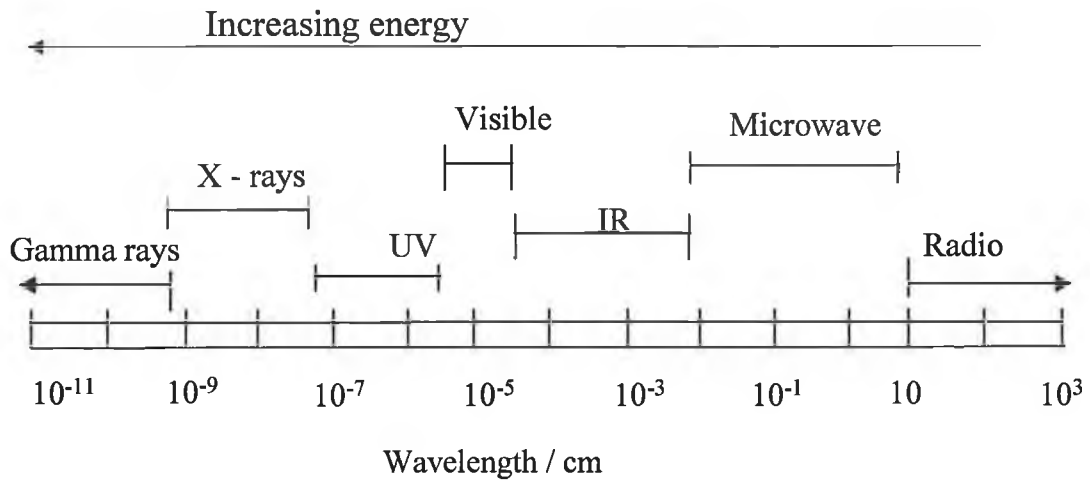

Figure 1-1: Electromagnetic Spectrum

The apparent colour of a material i.e. the light reflected by it, is complimentary to the colour of the incident light absorbed. Table 1-1 outlines the different colours of visible radiation and their compliment colours [8], with a white light used as a light source.

Table 1-1: Colours of reflected light and their corresponding absorbed light observed at various wavelengths in the UV-Vis spectrum.

Colour of reflected light and spectral range (nm)	Colour of absorbed light
Violet (400-465)	Yellow – green
Blue (465-482)	Yellow
Greenish blue (482-487)	Orange
Blue – green (487-493)	Red – orange
Bluish – green (493-498)	Red
Green (498-530)	Red – purple
Yellowish – green (530-559)	Reddish purple
Yellow – green (559-571)	Purple
Greenish – yellow (571-576)	Violet
Yellow (576-580)	Blue
Yellowish – orange (580-587)	Blue
Orange (587-597)	Greenish – blue
Reddish – orange (597-617)	Blue- green
Red (617-780)	Blue – green

Electrons within an atom occupy certain discrete energy levels. When light is absorbed at a specific frequency, an electron jumps to a higher energy level (absorption). In releasing this energy, the electron falls back to a lower energy state (emission). The electron cannot occupy levels between these quantized energy levels. These energy levels can be calculated by Equation 1-1.

$$E(n)=\frac{-hr}{n^2}$$ **Equation 1-1**

Where h is Planck's constant (6.626 x 10^{-36} Js), r, the Rydberg constant (3.29x1015 s^{-1}) and n, the energy level.

A molecule may undergo rotational, vibrational, electronic or ionisation processes. When the energy absorbed is greater than the maximum energy level (E_{max} is the limit of energy that an electron can have before escaping), the electron breaks the atomic bonds, and escapes, leaving the atom one electron short. This results in the formation of an ion.

The energy of the excited electrons must be released, in this case the energy is released as radiation, which can be in the form of, heat, vibrational or rotational energy and the electrons descend from a higher energy level to a lower energy level. The frequency of the released radiation energy can be calculated by using equation 1-2 and the wavelength of the photon can be calculated equation 1-3 [2].

$$\Delta E = h\nu \qquad \textbf{Equation 1-2}$$

$$\lambda = \frac{h\nu}{\Delta E} \qquad \textbf{Equation 1-3}$$

Where ΔE is the difference between the energy levels (J) and ν, the frequency of radiation (Hz). λ represents the photons wavelength.

1.3. Electromagnetic Spectra

There are two classes of spectra, absorption spectra (obtained when photons are absorbed and electrons are promoted to higher energy levels) and emission spectra (obtained from photons emitted when electrons relax from an excited state to a lower energy level).

1.3.1. Absorption Spectra

In a molecule the atoms can rotate and vibrate with respect to one another. These vibrations and rotations also have discrete energy levels. Absorption of ultraviolet and visible radiation in organic molecules is restricted to certain functional groups (chromophores) that contain valence electrons of low excitation energy. The spectrum of a molecule containing these chromophores is complex. This is because the superposition of the rotational and vibrational transitions on the electronic transitions gives a combination of overlapping lines. This appears as a continuous band. A schematic of an electronic transition caused by interaction with light and the corresponding absorption spectrum is shown in Figure 1-2[9].

(1)

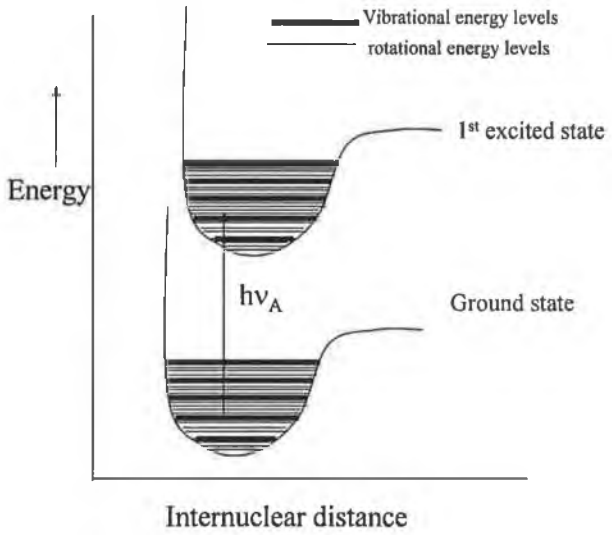

(2)

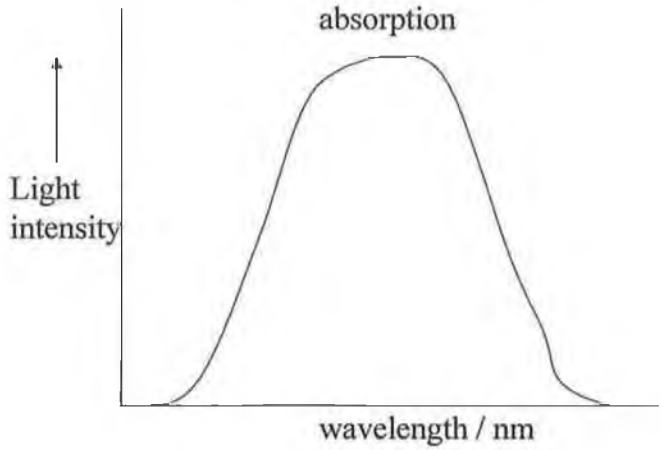

Figure 1-2: (1) Electronic transitions caused by interaction with light and (2) the corresponding absorption spectrum [9].

1.3.2. Emission Spectra

The excited molecules can loose their energy by rapid, weak collisions with neighbouring molecules. In this case the excited molecule relaxes from the excited state to the lowest vibrational level. If the molecule remains in the lowest vibrational energy level of the excited state long enough it can make the transition to the ground state either by strong collisions with another molecule or through radiation (fluorescence), see Figure 1-3.

(1)

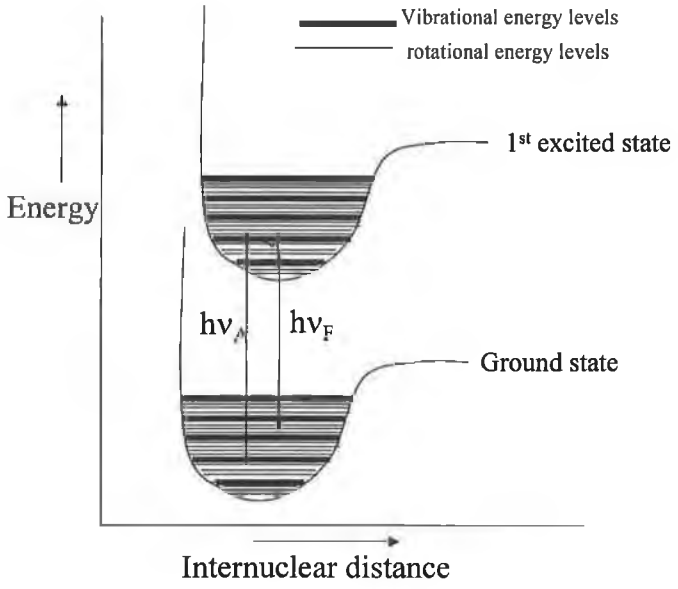

(2)

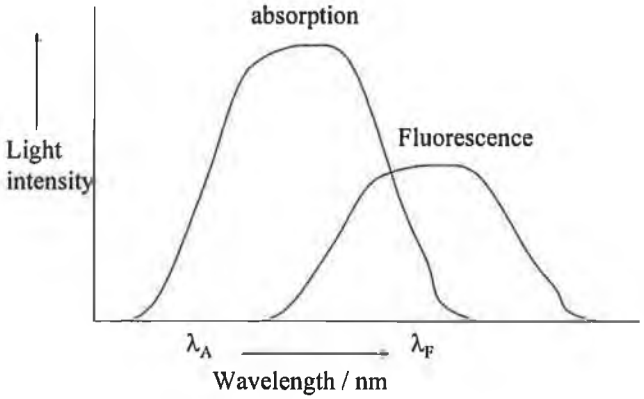

Figure 1-3: Absorbed energy dissipated non-radiatively to lowest vibrational level of first excited state. A transition from this level to the ground state is accompanied by a florescence radiation. (1) Electronic transitions caused by interaction with light and (2) the corresponding absorption spectrum.

Phosphorescence is similar to fluorescence but is based on a slightly different mechanism. The transition to the first excited state (singlet) on the absorption of light is the same, however if there is a triplet state (with two unpaired electrons) lying close to the first excited state, a non-radiative singlet – triplet transition can take place (Figure 1-4).

(1)

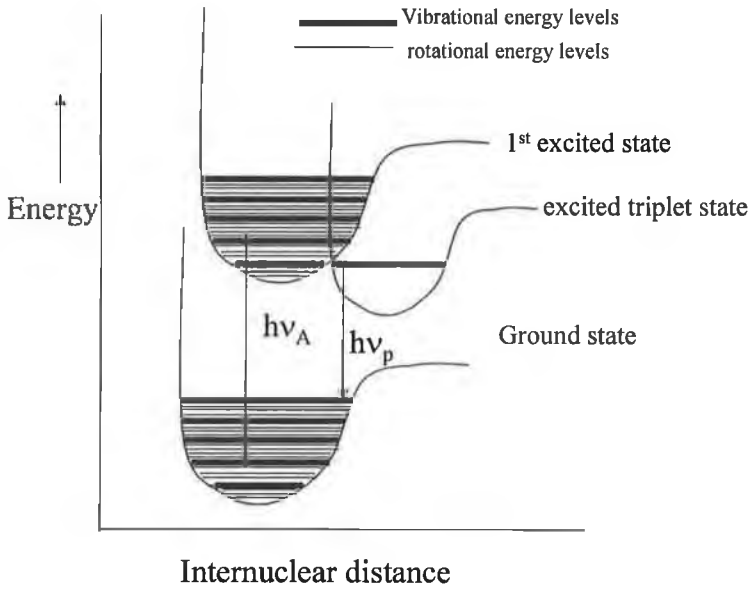

(2)

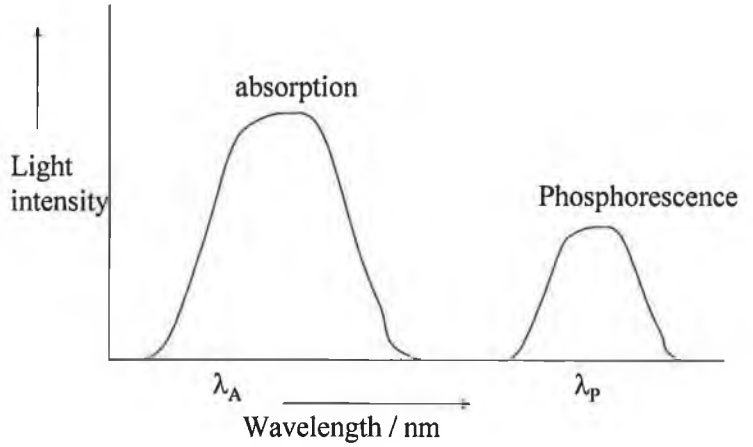

Figure 1-4: Transition from singlet to triplet state (phosphorescence). (1) Electronic transitions caused by interaction with light and (2) the corresponding absorption spectrum

Fluorescence and phosphorescence are distinguished from each other by the time between absorption and re-emission. In fluorescence the delay between absorption and reemission is 10^{-4} to 10^{-8} s while in phosphorescence the delay is much longer with a re-emission time ranging from nanoseconds to milliseconds [10].

1.4. UV-Vis Spectroscopy

Absorption spectroscopy in the ultraviolet and visible region is one of the oldest of the physical methods used for quantitative analysis. The absorption by molecules of photons in the UV-Vis region causes an excitation of the electrons, which promote them to a higher energy level. The lowest energy transition is that between the highest occupied molecular orbital (HOMO) and the lowest unoccupied molecular orbital (LUMO) in the ground state. The absorption of radiation creates an excited state promoting an electron to the LUMO. The more highly conjugated the system, the smaller the HOMO-LUMO gap (ΔE), and therefore the lower the frequency and longer the wavelength (λ) of the emitted radiation [11].

1.4.1. Laws of Absorption of Light

The amount of light that penetrates through a solution and the amount of monochromatic light absorbed by the solution are related to the thickness (Lambert, 1768) and the concentration of the sample, respectively (Beer, 1852) [12].

Both laws were combined to form the Beer-Lambert law. This law states that the fraction of the incident light absorbed by the sample is proportional to the number of molecules in its path. That is, if the substance is dissolved in a solvent, the absorption by the solution will be proportional to the molecular concentration providing the solvent itself does not have any absorption in that region [13].

This Beer-Lambert law is expressed as

$$A=\varepsilon C\lambda \qquad \textbf{Equation 1-4}$$

Where A is the absorbance (at a particular wavelength), ε, the molar absorbtivity ($M\ cm^{-1}$), C, the concentration of the sample (M) and λ, the path length (cm).

If a linear correlation is observed when the absorbance (at a particular wavelength) is plotted against the concentration of the sample then this indicates that the Beer – Lambert law is obeyed. An illustration of an absorbance versus concentration plot is shown in Figure 1-5.

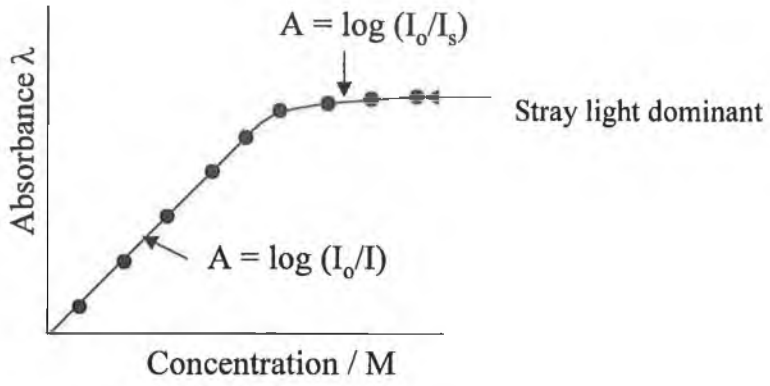

Figure 1-5: Illustration of concentration versus absorbance plot at a particular wavelength (λ)

The linear region of the plot shown in Figure 1-5 is in agreement to the Beer - Lambert Law, when the line starts to curve, this indicates that there has been a deviation from the Beer – Lambert law. Causes of non-linearity include, deviations in molar absorbtivity coefficients, ε, at high concentrations due to electrostatic interactions between molecules in close proximity, scattering of light due to particles in the sample, fluorescence or phosphorescence of the sample and / or changes in refractive index at high analyte concentration.

1.4.2. Conjugated Compounds

When a highly conjugated compound (a compound containing two or more double bonds each, separated from the other by a single bond) absorbs light in the UV-Vis region of the electromagnetic spectrum, an electron is promoted from HOMO to the LUMO. An example of a highly conjugated molecule used throughout this

research is bromocresol purple (BCP). The structure of BCP is shown in Figure 1-6.

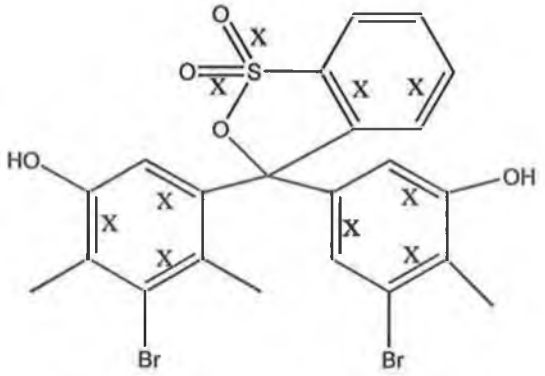

Figure 1-6: Chemical structure of bromocresol purple (BCP). X highlights the area of conjugation

Bromocresol purple is a pH indicating dye that is yellow when placed in an acidic solution and purple in a basic one. The reason for this colour change is due to a shift in the wavelength when the dye becomes deprotonated. When in its deprotonated form there is an overall negative change on the molecule (A^-), therefore the electrons are easier to promote hence a smaller ΔE is observed (Figure 1-7).

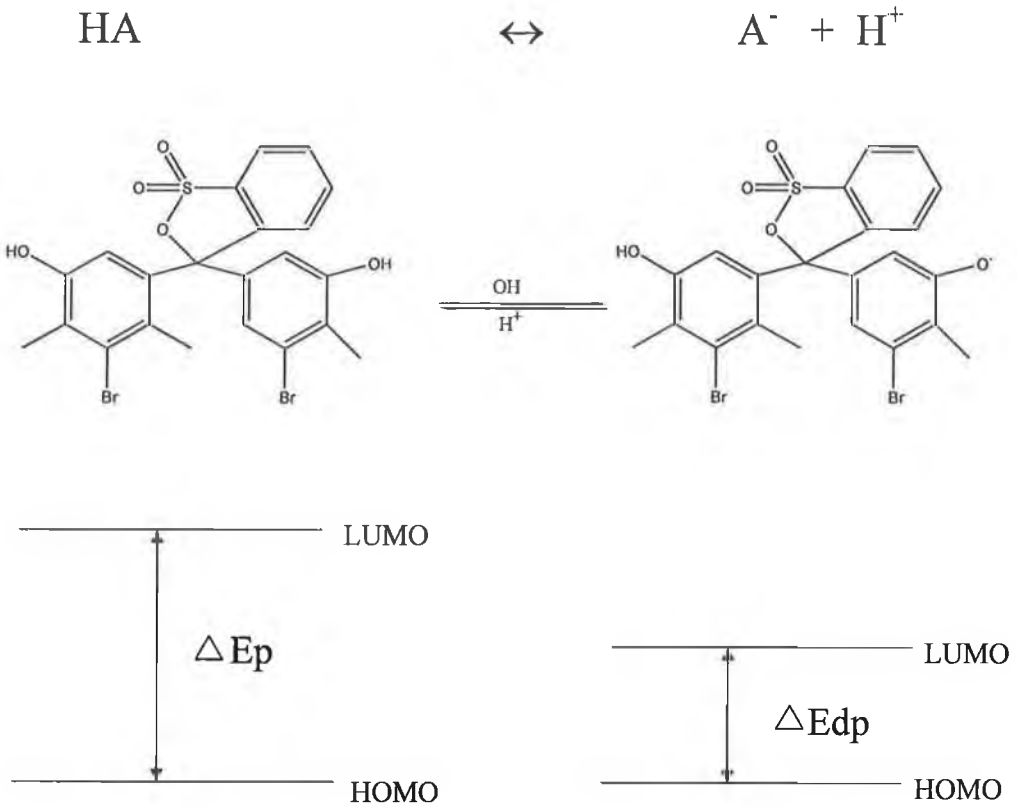

Figure 1-7: Chemical structure of protonated and deprotonated form of bromocresol purple and an illustration of their relative energy levels. Where p = protonated form and dp = deprotonated form of dye.

The absorption spectrum of 2 x 10^{-4} M BCP (obtained using a μQuant™ platewell reader, Bio-Tek Instruments, UK) is shown in Figure 1-8.

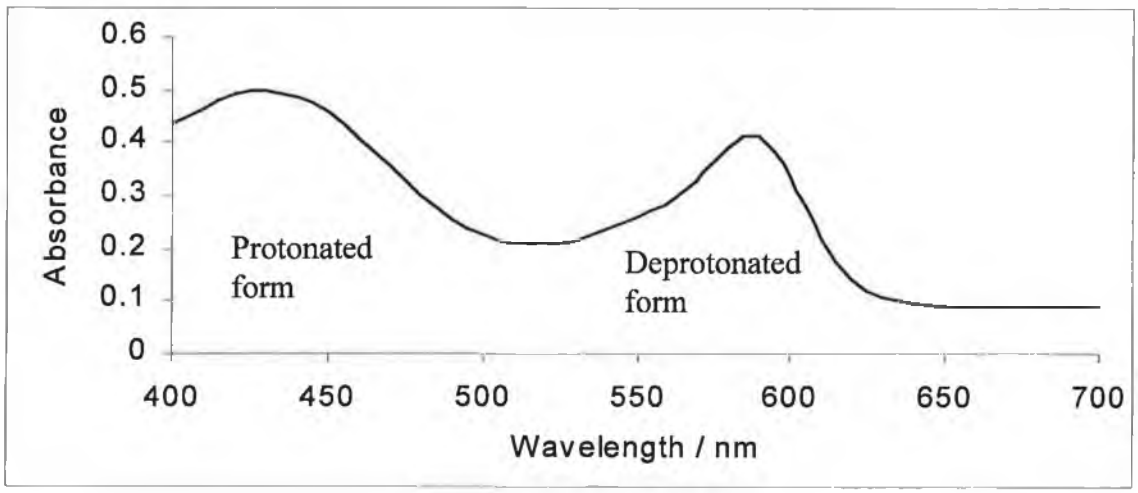

Figure 1-8: Plot of both the protonated and deprotonated form of the dye, bromocresol purple

Both forms of the dye can be seen. The protonated form absorbs at a lower wavelength than the deprotonated form of the dye as $\Delta Ep > \Delta Edp$.

1.4.3. UV-Vis Instrumentation

1.4.3.1 Bench-top UV-Vis Spectrometer

UV-Vis spectroscopy is typically used to measure the change in the light intensity with respect to the wavelength. The instrument is made up of the following components, a light source, a wavelength selector (monochromator), a sample reservoir, a detector, a signal processor and data acquisition through programmable software (Figure 1-9).

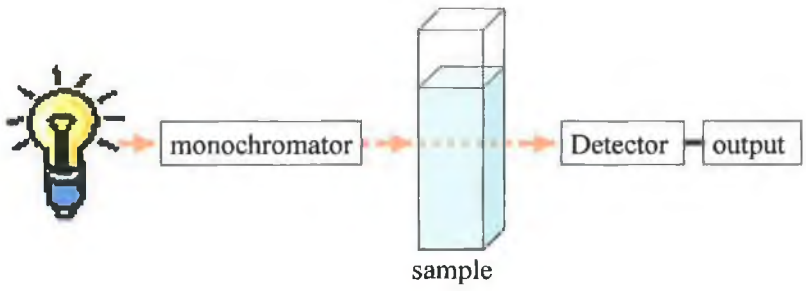

Figure 1-9: Schematic of typical components in a UV-Vis system

The **light sources** used are typically tungsten or hydrogen lamps. Deuterium and hydrogen lamps both emit in the range 160-375 nm. Tungsten lamps are used as a source for visible light, emitting in the wavelength region of 350-2500 nm [14]. The **monochromator** works as a wavelength selector in the following way, polychromatic radiation (radiation at more then one wavelength) enters the monochromator; the beam is collimated and then strikes a dispersing element at an specific angle. This splits the beams into its component wavelengths by a grating or prism [15]. The **sample reservoir** is usually a glass / quartz cuvette. A quartz or an optically transparent polymer cuvette must be used when analysing below 350 nm, as glass will absorb radiation of wavelength less than 350 nm. A **detector** commonly used with a UV-Vis instrument is a photomultiplier tube.

This consists of a photoemissive cathode (a cathode that emits electrons when struck by photons of radiation), several dynodes (emitting several electrons for each electron striking them) and an anode. The photomultiplier tube works in the following manner, a photon of radiation enters the tube and strikes the cathode causing the emission of several electrons. These electrons are then accelerated towards the first dynode causing the emission of several electrons for each incident electron; the electrons are then accelerated towards the second dynode to produce more electrons and then onto the third dynode and so on. Eventually the anode collects the electrons. The electrons have now produced up to 10^6 electrons. The resulting current is amplified and measured. Photomultiplier tubes are very sensitive to UV-Vis radiation and have extremely fast response times.

An example of a UV-Vis spectrometer commercially available is a PerkinElmer® Lambda 850 spectrometer (PerkinElmer®, USA Table 1-2 highlights the specifications of this instrument[♣]. This bench scale instrument is expensive to purchase and operate.

♣ Information obtained from PerkinElmer® Lambda 850 spectrometer operating manual.

Table 1-2: Table of specifications for PerkinElmer® Lambda 850 spectrometer – obtained from operating manual

Parameter	Specifications
Detector	Photomultiplier tube – R6872
Light source	Pre-aligned tungsten – halogen and deuterium lamp
Wavelength range	175nm – 900 nm
UV-vis resolution	< 0.05 nm
Wavelength accuracy	+/- 0.08 nm
Power	50 / 60 Hz
Temperature	10°C – 35 °C
Relative humidity	10 – 70 %
Size (W x D x H)	1020 mm x 630 mm x 300 mm
Weight	77 Kg

1.4.3.2 Platewell Reader

Another type of spectrometer that can be used to measure the absorbance of a sample is a platewell reader (Figure 1-10). This type of spectrometer is becoming more commonly used for spectral analysis. An example of a platewell reader is the μQuant™ reader and is available from Bio-Tek, Instruments, UK.

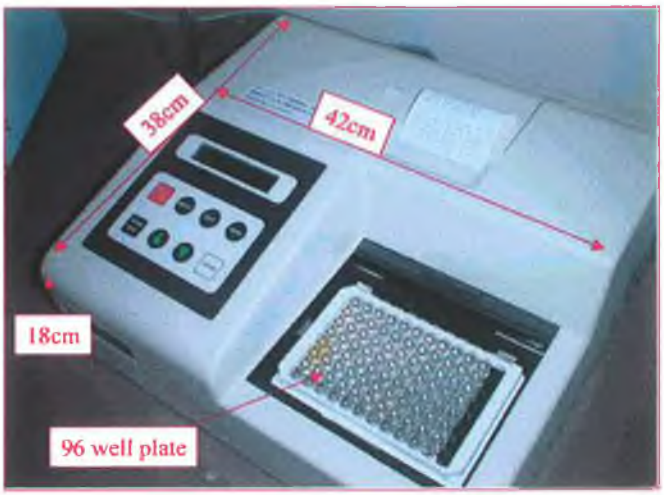

Figure 1-10: Photograph of platewell reader indicating dimension and 96 well plate.

The instrument is a single channel, automated, general-purpose analyser. It has the ability to measure the spectrum of multiple solutions in as many as 384 wells simultaneously. The optical reader has a wavelength range from 200 nm to 999 nm. The samples fit into a plate of dimension 12.8 cm (l) × 8.5 cm (w). The specifications of the instruments are shown in Table 1-3.

Table 1-3: Table of specifications for μQuant™ platewell reader

Parameter	Specification
Wavelength range	200 – 999 nm
Accuracy of wavelength	± 2 nm
Repeatability of wavelength	± 0.2 nm
Dimensions	42 cm x 38 cm x 18 cm
Weight	105 Kg
Detector	Photomultipling tube
Light source	Xenon flash
Environment	Operation temperature 18 – 40 °C

The instrument consists of a xenon flash light source, a monochromator and a photomultipling tube. All of the above information was obtained from the μQuant™ instrumentation handbook manual.

1.4.3.3 Portable Spectrometer

A conventional benchtop UV-Vis spectrometer is usually large in size and expensive; however newer generations of instruments are becoming increasingly smaller and more portable. Instrument miniaturisation ultimately brings down the unit cost. One example is a micro spectrometer (Ocean Optics S2000, OceanOptics, UK) as shown in Figure 1-11 [16], which is 20-fold cheaper than the bench scale PerkinElmer instrument described in Section 1.4.3.1.

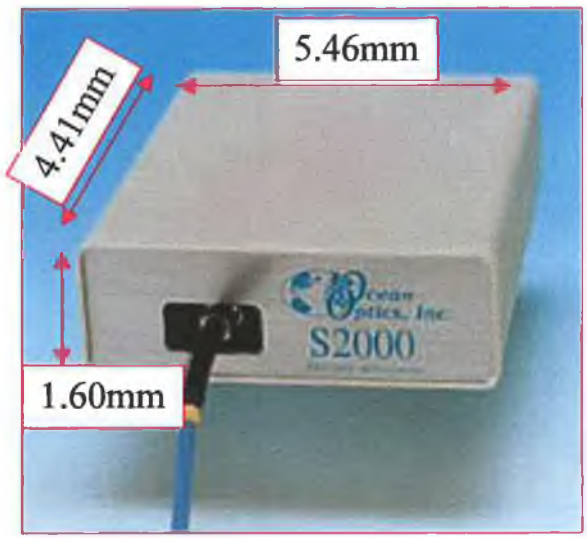

Figure 1-11: Photograph of Ocean Optics S2000 spectrometer

This spectrometer couples low cost with a high performance CCD – array detector. The S2000 accepts light energy transmitted through a single strand optical fibre and disperses it via a fixed grating across the linear CCD array detector from 200 – 1000 nm.

The specifications of the OceanOptics S2000 are listed in Table 1-4[♣].

Table 1-4: Table of specifications for S2000 OceanOptics spectrometer

Parameter	Specification
Weight	200 g
Dimensions	5.46 mm x 4.14 mm x 1.60 mm
Power regulations	130 mA at +5 V DC
Power up time	3 ms
Detector	Sony ILx511 CCD
Temperature	-3 °C - +70 °C
Humidity	0 % - 90 %

An external light source must be used, as one is not integrated into the spectrometer. Portable deuterium and halogen lamps can be used, which are obtainable from Top Sensor Systems, The Netherlands. The specifications for these lamps are listed in Table 1-5.

Table 1-5: Table of specifications for deuterium – halogen light source

Parameter	Deuterium lamp	Halogen lamp
Wavelength range	215 – 400 nm	360 – 1700 nm
Warm up time	30 minutes	20 minutes
Lamp life	1000 hours	900 hours
Power requirements	Europe 230 – 240 V	
Weight	Approximately 6 Kg	
Dimensions	150 mm x 135 mm x 319 mm	

[♣] Specifications obtained from their relative operating manuals.

1.4.4. pH

The pH of a solution is the negative of the logarithm of the hydrogen ion activity and can be expressed as outlined in Equation 1-5 [17]. It is a convenient way to represent very small concentrations of hydronium ion in solution and to show changes in very small concentrations

$$pH = -\log[H_3O^+] \qquad \textbf{Equation 1-5}$$

An equilibrium constant (K_a) is used to differentiate between strong acids and weak acids example acids and water.

$$HA + H_2O \leftrightarrow H_3O^+ + A^-$$

Where HA is a weak acid and A^- is the anion of the weak acid.
The equilibrium constant (K_a) can be obtained using the following equation,

$$K_a = \frac{[H_3O^+][A^-]}{[HA]} \qquad \textbf{Equation 1-6}$$

The larger the value of K_a the stronger the acid, and the greater the degree of dissociation into ions.

Like that of the pH scale, the negative logarithm of K_a gives the pK_a. This is a standard way to quote the strength of an acid. The stronger the acid the lower the pK_a (the negative logarithm inverts the relationship between the pK_a and the strength, just as it does for pH and acidity).

The Henderson-Hasselbach equation defines the pH of a solution of a conjugate acid-base pair in terms of the dissociation constant of the weak acid and the

equilibrium concentrations of the acid and its conjugate base. The definition of the Henderson-Hasselbalch equation is shown in Equation 1-7 [18].

$$pH = pK_a + \log\frac{[A^-]}{[HA]} \qquad \textbf{Equation 1-7}$$

This equation is used to calculate the effective pH of buffer solutions (typically mixtures of weak acids and its salt), using [A-] to approximate the concentration of the salt and [HA] to approximate the concentration of the acid. Then, if Ka is known, the pH of the mixture can be calculated.

1.4.5. Colorimetric Determination of pH

There are two main methods of measuring the pH of a sample, (1), a combination electrode (2), pH indicator dyes

(1) The combination electrode

A combination electrode is usually used to determine the pH of a solution; this contains both a pH-sensing electrode and a reference electrode in the same body. The pH sensing electrode is an ion selective electrode (ISE) for the hydrogen ion. An ISE is an electrode that responds selectively to certain ions in the presence of other ion without interference. The pH electrode has a membrane (usually glass) attached to the end of a tube that contains an internal reference solution (0.1M H^+ e.g. HCl). The reference electrode is used in combination with the pH electrode so that the difference in potential generated between it and the pH electrode can be measured. The reference electrode has a membrane attached to the end of a tube that contains an internal reference solution (usually saturated KCl). The combination electrode is immersed in the solution of interest. Since the potential of the reference is constant any change observed is due to the presence of H^+ ions. A schematic of a combination electrode is shown in Figure 1-12.

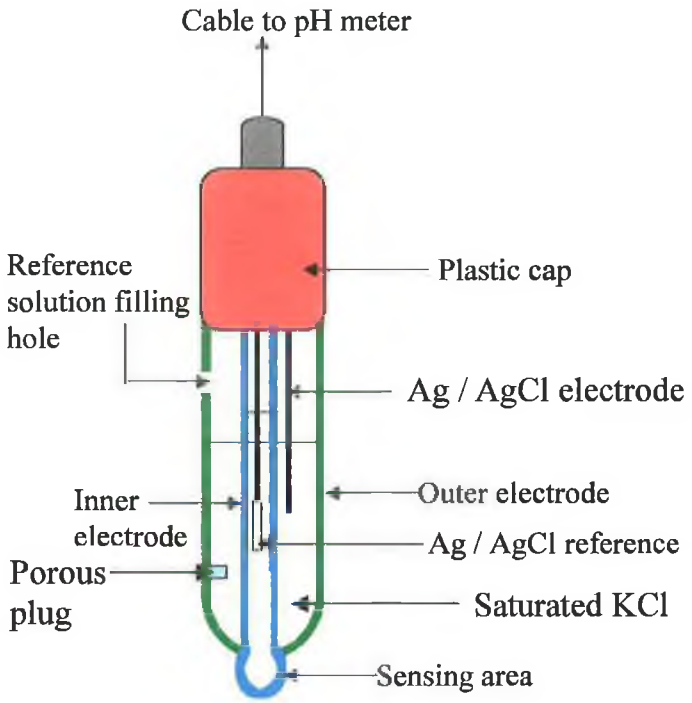

Figure 1-12: A schematic of a combination electrode

The potential difference between the two electrodes will depend on the activity of the H^+ ions. The activity is related to the concentration of H^+ ions, which facilitates analytical measurements of the concentration of H^+ present in solution. By measuring the potential generated and comparing it to the reference electrode (E^o), a net potential (E) is determined. The pH of the solution can then be obtained using Equation 1-8.

$$E = E° - S\,pH \qquad \textbf{Equation 1-8}$$

Where S = the Nearnst slope $\left(\frac{RT}{nF}\right)$ and R = gas constant (8.314 J K^{-1})

T = Temperature (K)

n = charge on the hydrogen ion (+1)

F = Faraday constant (96.485 KJ $V^{-1}mol^{-1}$)

(2) pH indicator Measurements

Figure 1-13 shows a pH titration curve when hydrochloric acid (strong acid) is added to an initial volume of sodium hydroxide (strong base). [19].

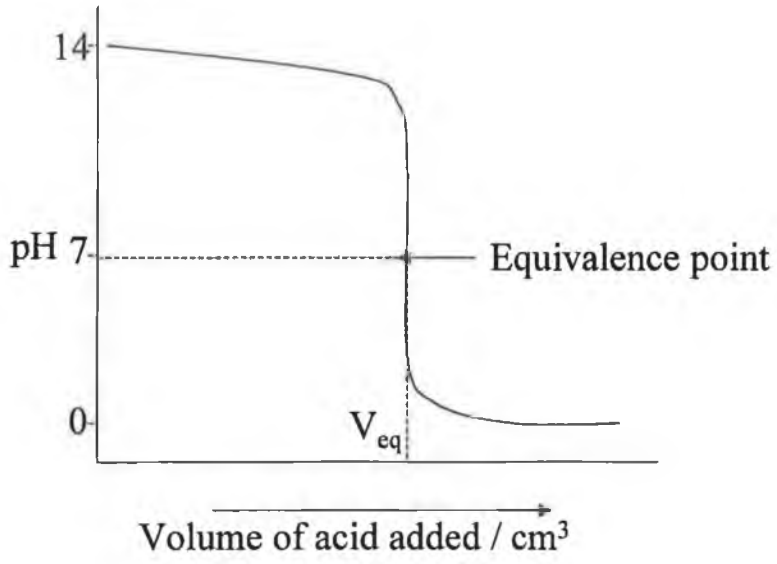

Figure 1-13: Plot of a titration curve for HCl and NaOH at the equivalence point, pH 7, at the equivalence volume, V_{eq}.

When the starting solution is a strong base and this is titrated with a strong acid initially there is a small change in pH. Once the equivalence point (point where there are equivalent amounts of acid and base in the solution) is approached there is a rapid change in the pH of the solution. If a small amount of pH sensitive dye is added to the mixture, then, if the pK_a of the dye coincides with the pH step generated by the change from acid to base dominated regions, the dye colour will change, and indicate when the change has happened.

This is the basis of a pH indicator dye (e.g. bromocresol purple) measurements of pH titrations. Note that for accurate measurements, a minimum amount of dye should be added (strong chromophores preferred), and the pK_a of the dye must coincide with the pH step accompanying the equivalence point.

1.5. Aims of Project and Work Plans

As already outlined, UV-Vis spectrometers in their various forms can be used to measure light intensity as a function of wavelength. These instruments all differ from one another in various aspects such as size, cost and accuracy. The most sensitive system out of those outlined above is the Perkin Elmer UV-Vis spectrometer, this is due to the excellent sensitivity of the monochromator and photomultiplier tube, which are explained in Section 1.4.3.1. However there is a growing need for smaller, inexpensive, low-powered optical devices for colorimetric analysis that are capable of operating autonomously in field deployment, performing real-time measurements over long time periods. A small, inexpensive low powered optical device cannot replace the bench top instrument in terms of sensitivity and accuracy, but a trade-off is acceptable when the miniaturised system can perform simple tasks efficiently and reproducibly with the added advantages of having quick response times, lower sample volumes, costing less and being portable.

The main aim of this project is to investigate an alternative method of light sensing using LEDs as both the light source and detector components of the system, and evaluate the systems validity for chemical analyses. Mitsubishi Electric Research labs (MERL)[*] investigated the use of LEDs as a way to improve existing infrared remote controls [20]. Normally in order to activate the backlight of a remote control a button must be pressed, which can be difficult to locate in the dark. MERL initially investigated the use of a capacitance proximity sensor; which functioned by turning on the backlight every time the control was handled. This technique was not very appropriate as it runs down the lifetime of the battery very rapidly. Also when the remote control was used in good lighting conditions, the backlight was unnecessary. Instead a light sensor was added that could turn on the backlight only when required. LEDs were investigated as light sensors [20]. In using LEDs as the optical components (as both a light source and

---

[*] Mitsubishi Electric Research Laboratories, 201 Broadway, Cambridge, MA 02139.

a detector) for the device instead of a tungsten lamp and photomultiplier tube this reduced the cost of the device significantly.

1.5.1. LED v's photodiode

A cadmium sulfide (CdS) photochemical cell (that of a photodiode) could also be used to detect light. The advantages of using a LED over a photodiode are listed below

1. LEDs have flatter sensitivity in the blue and UV region, where silicon photodiodes roll off.

2. LEDs have ~ zero quantum efficiency for wavelengths longer than their emission wavelength. Thus, they have a built-in short-wavelength pass filter, and the cutoff frequency can be hand picked depending on the colour of the LED. This is important down in the IR where a lot of LED emission sources have a secondary emission, and where silicon photodiodes will see the emission and not differentiate it from emission in the reagent passband. To fix this issue with a silicon photodiode an extra blocking filter is needed at the 99.99% level to be as good as the LED.

3. With the LED there is the potential that the LED can be used as a single device (detector only). The LED also has the potential to signal to other LED's or light sensitive detectors e.g. low cost digital cameras.

4. At night a LED can be seen over long distances e.g. under sea green LEDs are very efficient.

1.5.2. Construction of LED based Optical System

The construction of the optical device will vary depending on whether the device will be used for indoor lab based experiments or outside in the environment; for example, does the device have to be water tight or gas tight. These are all important factors that will determine how the device is constructed. The work carried out in this thesis evaluates the generic optical LED based sensing device for the use in either the environment or lab-based measurements. The devices (circuitry and optics) are not airtight or water tight as this is not a requirement for the applications explored. However if the application required that the devices are airtight or water tight all of the device can be easily altered to meet this requirement.

There are a number of important considerations when developing a low cost optical sensing device including, cost of material, cost of fabrication, manufacturability, power consumption, ease of operation, sensitivity and compatibility with a digital system.

The cost of the material for the system includes the optical device itself and the electronics used to run the device. As the main optical components of the device are LEDs and these are relatively inexpensive, the overall cost of the device will be a lot lower then that of a conventional UV-Vis instrument that uses tungsten light sources and photomultiplier tube detectors. There are various types of LEDs commercially available e.g. a 3 mm round LED (HLMP1700) (Radionics, Dublin, Ireland) costing approximately €1, with a surface mount LED (LSYT676, Radionics, Ireland) costing about double this.

If small quantities of the device are required then the components can be manually soldered onto the circuit boards, no special instrumentation is needed, however if large batches are required then an injection moulding technique can be used to rapidly and accurately manufacture the device in bulk.

The power consumption of the device is a lot lower than that of other portable optical based light sensors. For example the OceanOptics S2000 consumes 130 mA / hr. at 5 V DC. The power consumption for the LED-based optical device can be estimated to be 7 mA / hr at 5 V DC. A Duracell alkaline 9 V battery has a battery capacity of 580 mA / hr; therefore using this battery the LED based optical device can operate continuously for approximately 83 hrs.

The use of autonomous wireless network sensing for environmental chemical sensing is growing rapidly. In principle, this drastically reduces the time of human intervention required to incidents detected through continuous monitoring. Networked sensors contribute reliable data with the additional benefit of real time geographically distributed information. The basic requirements for these network sensors are that they have to be robust, cost effective, energy efficient and the data must be readily digitised for transmission. The aim of this work is develop a generic circuit and optical device that can meet these requirements.

The sensitivity of the colorimetric sensing device can be tuned by using a light emitting diode with the appropriate waveband. The emission band of the LED must overlap exactly with the maximum of the absorption band of the sample in order to achieve maximum sensitivity.

1.5.3. Evaluation and Optimisation of System

The LED based optical system was evaluated to ensure that it can be used as an alternative method for light sensing. This was done by experimenting with different configurations of the optical components. Each configuration was evaluated in turn.

Once each individual component has been screened for suitability, then the instrument comprised of these components can be optimised. Parameters to be optimised include the path length, light intensity, sample size, LED configuration and LED emission band.

When the system has been fully evaluated and optimised, it can then be calibrated, using pH indicator dyes. These dyes should have absorbance characteristics in agreement with the Beer-Lambert law (Section 1.4.1). Hence, when analysed using the LED based optical system the dyes exhibit a 'Beer-Lambert law' like behaviour. A true Beer-Lambert law plot is not observed as the LEDs emit a band of light rather then monochromatic light, as it is based on the use of monochromatic light. However, if the absorbance across the band is broadly Beer-Lambert compliant, then a linear relationship between sample concentration and instrument output can be expected (at least for a certain range of concentrations).

If a linear working range is obtainable for the indicating dyes using the novel optical device then it can be concluded that the device has been successfully calibrated to monitor the pH of a solution using that particular dye.

1.5.4. Applications of LED Based Device

The LED based optical system is a generic platform for any colorimetric sensing. The main aim of this work was to prove that these LED-based sensing devices are suitable for colorimetric sensing. The applications investigated in this study to demonstrate this principle are,

- The determination of the pH of a solution in both liquid phase and solid phase sensing, and;
- The determination of the amount of iron (II) present in a solution.

The iron (II) determination was undertaken using the iron complexing reagent 1,10 phenanthroline while the pH determination was determined using pH indicator dyes. These will be discussed in Chapters 3, and 4 & 5, respectively. Chapter 2 will discuss in detail how the LED sensor and circuitry function.

1.6. References

[1] www.epa.ie/OurEnvironment/Water/Rivers/RiverQualityReport2003/ [Last accessed 10/06/05]

[2] Eric Bakker and Ernö Pretsch, *TrAC Trends in Analytical Chemistry*, 2005, **24**, 199.

[3] S. Alcock, D. Barcelo, P.D. Hansen, *Biosensors and Bioelectronics*, 2003, **8**, 1077.

[4] D. Diamond, *Principles of chemical and biological sensors*, J. Wiley & Sons, 1998, 2.

[5] R.J Forster, D. Diamond, *Anal. Co*mm., 1996, **33**, 1H.

[6] X. Yang, K.G. Ong, W.R. Dreschel, K. Zeng, C.S. Mungle, C.A. Grimes, *Sensors*, 2002, **2**, 455.

[7] http://www.geo.mtu.edu/rs/back/spectrum/ [Last accessed 02/02/05]

[8] T. Frost and M.A. Russell, *Techniques in Visible and Ultraviolet Spectrometry*, BJ Clark, **4**, 1993, 26.

[9] J. Janata, *Principles of Chemical Sensors*, D. Hercules, **2**, 1990, 245.

[10] C.N.R. Rao, *Ultraviolet and Visible Spectroscopy Applications*, Butterworths, **3**, 1992, 144.

[11] E. D. Olsen, *Modern Optical Methods of Analysis*, Mc Graw – Hill, 1975, 83.

[12] D.T. Burns, Aspects of the Development of Colorimetric Analysis and Quantitative Molecular Spectroscopy in Ultraviolet-Visible Region, in Advances in Standards and Methodology Spectrophometry, C. Burgess and K.D. Mielenz, 1987, 10.

[13] C.N.R. Rao, Ultraviolet and Visible Spectroscopy Applications, Butterworths, **3**, 1992, 3.

[14] D. Heinz-Helmut Perkampus, *UV-vis Spectroscopy and its Applications*, H. Charlotte Grinter, T.L. Threlfall, 1992, 12.

[15] R. C. Denny, R. Sinclair, *Visible and Ultraviolet spectroscopy*, Mowthorpe, 1987, 39.

[16] http://www.oceanoptics.com/products/s2000.asp
[Last accessed 02/02/05]

[17] P. Atkins, L. Jones, *Chemistry Molecules Matter and Change*, W.H. Freeman and Company, **3**, 1992, 564.

[18] H.F. Holtzclaw, W.R. Robinson, J.D. Odom, *General Chemistry*, D.C. Health and Company, **9**, 1991, 557.

[19] H.F. Holtzclaw, W.R. Robinson, J.D. Odom, *General Chemistry*, D.C. Health and Company, **9**, 1991, 518.

[20] P. Dietz, W. Yerazunis, D. Leigh, *Mitsubishi Electric Research Laboratories Internal Report* TR2003-35, July 2003.

2. LIGHT EMITTING DIODES

2.1. Introduction

The use of light emitting diodes (LEDs) is widespread these days particularly in a multitude of electronic devices found around the home and workplace. They are for various reasons including, transmitting information (remote controls), illumination of the screen in digital watches and as visual indicators showing when an appliance is switched on. When LEDs are grouped in high density arrays, they can be used to form images on television screens or illuminate traffic lights. They are available in many different colours, shapes and sizes. The original and most common LED has a standard domed body of 5 mm diameter (see Figure 2-1 (3)). Nowadays a range of LEDs are available in many different sizes, e.g. 3 mm, 8 mm and 10 mm. Other shapes include square, rectangular and triangular LEDs. Bicolour and tricolour LEDs are also available, a bicolour LED consists of two colours, e.g. a red and green, in a single package connected back to back so that the cathode is connected to the other diodes anode. A tricolour / full colour LED contains a red, green and blue LED housed in a single epoxy package. Surface mount LEDs are also available. These can be found in standard benchtop computers. Figure 2-1 shows a diverse range of commercially available LEDs [1].

Figure 2-1: A selection of LEDs available (1) surface mount LED (3.2 mm x 2.8 mm), (2) 3 mm clear domed LED, (3) 5 mm clear domed LED, (4) 3 mm tricolour LED, (5) 3 mm domed LED, (6) 3 mm rectangular LED, (7) 10 mm domed LED.

LEDs also vary in their viewing angle. The viewing angle of a LED controls the light emission beam. Standard LEDs have a viewing angle of 60 degrees where as others have a narrower beam of 30 degrees or less.

The cost of LEDs varies significantly depending on the size and the material used to fabricate the LEDs. For example, 5 mm GaAlAs ultra-bright round LED can be purchased from Radionics [2] at a starting price of €0.52 while a 5 mm ultra-bright precision optical performance round LED has a starting price of €2.21 (Radionics, Dublin, Ireland). LEDs appear to have a very exciting commercial future. For example it was reported in the Engineering Times (2004) [3] that within the next 5 years the LED would replace the conventional light bulb.

From the point of view of colorimetric analytical measurements LEDs offer significant advantages compared to conventional light sources such as a tungsten filament light bulbs including:

- Small size: enabling the scale of the instrumentation to be reduced.
- Consume low power: Example can be operated using a < 5 V battery supply for many hours (approximately 30 hours).
- They can be suitably used for a wide range of the colorimetric methods: The LED most desirable (in terms of λ_{max}) for a particular application can be handpicked.
- Simplicity: They are very easy to use, assemble and incorporate into a system
- Cost efficient: LEDs are cheap, particularly when bought in bulk.

2.2. LED Structure

The first commercially available LED was developed in the 1960's by combining 3 primary elements gallium, arsenic and phosphorus (GaAsP) to obtain a red light source with a λ_{max} 655 nm. The basic structure of a LED consists of a LED chip (light emitting semiconductor material), a mild steel lead frame upon which the

semiconductor material is placed and an encapsulating epoxy, which surrounds and protects the chip (Figure 2-2). A typical LED is made from a GaAsP n-doped substrate with a thin p-doped layer grown on the top of this substrate, (for more information on p and n type material see section 2.3.1). The p-n junction (where the radiation is generated) is between these two layers. The GaP layer is inherently transparent and hence the radiation escapes through the top layer and a reflective layer is added to the bottom electrode of the GaP substrate [4]. The flux escape mechanism is shown in Figure 2-3. All of the components that make up a LED are then encapsulated into a plastic housing, typically a transparent epoxy. This improves the optical efficiency of the LED, and holds all of the components together. The shape of the plastic dome dictates the output pattern of the LED.

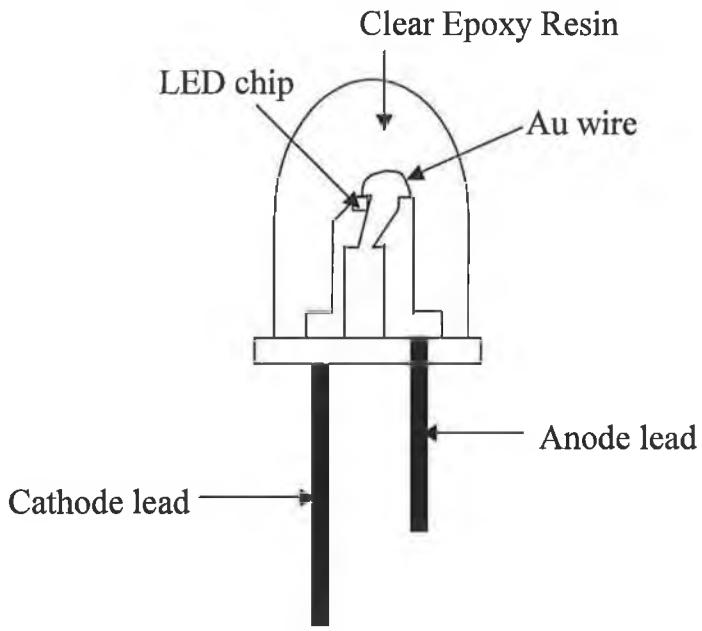

Figure 2-2: Sketch of a typical LED.

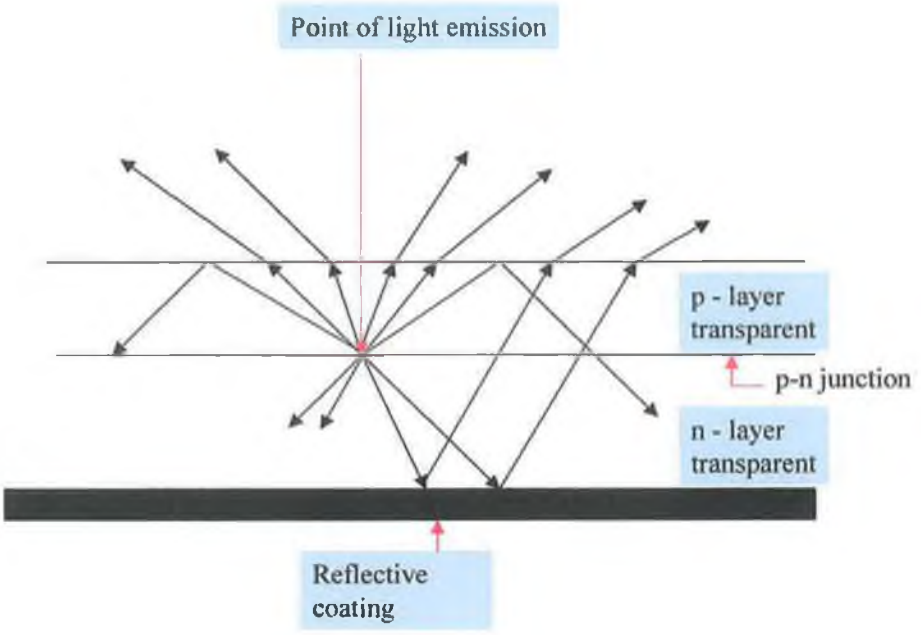

Figure 2-3: LED with absorbing and transparent n-layer

The materials used to fabricate the diodes are usually silicon (Si), germanium (Ge) and gallium (Ga). An example of the electron shells present in a Ge atom is shown in Figure 2-4 [5].

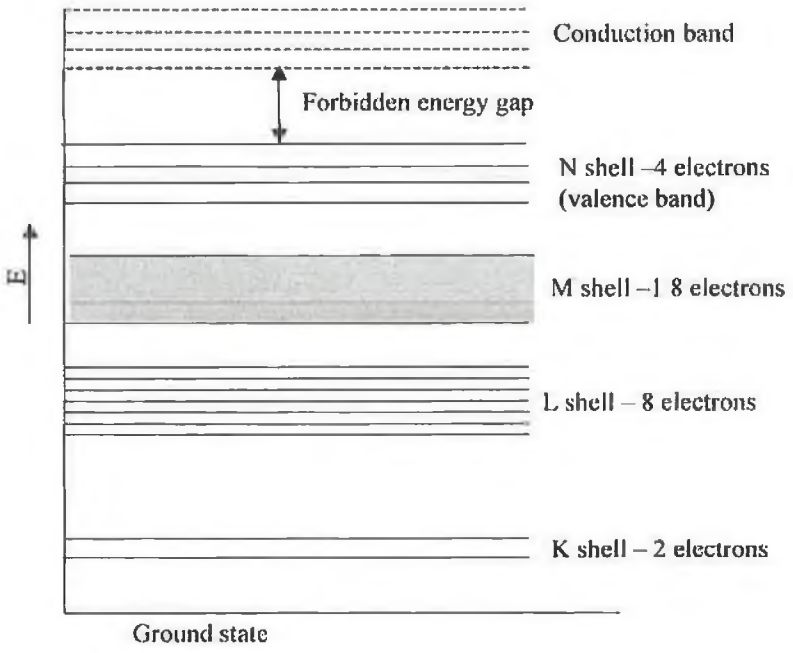

Figure 2-4: Shells in a germanium atom.

Generally the electrons that are present in the valence band (N shell in Figure 2-4) are known as valence electrons. If appropriate energy is provided to the atom then these valence electrons are promoted into the conduction band where they are free to follow electrical forces and become carriers of electricity. The electrical property of a material depends on the number of electrons and the availability of the carriers in the conduction band. A good conductor can have up to 10^{23} carriers / cm^3 and a good insulator 10 carriers / cm^3. A semiconductor has between 10^8 – 10^{14} carriers / cm^3 [6]. In a conductor the energy gap between the valence band and the conduction band is non-existent, in an insulator this gap is approximately 6 eV and in a semiconductor this gap is in-between that for a conductor and insulator (approximately 1 eV).

2.3. Conduction in Semiconductors

Silicon is a semiconductor material commonly used in the fabrication of LEDs; this atom has four electrons in its outer shell. These electrons are all involved in forming bonds between the silicon atom and other atoms. In a crystal of silicon each atom is bonded to four other silicon atoms, each bond consisting of two shared electrons (Figure 2-5) [7].

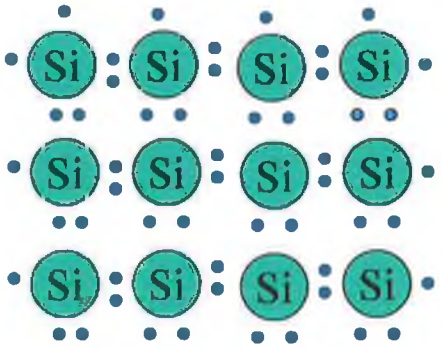

Figure 2-5: Schematic of silicon crystal [7]

At temperatures above absolute zero some of these electrons leave the bond and become free to move through the crystal. When a silicon atom looses one of its four electrons the "space" left behind is known as a hole, which behaves as if it

has a positive charge (having a strong attraction for negative electrons), see Figure 2-6.

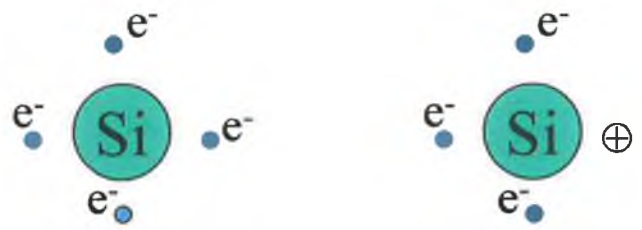

T = 0 K (a)

T > 0 K (b)

Figure 2-6: (a) Schematic of silicon at 0 K with no free electrons, (b) at higher temperatures some electrons are freed leaving positive holes [7].

When a piece of silicon is placed in an electric field, the free electrons drift towards the positive electrode, at the same time a bound electron near a positive hole may gain enough energy to move from its own atom into the positive hole thus creating a positive hole in its original position. As this process is repeated the positive hole in effect moves towards the negative electrode (Figure 2-7). The higher the temperature of the semiconductor material the more free electrons and holes available for conduction i.e. the resistance of a semiconductor decreases with an increase in temperature (unlike metallic conductors).

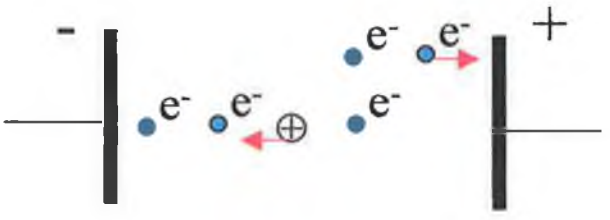

Figure 2-7: In an electric field the electrons move towards the positive potential while the holes move towards the negative potential [7].

2.3.1. Doping

The conductivity of a semiconductor material (e.g. silicon) can be increased by the addition of small controlled amounts of "impurities" that have roughly the same atomic size but more or less valence electrons then the semiconductor itself. This process is known as doping.

2.3.1.1 N type semiconductor

In an N-type semiconductor the semiconductor (e.g. Si) has been doped with an impurity containing a higher concentration of electrons then holes (e.g. phosphorous (P)). The electrons are the major carriers and dominate the conductivity (e.g. silicon with the addition of phosphorous shown in Figure 2-8).

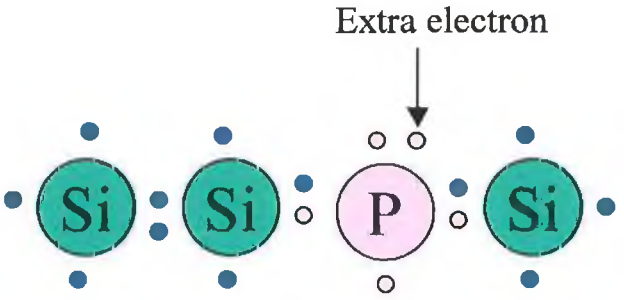

Figure 2-8: Doping of silicon with phosphorous (N-type semiconductor)

This extra electron becomes available for conduction therefore the conductivity of the material is increased.

2.3.1.2 P type semiconductor

In a P type semiconductor the impurity / dopant has a greater concentration of holes then the concentration of electrons. These holes are the major carriers and dominate the conductivity. For example the resistance of a piece of silicon decreases significantly by doping it with boron (B) (Figure 2-9).

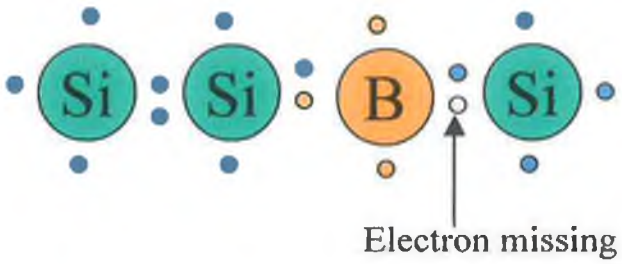

Figure 2-9: Doping of silicon with boron (P-type semiconductor)

The doping process does not introduce an overall charge to the crystal. The impurity atoms have a different number of electrons in their outer shells to the silicon atom. However the number of protons and electrons are the same, therefore they are electrically neutral.

2.3.2. P-N Junction

When a P-type and N-type material combine a junction is formed, this junction is known as the P-N junction. The electrons near the junction move into the P-type material, where they combine with the holes and at the same time the holes move into the N-type material, where they combine with the electrons. This causes a layer to form (depletion layer) on either side of the junction; there are virtually no free electrons or holes in this layer (Figure 2-10) and hence this region has a relatively high resistance.

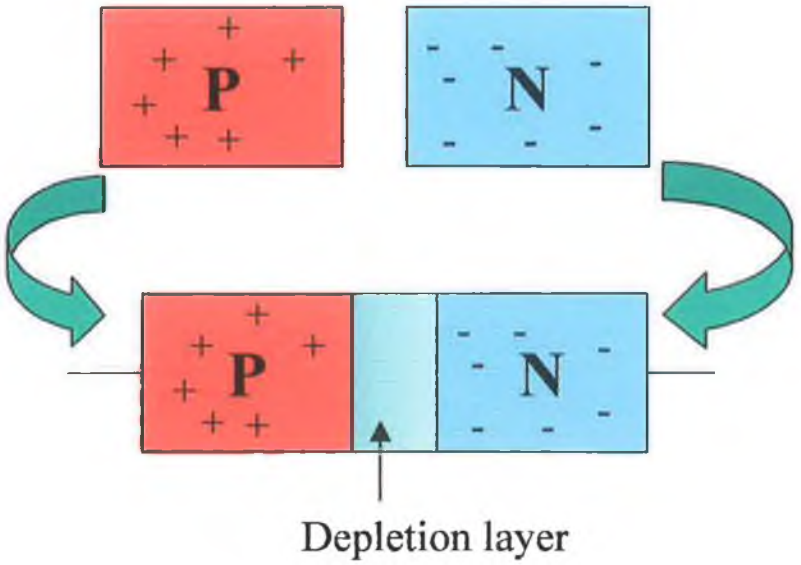

Figure 2-10: Schematic of P-N junction where P-type material and N-type material combine and a depletion layer forms.

2.3.3. Junction Diode

2.3.3.1 Forward Bias

When a diode (P-N material) is connected in a circuit in such a way that the P-type material is positive with respect to the N-type material, then the diode is referred to as being forward biased. Here the free electrons in the N-type material are repelled from the negative end of the battery terminal and driven into the depletion layer, at the same time the holes are driven into the depletion layer by the positive potential. This causes the width of the depletion layer to reduce significantly or disappear and current starts to flow (Figure 2-11). When a LED is connected to a battery in the forward biased mode (the N side of the LED is connected to the negative side of the battery) photons of light are emitted.

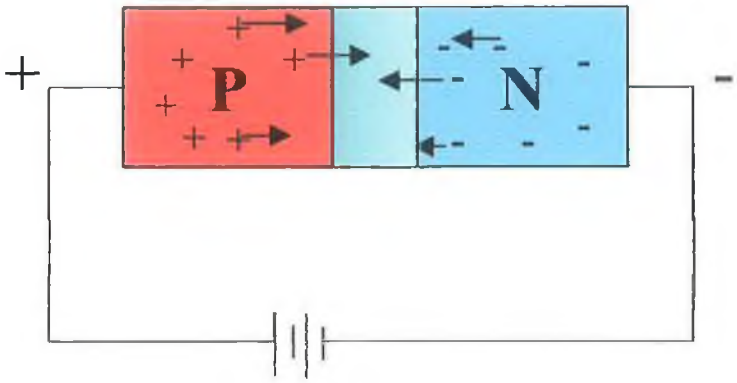

Figure 2-11: Forward biased diode, the P-type material is positive with respect to the N-type material and the depletion layer is reduced or disappears enabling current to flow more easily.

2.3.3.2 Reverse bias

When the diode is connected to a circuit in such a way that the N-type material is positive with respect to the P-type material then no current flows and the diode is said to be reverse biased. This is due to the fact that the N-type material is positive and the electrons are attracted towards the positive end of the battery. At the same time the holes in the P-type material are attracted towards the negative end of the battery (Figure 2-12). This causes the depletion layer to widen and no current flows (capacitor).

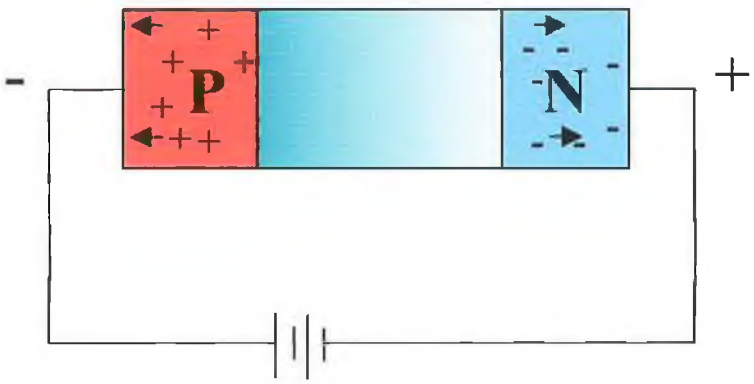

Figure 2-12: Reverse biased diode, the N-type material is positive to the P-type material and the depletion layer is widened causing no current to flow.

A photodiode is a diode that is configured in reverse biased mode and can be used to sense light. If a reverse biased junction is illuminated with light, free electrons-hole pairs are created in the depletion layer and a small photocurrent will flow. Since each photon of incident light creates one electron hole pair, the current flowing is proportional to the intensity of light.

Photodiodes generally require a pre-amplifier to give a signal gain for applications when needed to detect Pico Watts of light power. Silicon (Si) based photodiodes cover a wide range of wavelengths from 190 nm to 1100 nm. Germanium (Ge) photodiodes overlap with the Si response spectrum can detect up to approximately 1600 nm. Photodiodes are widely used in everyday applications, e.g. sensors for door openings, assembly line controls, load levellers in luxury cars, tanning exposure meters, smoke detectors, x-ray baggage inspection systems and personal blood sugar meters for diabetics [8].

2.3.4. Measurement of Light Intensity

The Sun Spectrometer

Recently research has been carried out utilizing LEDs as light detectors. Mims et al. [9, 10] were the first to develop a method for the detection of light using a LED. The application developed by Mims et al. was a sun spectrometer. This method of detection used an operational amplifier (op amp) to amplify the photocurrent obtained.

An op amp amplifies the difference between two inputs, conventionally labelled as (+) and (-). In an op amp (1) input impedance is infinite therefore all of the current flows through the feedback loop, (2) the voltage difference between (+) and (-) inputs is zero therefore V (-) = 0 (same as V (+) and (3) if the input voltage is example 1V then the current is I = V/R which is 1 mA, the current through 10 KΩ is also 1 mA therefore the voltage drop across the resistor is 10 V.

An example of a typical op amp is shown below in Figure 2-13. Here the resistances of R1 and R2 are 1 KΩ and 10 KΩ, respectively. According to Ohms law (Voltage = resistance x current) if there is a current of 1 mA flowing through R1 then the output will have to move to – 10 mV's to supply the same current through R2. The voltage gain therefore is R2/R1, which in this case is equal to 10 (Figure 2-13).

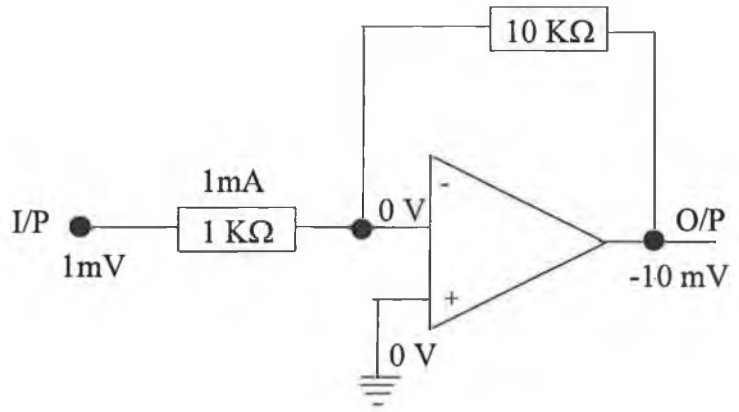

Figure 2-13: Schematic of inverted operational amplifier.

With the sun spectrometer the photocurrent was fed to the op amp via two resistors (R1) and (R2) as shown in Figure 2-14, in such a way that the input signal applied was in series with R1 and the output was connected back to the inverting input through R2 (negative feedback). The non-inverting input was connected to the ground. When in operation the input signal moved to the positive and the output signal the negative and visa versa. The voltage change at the output relative to the input was dependent on the two resistors. The light from the sun caused the LED detector to generate an electrical current; the current was transmitted directly to the op amp, which was connected to convert the LED current to a voltage. This voltage was then measured using a voltmeter. The ambient light acted as the light source and a LED was used as the detector. This approach could be used for chemical sensing but would require an A/D converter. A signal amplifier may also be required for low concentration solutions.

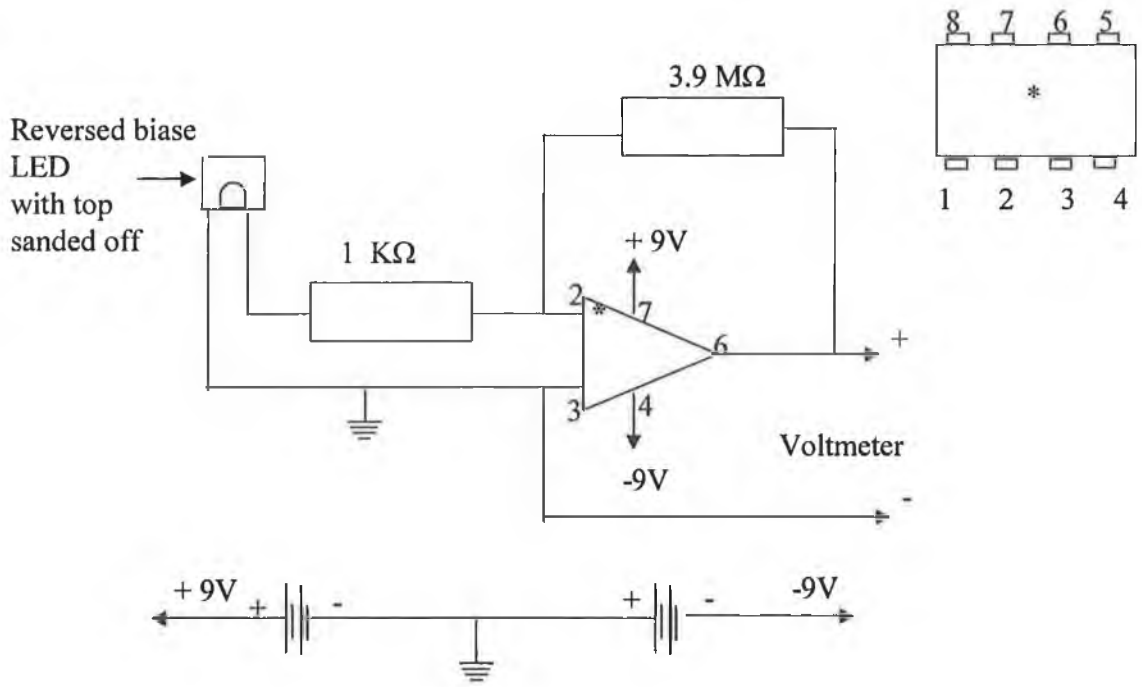

Figure 2-14: Schematic of circuitry used by Mims et al. to measure the intensity of light using an LED [9].

Backlight Detector

Mitsubishi Electric Research Laboratories (MERL) has developed a backlighting system for remote controls that use a LED as a light detector [11]. The LED in the remote control is configured to automatically sense when the backlight is needed. A MERL - DCU collaboration was set up to explore the possibility of using a LED as part of an integrated device for the application of chemical sensing.

An example showing how the LED is used for the detection of light is outlined in Figure 2-15. This plot was obtained using a Fluke 199C 200 MHz dual channel floating input portable oscilloscope (Fluke Corporation, USA). The figure illustrates the principle employment in the measurement.

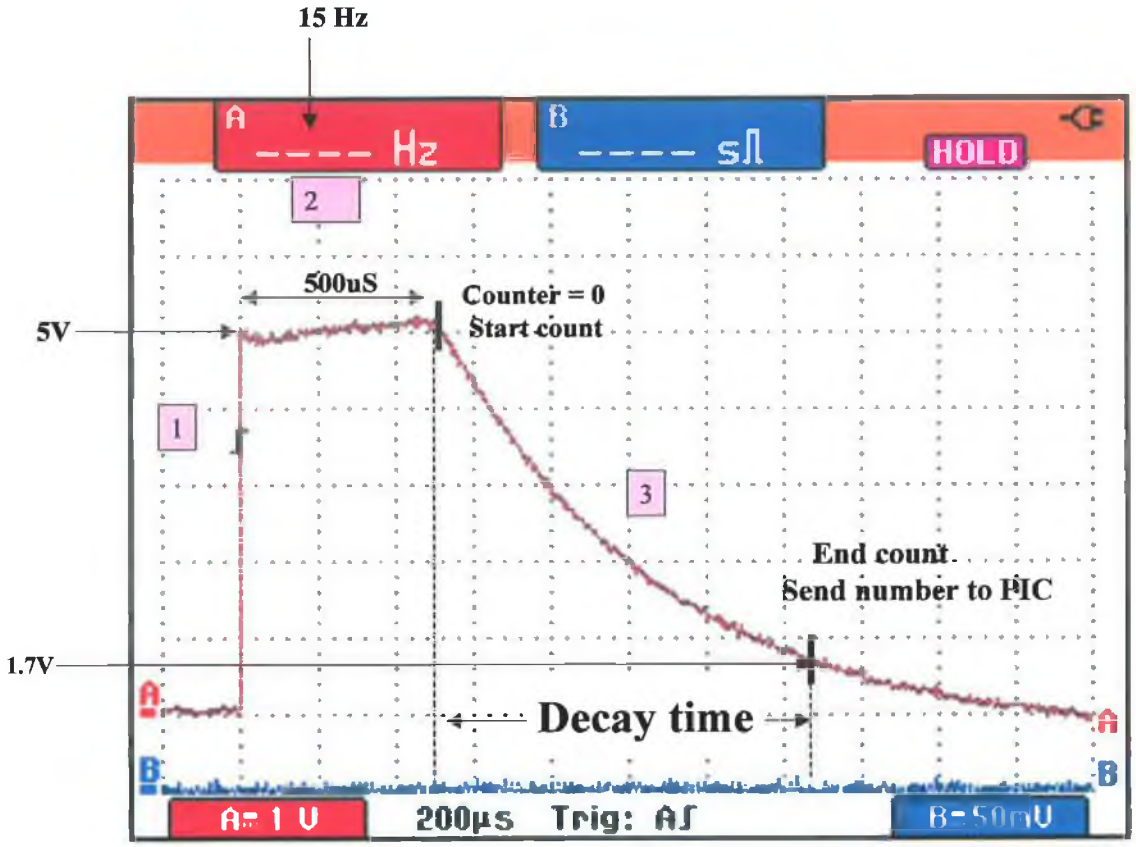

Figure 2-15: Results from Fluke 199C of charge and discharge of capacitance decay, (1) LED reversed biased, (2) held at 5V and (3) output pin switched to input and the decay time measured.

The detector LED was reversed biased to 5 V, inducing a capacitance (1). Once completely charged it was held at 5 V for 500 µs. This ensured that the voltage was at a constant 5 V (2). Next the output pin was switched to input and the photocurrent arising from incident photons (e.g. from the emitting LED) begins to discharge the capacitance (3). The time taken for the junction to discharge from 5 V (logic 1) to 1.7 V (logic 0) was captured and is directly related to the intensity of light reaching the detector. Note that this simple timer circuit provides an inherent digital output i.e. no A/D converter is required.

2.4. Theory of Operation

The total discharge time (t) for the LED equivalent circuit can be described as [12],

$$t = \frac{Q}{i_{light} + i_{discharge}} \qquad \textbf{Equation 2-1}$$

Where Q = CV (voltage × capacitance) is accumulated charge and is a constant

i_{light} is the photocurrent,

$i_{discharge}$ is the discharge current arising from non photocurrent sources

When $i_{light} >> i_{discharge}$

$$t = \frac{Q}{i_{light}} \qquad \textbf{Equation 2-2}$$

Because the photocurrent is proportional to the light intensity (I) Equation 3-2 can be rewritten as

$$t = \frac{Q}{kI} \qquad \textbf{Equation 2-3}$$

Where k is a constant

When the conventional absorbance model (Beer-Lambert's Law) is considered, then,

$$\log \frac{I_o}{I} = A = \varepsilon C \lambda \qquad \textbf{Equation 2-4}$$

Where A is the absorbance (at a particular wavelength), ε, the molar absorbtivity ($M\ cm^{-1}$), C, the concentration of the sample (M) and λ, the path length (cm).

When (Equation 2-3) is combined with (Equation 2-4), (Equation 2-5) is obtained.

$$\log t = \varepsilon C \lambda + \log t_o$$ **Figure 2-5**

Therefore under conditions where the Beer-Lambert Law is obeyed, plotting log t verses c yields a straight line with intercept at log t_0.

2.5. Circuitry for LED Light Sensing

A photograph of the circuitry used is shown in Figure 2-16.

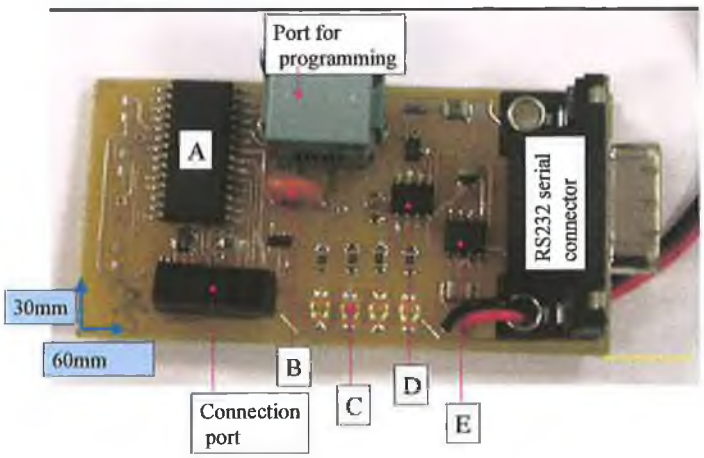

Figure 2-16: Photograph of circuitry (A) = Programmed Integrated Circuits (PIC) microcontroller, B= 20 MHz resonator crystal, C = indicator LEDs, D = low power serial communication transceiver and E = 5 V voltage regulator.

A schematic diagram of the circuitry used is shown in Figure 2-17.

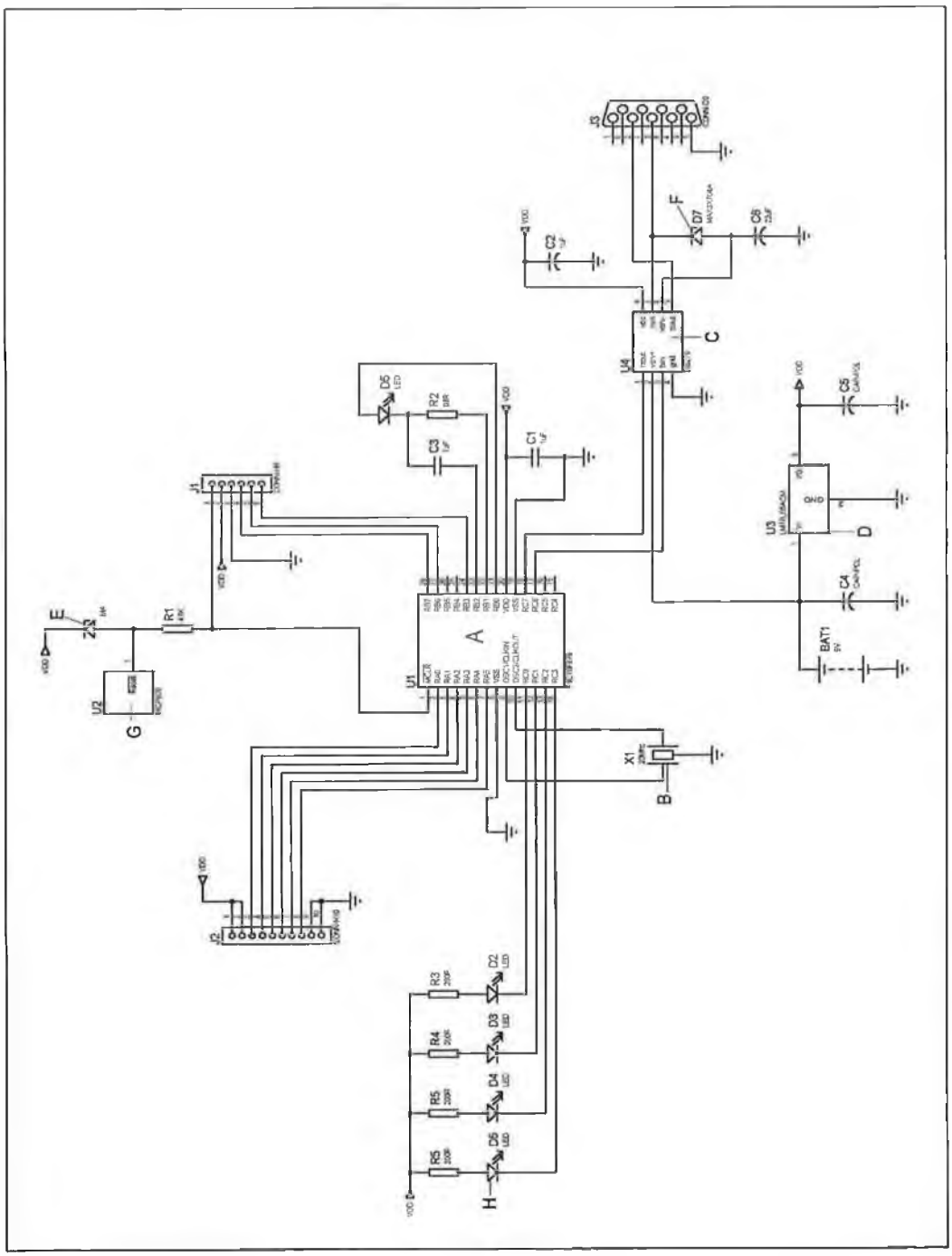

Figure 2-17: Schematic of Circuitry used; (A = PIC microcontroller, B= 20MHz resonator, C = low power serial communication transceiver, D = 5V voltage regulator, E +F = Schottkey diodes, G = reset supervisor and H = indicator LEDs.

The main components of the circuitry for the LED-based optical system are (from the photograph), (A) a Programmed Integrated Circuit (PIC) microcontroller, (E) a 5 V voltage regulator and a RS232 port for communication with a PC.

The microcontroller (A) used (PIC 16F876), was a 16-bit microcontroller that has a resolution of 65,536 (2^{16}). The microcontroller is the core of the circuitry controlling all actions taken. It is programmed to run and control the tasks desired by the end user. Other components on the board include (B) a 20 MHz oscillator, (D) a low power serial communication transceiver chip (DS276) that translates the RS232 signal levels to common CMOS/TTL levels. (E) A 5 V voltage regulator (LM78L05ACM), which controls the voltage of the system to 5V. All of the components used on the board are surface mount components.

The microcontroller used requires 23 instruction cycles to perform a check on the logic state of the pin (i.e. logic 1 or logic 0). If the pin is above 1.7 V then it is classed as logic 1 and an increment of 1 is added to the count until a maximum of 14130 loops are done at which the counting is stopped. The 20 MHz oscillator provides 20 x 10^6 clock cycles per second, 1 cycle takes 5 x 10^{-8} s, i.e. 0.05 x 10^{-6} s, therefore 20 clock cycles takes 1 μs (1 x 10^{-6} s). As each loop cycle requires 23 instructions, each of which takes 4 clock cycles, 1 loop will require 23 x 4 = 92 clock cycles, i.e. 4.6 μs.

2.6. Data Capture

Each measurement takes approximately 65 ms (4.6 μs x maximum count 14130). Every second 8 ambient light measurements and 8 measurements with the LED ON are recorded. Before any data point is printed a total of 32 measurements are taken and averaged. These results in a new averaged data point being printed approximately every 2 s (65 ms x 32). The data point printed is comprised from 16 ambient light readings and 16 readings obtained with the LED ON. HyperTerminal (Windows 2000) is used to transfer the data from the microprocessor into a Microsoft Excel file. The settings connect to COM PORT 1

at a band rate of 9600 bits / sec. When this is set up the data is then captured and saved to a text file. Figure 2-18 shows a screen image of data collected using HyperTerminal. The software is configured to capture 2 columns of data; (1) The data obtained when the LED is off (sometimes called dark current) and (2) the data obtained when the LED is on. A third column is then calculated by the software that contains the values obtained when the dark current data is subtracted from the data obtained with the LED on and corrects for the presence of ambient light.

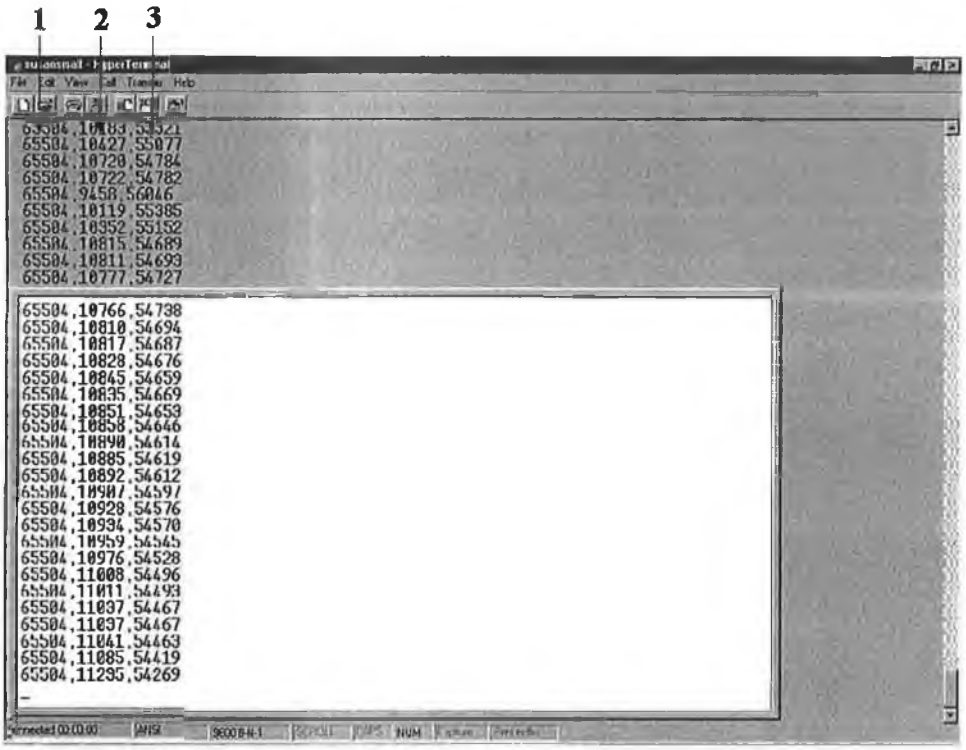

Figure 2-18: Screen capture of data being collected by HyperTerminal, column 1 = dark current response, column 2 = response with LED on, column 3 = dark current response -response with LED on.

Once all data has been captured the process is stopped. Data is exported to Microsoft Excel and processed. This is the method of data collection used for all experiments carried out using the LED-based optical devices throughout this thesis.

The circuitry that was described in Section 3.5 was utilized with all of the LED based optical devices developed throughout this work. Both the emitter LED and detector LED are connected to the circuitry via the connection port shown in Figure 2-16 and a 9 V battery is used as a power source.

2.7. References

[1] http://www.peats.ie/cgi-bin/shop/db.cgi?q=LED
[Last accessed 01/02/05]

[2] http://www.radionics.ie/cgibin/bv/search/searchdisplay.jsp?3287682619=3287682619&cacheID=ieie
[Last accessed 01/02/05]

[3] http://www.eetimes.com/at/news/showArticle.jhtml?articleID=25600144
[Last accessed 10/01/2005]

[4] E. Uiga, Optoelectronics, Practice – Hall inc., 1995, 95.

[5] E. Uiga, Optoelectronics, Practice – Hall inc., 1995, 79.

[6] J. J. Brophy, Basic electronics for scientists, Mc Graw-Hill, **2,** 1990, 5.

[7] G. Porter, *senior physics*, Folens, 297.

[8] J.J. Sparkes, Semiconductor devices, VNR international, **2,** 1987, 69.

[9] F.M Mims, Siliconnections - coming of age in the electronic era, Mc Graw Hill. 1986, 91.

[10] F.M. Mims, LED circuits and projects, Howard W. Sams and Co. Inc., 60.

[11] P. Dietz, W. Yerazunis, D. Leigh, Mitsubishi Electric Research Laboratories internal report TR2003-35, July 2003.

[12] K.T Lau, S. Baldwin, M.O'Toole, R. Shepherd, W. Yerazunis, S. Izuo, S. Ueyama, D. Diamond, submitted for publication, *Analyst,* ref: B412706D.

3. DEVELOPMENT OF A LED BASED PHOTOMETER

3.1. Summary

This chapter presents the development of a photometer used for transmittance-based measurements. The photometer is based on two LEDs; one functions as a light source and the other as a light detector, with the light emitting LED positioned directly opposite the light sensing LED. The basis of this configuration is similar to that of a conventional UV-Vis spectrometer where the light passes from the emitter through the sample to the detector. Some basic evaluations of the LED components used in the construction of the photometer are presented along with the use of the photometer for the colorimetric analysis of iron (II).

3.2. Effect of LED Separation on Discharge Time

The aim of this experiment was to evaluate the detector response to a variation in the light intensity of the emitting LED as a function of the distance between the emitter and the detector.

Two LEDs (LTL-2V3SRKW, LiteOn, USA, dominant wavelength 630 nm, luminous intensity 3200 millicandellas (mcd)) were securely placed at either end of a piece of black heat shrink tubing (l=24.5 cm x d=5 mm) obtained from Radionics, Dublin, Ireland. Shortening the heat shrink tubing varied the distance between the two LEDs. The following distances were investigated, 21.8 cm, 19.5 cm, 16.9 cm, 14.9 cm, 12.7 cm, 9.7 cm, 6.9 cm, 4.4 cm, 2.4 cm and 0.9 cm. The light emitter was forward biased while the detector was reversed biased, the emitting LED was connected to a 5 V power supply and the detector LED was connected to the circuit board, as shown in chapter 2, section 2.5. The set up was clamped between two rulers in order to keep the heat shrink tubing straight. The signal at the detector LED was measured through an air gap at each separation point. A schematic of the experimental set up used is shown in Figure 3-1.

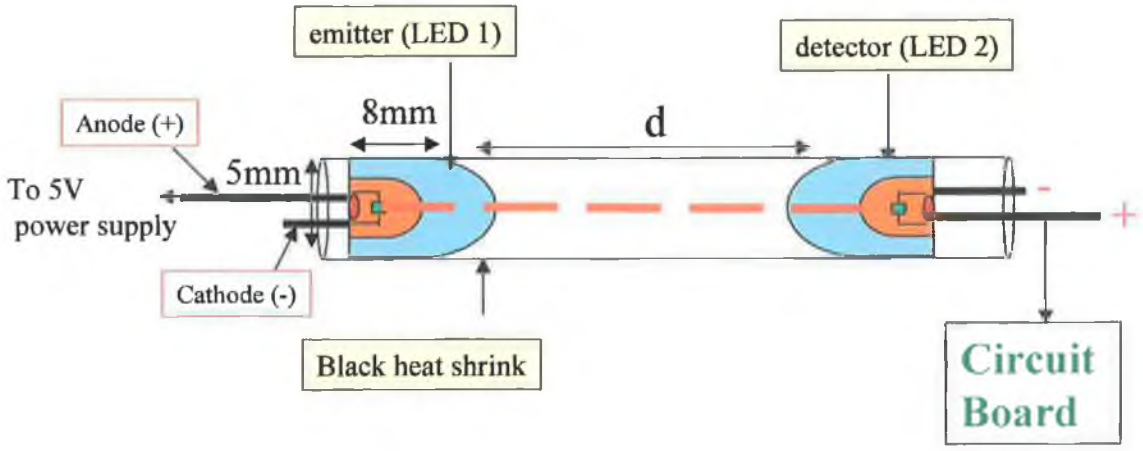

Figure 3-1: Schematic of experimental set up used to determine the effect of the separation distance of the LEDs on the response time.

The raw data was captured via the PC serial port using HyperTerminal. The microcontroller on the circuit board, which controls data capture, was set to capture 16 data points per second (see chapter 2 section 2.6). The raw data was then exported from Hyper Terminal (Windows 2000) to Microsoft Excel where it was further analysed. For further details on data transfer refer to chapter 2, section 2.6. Table 3-1 shows the responses observed at each separation distance.

Table 3-1: Table of distances used and responses observed (Detector LED discharge time in μs).

Distance	21.8	19.5	16.9	14.9	12.7	9.7	6.9	4.4	2.4	0.9
Response / μs	1479	1046	931	562	503	368	331	147	110	73

The graph obtained when the discharge time (μs) observed for each distances was plotted against the distance (cm) is shown in Figure 3-2.

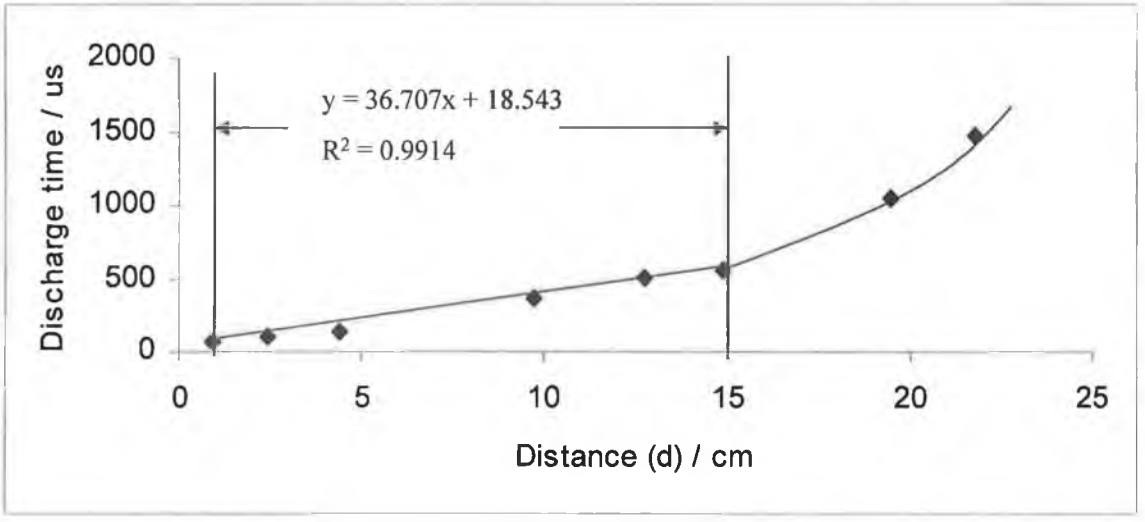

Figure 3-2: Plot of results obtained as the distance of the emitting LED (LED 1) from the detector LED (LED 2) was varied.

From Figure 3-2 it can be see that as the distance (d) between the LEDs increased, the discharge time (D_T) increased i.e. the intensity of light emitted from LED 1 reaching LED 2 decreased with an increase in separation distance. The typical resetting error associated with the LEDs in the device was approximately 100 microns (0.01 cm). At 10 cm the D_T was 385.61 μs (found by substituting 10 cm into the equation of the line for x), the D_T at 10.01 cm was then calculated in the same manner and "y" was found to be 385.98 μs. This resulted in an extremely small resetting error of 0.095 %. The slope of the linear portion of the plot was found to be 36.71 μs / cm; this implies that in air, small movements of the LEDs laterally will make very little difference to the measurement. In later experiments D_T was found to be very large (1000's of μs) this implies that the error present will be very small. Hence, it can be concluded that in air small variations in separation distance will have minimal effect on the intensity of photons incident on the detector junction.

3.3. Relationship Between Emitter Current and Light Intensity.

The following experiment evaluated the variation in the intensity of the emitter LED by controlling the current going to the emitter. A light dependant resistor

(LDR) was used as the light detector. The distance between the LED and LDR was kept constant and a variable resistor (0-10 KΩ, Peats, Dublin, Ireland) was placed in line with the light emitter. The LDR used came packaged in a sealed epoxy case with a clear lens window. The specifications for the LDR are outlined in Table 3-2.

Table 3-2: Specifications of LDR obtained from Peats, Dublin, Ireland

LDR Parameter	Value
Peak Spectral response	Typically 560 nm
On resistance	6.5 – 13.5 KΩ
Off resistance	0.5 MΩ
Maximum dissipation	250 mW at 25°C
Maximum voltage	32 V

The experiment was based on the assumption that the light intensity of the emitting LED increased as the current reaching the emitter increased and visa versa. Both the LED and LDR were placed into a piece of heat shrink tubing (16 mm in length) obtained from Radionics, Dublin, Ireland. The LDR resistance was monitored with a HP multimeter (model 34401A) and the LED was driven with a 5 V battery supply. The variable resistor was placed in line with the light emitting LED. A schematic of the experimental set up used is shown in Figure 3-3.

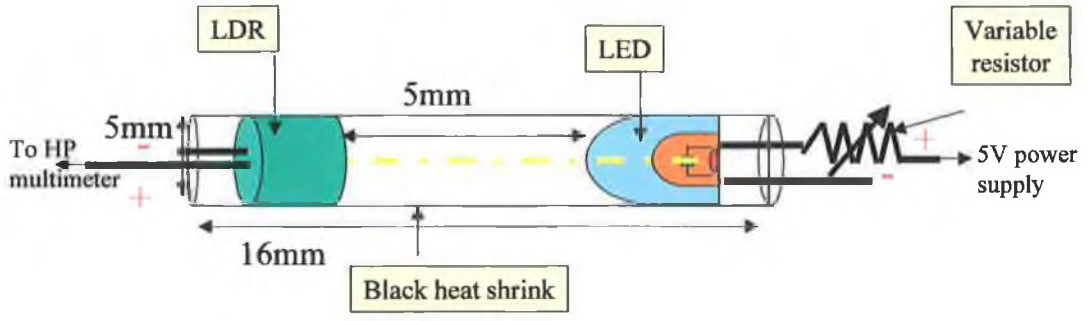

Figure 3-3: Schematic of experimental set up to determine the effect of varying light intensity.

It was assumed that as the current reaching the detector increased, the intensity of light also increased; therefore this approach (introducing a resistor) would reduce the amount of light reaching the detector without having to change the positioning of the optical components. The result observed when the LDR resistance was plotted against reciprocal of the applied resistance is shown in Figure 3-4.

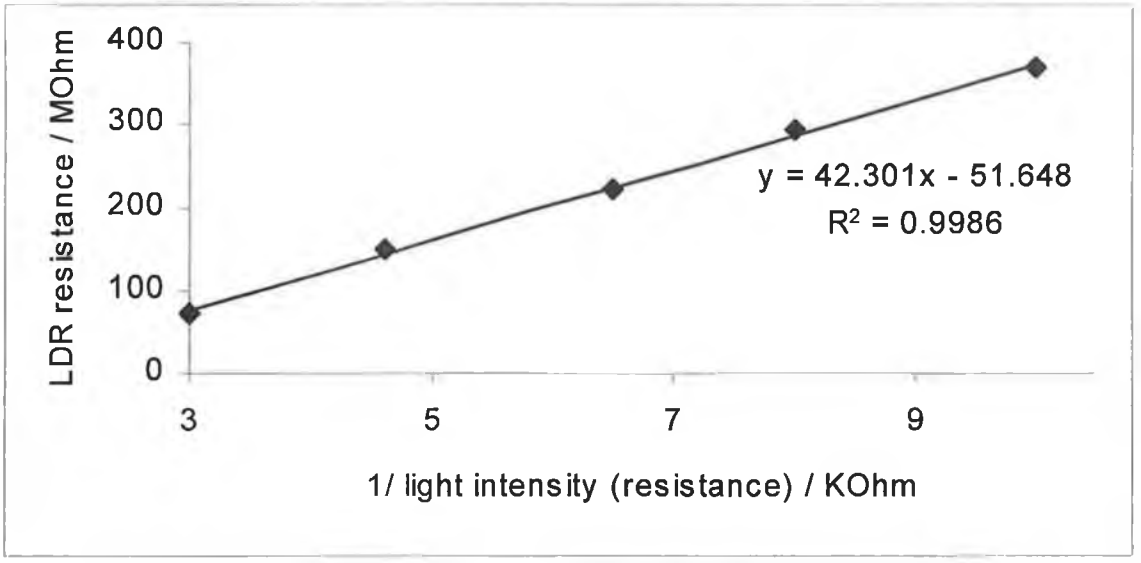

Figure 3-4: Response observed by LDR with a change in light intensity. The intensity of light was varied using a variable resistor (range 0-10 kΩ).

From Figure 3-4 it can be seen that when the current entering the emitter LED was increased, then the light intensity increased proportionally i.e. a linear relationship was observed between the LDR resistance and the reciprocal of the applied resistance in the emitter LED circuit. This indicates that for analytical measurements the emitter LED current must be kept constant. This finding highlights that the baseline of the detector can be tuned for a particular application using a simple variable resistor on the emitter LED supply, which is important for maximising the sensitivity of the detector response for a particular analyte concentration range.

3.4. Construction of LED Based Photometer

The device was made from two identical pieces of black nylon plastic (Radionics, Dublin, Ireland) (width 2 cm, height 2.8 cm, length 3.2 cm). Firstly a cavity (1.3 cm length x 0.4 cm width x 2 cm height) was milled into the two pieces of black nylon, the two sections were then joined together using black silicon glue (RS Components, Dublin, Ireland. A small hole (diameter 5 mm) was made on either side of the device for the LEDs. PMMA transparent slides (width 1.5 cm, height 2.5 cm) were fixed in front of the LEDs using Araldite glue (RS Components, Dublin, Ireland), finally, to exclude ambient light, a lid was made (2 cm x length 3.2 cm). This was constructed out of the black nylon material. Once fabricated and fully sealed this cell can hold up to 1 mL of sample. A schematic of the device is shown in Figure 3-5.

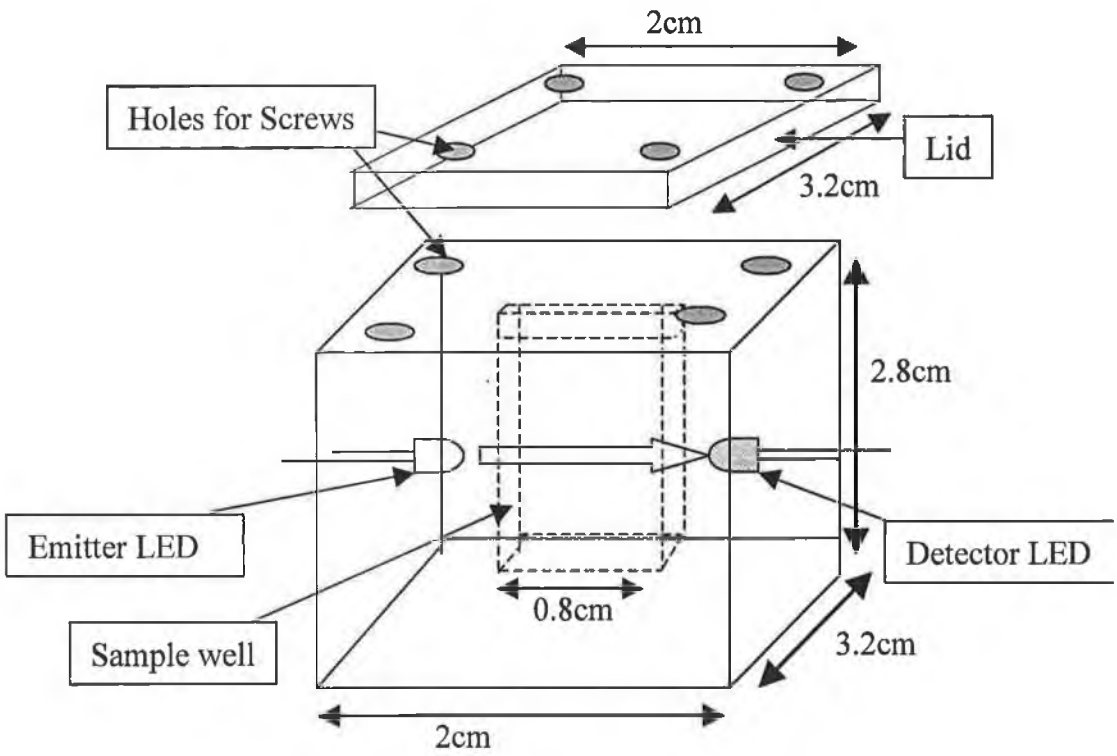

Figure 3-5: Schematic of design for transmittance based optical photometer.

The LEDs were fixed in position so that they could not move. The colour of the sample solution now functioned like a variable resistor i.e. it affected the intensity of light reaching the detector. If the absorbance spectrum of the sample coincides with the emission spectrum of the emitter LED, then in concentrated sample solutions, most of the light energy will be absorbed, and relatively little light will reach the detector. In more dilute solutions, a much greater intensity of light will reach the detector, which will be manifested in shorter discharge times.

3.5. Application

3.5.1. Background and Instrumental Methods

The application chosen to present this device as a working photometer was in the detection of iron II (Fe II). Iron is one of the earth's most plentiful resources; it makes up at least 5 % of the earths crust. It is present in almost all natural water supplies due to rainfall seeping through the soil. Iron is not considered detrimental to health; in fact it is essential for good health as it is iron that transports the oxygen in the blood, through its presence in haemoglobin.

There are two classes of contaminants (1) primary contaminants and (2) secondary contaminants. These are assigned depending on how they influence human health. Primary contaminants include pollutants such as pathogens; radioactive elements and toxic chemicals while secondary contaminants are based on taste, odour, colour, corrosivity, foaming and staining properties of water. Iron is classed as a secondary contaminant. According to the Environmental Protection Agency (EPA) the recommended limit of iron allowed in Irish water is 0.2 ppm [1]. This limit is based on the taste and appearance of the water. When the level of iron in water is greater then 0.2 ppm, the water turns a cloudy yellow / brownish colour and may have a bad taste. There are two forms of iron that can be present in water, Fe (II) and Fe (III). Fe (II) is faint yellow in colour but when allowed to settle for a long period of time will eventually oxidise to form reddish brown particles (Fe (III)) that will settle to the bottom of the container.

Fe (III) is the most common form of iron found and it also causes the most damage. Simultaneous determination of Fe (II) and Fe (II) can be achieved based on the photo reduction of the Fe (III). The amount of Fe (III) in a solution can be measured then all of the Fe (III) can be reduced to Fe (II) using a reducing agent e.g. hydroquinone and the actual concentration of Fe (II) present can be determined by subtracting the concentration of Fe (III) from the amount of Fe (II) found after the Fe (III) was reduced to Fe (II) [2].

A survey of drinking water in Ireland held in 2002 comprising of 22,891 samples i.e. 141,955 individual tests reported [3] that 5.71 % of samples exceeded the specified allowed amounts of elements allowed in drinking water. Iron frequently exceeded the required amount, along with manganese. The following is an example of a possible cause of excess iron and manganese in water and the required treatment needed to reduce these high levels found [4].

Indication: Water clear when drawn but red-brown or black particles appear upon standing.

Cause: Dissolved iron or manganese.

Treatment:

- Phosphate compounds *(*< 3 ppm iron*)*
- Water softener (<5 ppm combined concentrations of iron and manganese)
- Oxidizing filter (manganese greensand or zeolite) (<15 ppm combined concentrations of iron and manganese)
- Aeration (pressure) (<25 ppm combined concentrations of iron and manganese)
- Chemical oxidation with potassium permanganate or chlorine; followed with filtration (>10 ppm combined concentrations of iron and manganese)

There are numerous methods published for the determination of Fe (II) in water. Some of the methods include capillary electrophoresis [5,6], atomic absorption spectroscopy [7,8], electrochemical methods [9] and spectrometric methods of analysis [10]. An overview of recent methods used for the determination of Fe (II) was carried out by Achterberg *et al.* [11] and is shown in Table 3-3.

Table 3-3: Table showing methods of detection for various forms of iron present in water. [1] Graphite furnace atomic absorption spectroscopy, [2] inductively coupled plasma mass spectrometry, [3] liquid chromatography, [4] Adsorptive cathodic stripping voltammetry

Iron species determined	**Detection method**	**Reported LOD (ppm)**	**References**
Total dissolved iron	GFAAS [1]	5×10^{-11}	[12]
Total dissolved iron	ICP-MS [2]	1.5×10^{-11}	[13]
Dissolved iron (II)	LC [3] and colorimetry	1×10^{-10}	[14]
Dissolved iron (II)	Chemiluminescence	1×10^{-11}	[15, 16]
Dissolved iron (II) and (III)	Colorimetry	1×10^{-10} Fe (II) 3×10^{-10} Fe (III)	[17]
Total iron	Catalytic kinetic spectrophotometry	2.5×10^{-10}	[18]
Total dissolvable iron	Chemiluminescence	Not reported	[19]
Iron (II) and (III)	AdCSV [4]	1.2×10^{-10} Fe (II) 7.7×10^{-10} Fe (III)	[20]
Organic iron	AdCSV [4]	Not reported	[21]
Total dissolvable iron	Chemiluminescence	4×10^{-11}	[22]
Total iron	ICP-MS [2]	5×10^{-11}	[23]
Total dissolved iron	ICP-MS [2]	6×10^{-11}	[24]
Dissolved iron (III)	Chemiluminescence	2.1×10^{-11}	[25]

The majority of the methods outlined in Table 3-3 require large, expensive instrumentation, e.g. ICP-MS, GFAAS and LC to monitor the presence of iron. Due to the size of these instruments all analysis must be carried out in the laboratory. The colorimetry method of iron detection used [17] required a pre concentration step in order to remove other major ions that may be present and also to concentrate the iron content. A C-18 column was impregnated with ferrozine (a selective ligand for Fe (II)). The sample solution was passed through the C-18 column and then passed onto the detector (a spectrophotometer) where the presence of iron was detected. The advantage of using the proposed LED based photometer over the above methods listed above is that it is small in size, relatively inexpensive and it does not require a pre concentration step.

O' Connor *et al.* [26] have used ICP-MS in a study of the metal ion content in Irish canals. Part of this study included the testing for the presence of iron. It was found that the ICP-MS method of analysis was quick and reliable. This study found the iron content to be very high in the Shannon – Erne area (1.165 ppm iron), which is approximately an order of magnitude higher than the content of iron found in other areas. This high iron content, which exceeds the maximum allowed content of iron as specified by the EPA (0.2 ppm Fe), arises because a feed river to the canal passes through a mountainous area of shale, sandstone and coal that is rich in iron (the area is known locally as "The Iron Mountains"). ICP-MS was successful in the determining the presence of iron in waters but as previously mentioned the disadvantage of using this system is that when using this technique one is restricted to lab-based analysis of samples due to the weight, size and cost of the instrumentation.

3.5.2. Complexometric Detection of Fe (II)

The 1,10 phenanthroline family includes the use of dihydroxy, dimethyl, nitro and diphenyl derivatives [27], all of which have been applied for the colorimetric determination of Fe (II). 1,10 phenanthroline combines with Fe (II) to form an

orange-red iron (II) phenanthroline complex. The structure of 1,10 phenanthroline (Phen) is shown below in Figure 3-6.

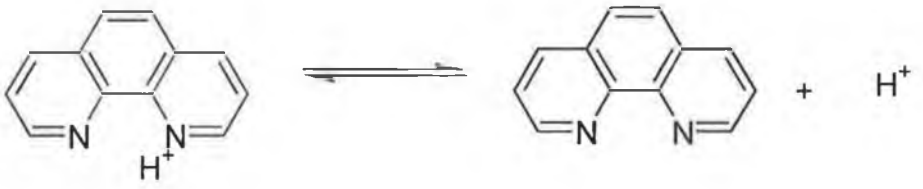

PhenH$^+$ **Phen**

Figure 3-6: Structure of 1,10 phenanthroline (Phen) and PhenH$^+$

Phenanthroline is a weak base and in acidic conditions it acts as a phenanthrolium ion (as shown in equation 3-1). Each *o*-phenanthroline molecule binds to the Fe (II) ion by the two nitrogen atoms and a proton is displaced in the process. Three Phen molecules combine with Fe (II) in a series of stepwise reactions as shown below.

$$PhenH^+ + Fe^{2+} \leftrightarrow Fe(Phen)^{2+} + H^+$$
$$PhenH^+ + Fe(Phen)^{2+} \leftrightarrow [Fe(Phen)_2]^{2+} + H^+ \quad \textbf{Equation 3-1}$$
$$PhenH^+ + [Fe(Phen)_2]^{2+} \leftrightarrow [Fe(Phen)_3]^{2+} + H^+$$

This presence of H^+ indicates that the complexation reaction is pH dependant. Normally, a pH of 3.5 – 4.0 is used; however at lower pH values, the stepwise formation of the complex is suppressed, as at higher pH values, the complexation will not occur due to the iron precipitating out of solution as $Fe(OH)_2$.

Demirhan *et al.* [27] developed a spectrometric method for the determination of Fe (II) by complexing the Fe (II) with 5-nitro-6-amino-1,10 phenanthroline. The Fe (II) was complexed with the 5-nitro-6-amino-1, 10 phenanthroline to form a coloured product, which absorbed at 520 nm. A working range of 0.1 - 0.4 ppm was achieved.

Interference studies were carried out by analysing spiked samples in a UV-Vis single beam spectrometer. Iron (II) could be determined in concentrations below 2.9 ppm Ni (II), 5.7 ppm Co (II), 4.4 ppm Cu (II), 3.10 ppm Zn (II), 4.50 ppm Mn (II), 0.4 ppm Al (II), and 2.43 ppm Mg (II). Adjusting the pH within a narrow range minimized the interferent's effects.

Flow injection analysis is also a commonly used technique for the detection of iron. The concentration of Fe (II) present in waters is commonly calculated by a difference method after the reduction of Fe (III) to Fe (II) [28, 29]. We chose to use 1,10 phenanthroline as the complexing agent for the detection of Fe (II). As previously discussed there are numerous forms of the 1,10 phenanthroline family which can be used in the detection of Fe (II) but 1,10 phenanthroline was chosen as it is readily available and has proven to be capable of detecting sub ppm levels of iron (II) [30,31]. This reagent is also appealing as it forms a strong coloured complex in the presence of iron within the visible region of the electromagnetic spectrum and should be easily detected the newly developed photometer provided the appropriate emitting LED is used.

3.6. Experimental Reagents

All of the chemicals and reagents used were of analytical grade. Ferrous ammonium sulphate hexahydrate (Sigma Aldrich, Dublin, Ireland) was used as a source of Fe (II); an alternative source of iron (II) is ferrous sulphate. The binding ligand used was 1,10 phenanthroline (Sigma Aldrich). All of the solutions used were buffered to pH 4 using pH 4 buffer tablets obtained from BDH Laboratories, (Poole, England). The buffer solutions were prepared by dissolving 1 buffer tablet in 100 mL of deionised water. Stock solutions of both ferrous ammonium sulphate hexahydrate and 1,10 phenanthroline were prepared by dissolving 0.1 g and 0.3 g respectively of each chemical in 100 mL of buffer solution. Working samples were then obtained by diluting the stock solutions.

3.7. Results and Discussion

3.7.1. Choice of LEDs

In order to achieve the maximum sensitivity for the photometer, the appropriate emitting LED had to be chosen. The basic requirements for the LED are that the emission band of the LED must overlap with the absorption spectrum of the complex and the LED must provide photons with enough energy to create a photocurrent in the detector diode. Using an Ocean Optics 2000 spectrometer (Ocean Optics, UK) the emission spectra of a red LED (LTL-2V3SRKW), yellow LED (LTL – 2V3SKS), green LED (LTL – 2T3TGK6), and blue LED –(LTL – 2R3CBK5) were taken and compared to the absorption band of a 3.2 ppm Fe (II) - 1,10 phenanthroline complex (obtained using the μQuant™ platewell) (see Figure 3-7). All LEDs were obtained from LiteOn, USA. The LED with the emission band most similar to the absorption band of the complex was chosen as the optimum LED.

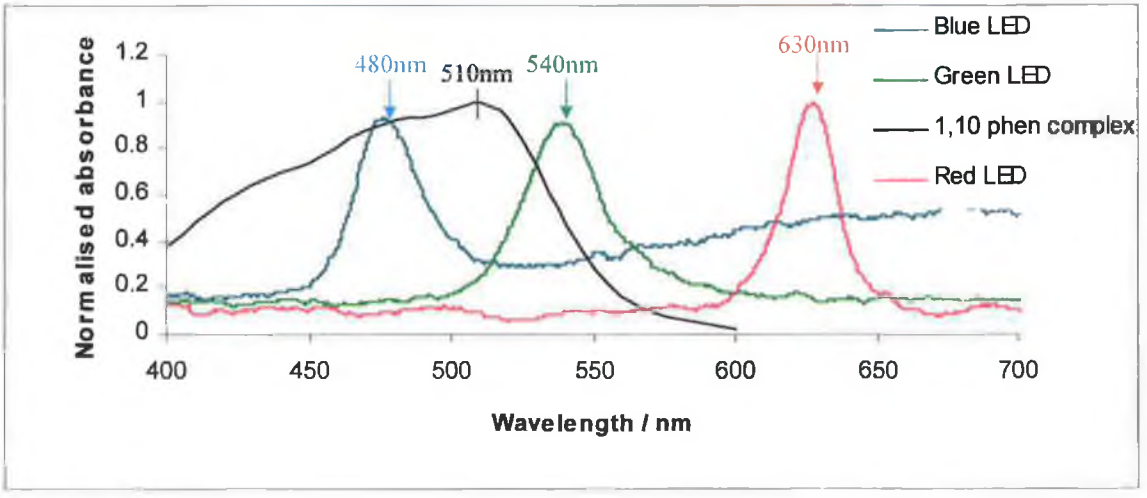

Figure 3-7: Emission spectra of red LED – LTL-2V3SRKW, green LED – LTL – 2T3TGK6, blue LED – LTL – 2R3CBK5 and absorption spectrum of 3.2 ppm Fe (II) – 1,10 phenanthroline.

The complex was found to absorb strongly in the region of 450 – 520 nm. The blue LED (LTL – 2R3CBK5) had a dominant wavelength of 480 nm therefore it was chosen as the optimum emitter LED to use for the photometer.

A study was carried out to determine the effect of the LED λ_{max} on the sensitivity of LEDs as light sensors [32]. This was done using a constant emitter LED (emission λ_{max} = 660 nm) as an energy source, and series of neutral density filters to vary light output intensity (relative intensities of 1, 2.8 and 8.3). The results observed are shown in Figure 3-8.

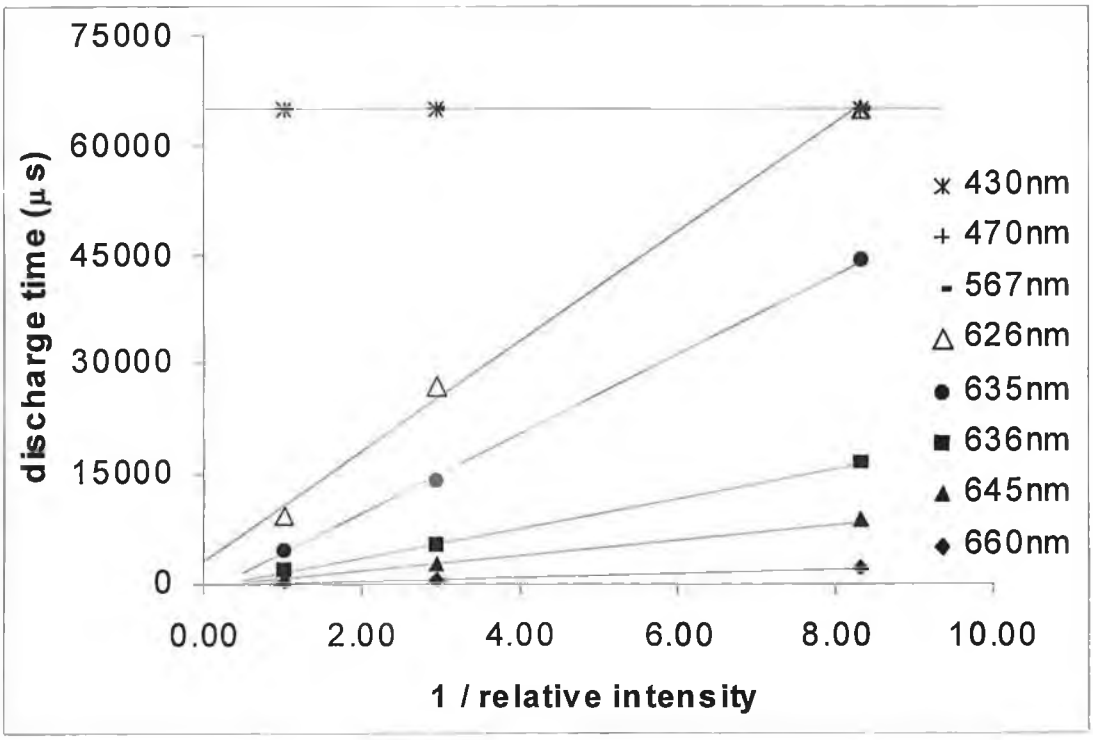

Figure 3-8: Detection characteristics of LEDs with varying λ_{max} (see list on right) configured as light sensors. The source used was an LED with emission λ_{max} at 660 nm.

The results showed that the LEDs have a linear response to the inverse of incident light intensity. The discharge time is fastest for the 660 nm LED sensor, and the discharge time increased with decreasing λ_{max}. The 567, 470 and 430 nm LEDs

did not produce a photocurrent large enough to be detected by the timer circuit (points are superimposed on the maximum 65536 μs line). The plot indicates that the flux of photons with sufficient energy to generate electron-hole pairs in the detector LED junction decreased sharply as the λ_{max} of the detector was lowered relative to the fixed λ_{max} of the emitter LED. As wavelength is reciprocal to frequency (and therefore energy), this highlights that the work function of the junction is being raised as λ_{max} decreases, and photons need more energy in order to generate a photocurrent. LEDs have a bell shaped distribution of emission wavelength around the λ_{max}, and a similar curve will describe the work function distribution when in detector mode. The efficiency of photocurrent generation depends on what fraction of the emission LED photons have energy greater than or equal to the work function of sites in the receiving junction.

In conclusion this work demonstrates that in order to generate a photocurrent in the detector LED the λ_{max} of the emitter must be $\leq \lambda_{max}$ of the detector.

3.7.2. Limit of Detection

The detection limit of the device is the minimum analyte concentration that can be observed or measured by the device. The equation used to calculate this limit of detection (LOD) is shown in equation 3-2.

$$D = 3\sigma_{blank} + mean_{(blank)} \qquad \textbf{Equation 3-1}$$

D = mean response of blank + 3x standard deviation of blank (where the blank solution is a solution containing no iron.
σ_{blank}= standard deviation of blank solution.

D is placed into the equation of the line (y =mx + c) and x is determined. This is equivalent to the LOD detectable using the photometer.

3.7.3. Background Studies

The aim of this study was to determine if the change in the concentration of iron alone in solution would result in a change in the discharge time observed by the photometer. Figure 3-9 shows the plot observed when a 10ppm Fe (II) solution, a 750 ppm 1,10 phenanthroline and a Fe (II) – 1,10phenanthroline solution were analysed using a UV-Vis spectrometer. A scan was performed from 250 – 600 nm or 700 nm (in the case of the complex).

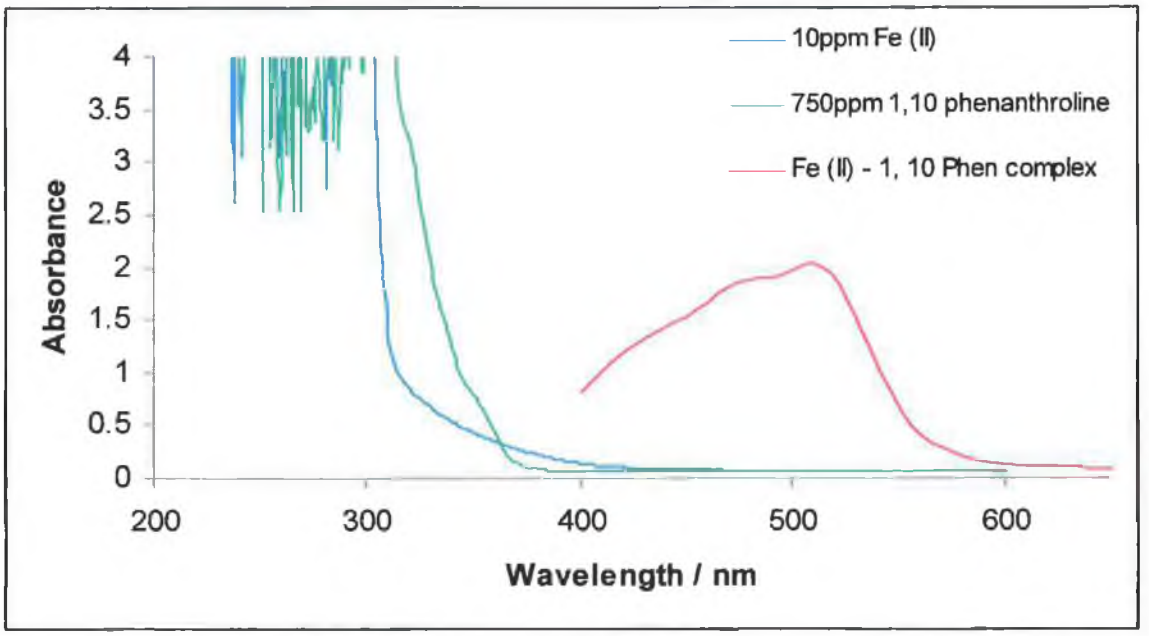

Figure 3-9: Plot showing spectra of the Fe (II) – 1,10 phenanthroline complex 10 ppm Fe (II) and 750 ppm 1,10 phenanthroline. All data scanned from 250 nm to 600 nm or 700 nm (in the case of the complex).

From Figure 3-9 it can be seen that there is a large shift in wavelength (from the ultraviolet region into the visible region) due to the complexation of the Fe (II) to the 1,10 phenanthroline. The reason for this large shift in the wavelength is due to the presence of conjugation within the molecule. For a more detailed discussion on conjugated compounds and their relative wavelengths see chapter 1 section 1.4.2.

Figure 3-10 shows the plot observed when the concentration of Fe (II) in a pH 4-buffered solution was varied from 1 - 36 ppm Fe (II) with no complexing reagent.

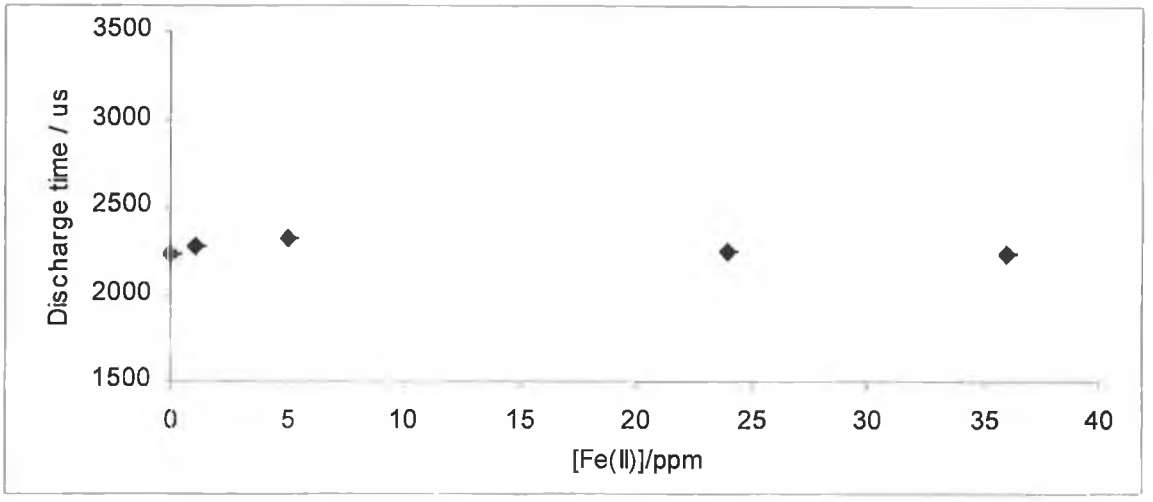

Figure 3-10: Plot of response observed with a change in concentration of Fe (II) with no complexing reagent, n=3. Points as mean of n = 3 measurements, error bars = standard deviation.

The plot observed shows that there was no change in response observed by the photometer with a change in the concentration of Fe (II). This proved that an increase in the presence of iron in solution does not change the discharge time observed by the photometer. Also the average D_T observed was approximately 2250 μS, which implies that the light intensity is always large, i.e. there is a large photocurrent reaching the detector LED. The reason for this is clearly evident from Figure 3-10 above, which shows that Fe (II) does not absorb near the λ_{max} of the LED emitter (450 nm), increasing the Fe (II) concentration therefore has no effect on the light intensity incident on the detector LED.

3.7.4. Optimisation of Reagent Concentration

This experiment determined the concentration of complexing reagent (1,10 phenanthroline) needed to achieve the optimum response using the photometer.

Here the concentration of Fe (II) remained constant at 10 ppm while the concentration of 1,10 phenanthroline was varied. The absorbance of the complex, observed by the platewell reader was plotted against the concentration of 1,10 phenanthroline present in the complex and this plot is shown in Figure 3-11.

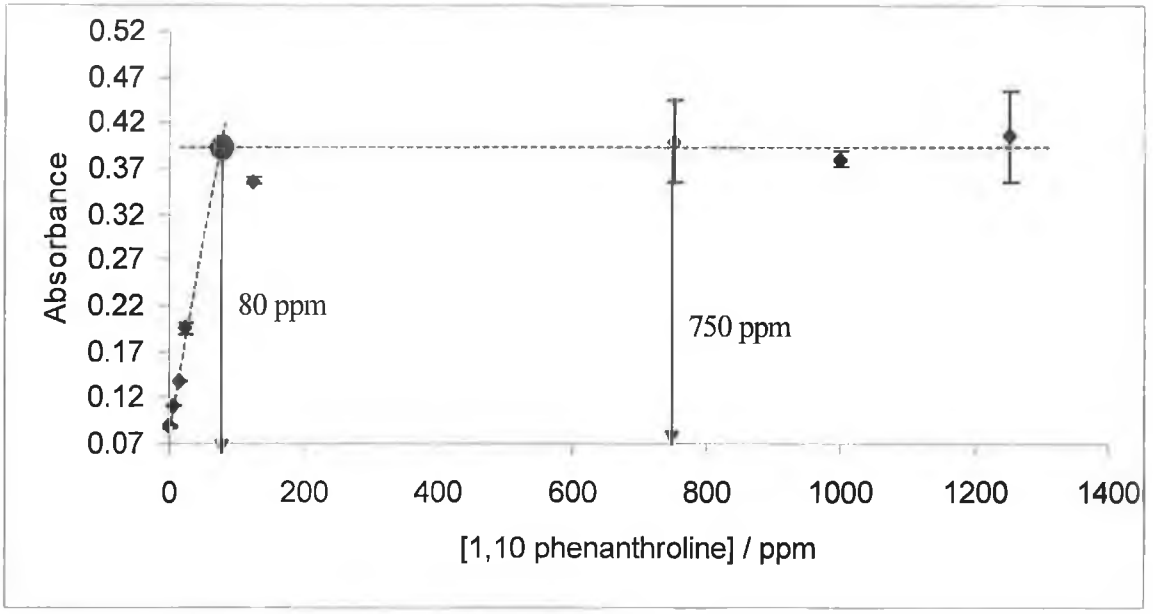

Figure 3-11: Effect of reagent concentration on the formation of Fe (II) – 1,10 phenanthroline complex. Absorbance was monitored at 510 nm. Points as mean of n = 3 measurements, error bars = standard deviation. The dotted lines act as visual aids only for the best-fit lines.

From Figure 3-11 it is clear that the minimum concentration of 1,10 phenanthroline required to give the maximum absorbance is approximately 80 ppm, 750 ppm 1,10 phenanthroline was chosen to ensure that the reagent concentration was in large excess.

3.7.5. Calibration Study

A range of 1,10 phenanthroline and Fe (II) solutions were prepared from the stock solutions (0.1 g and 0.3 g of ferrous ammonium sulphate hexahydrate and 1,10 phenanthroline respectively in 100mL of pH 4 buffer solution). These solutions were mixed in a 1:1 ratio to result in the following concentrations (Table 3-4).

Table 3-4: Table indicating Fe (II) - 1,10 phenanthroline solutions used for calibration study.

1, 10 phenanthroline concentration / ppm	**Fe (II) concentration / ppm**	
750	0.005	5
750	0.01	6
750	0.015	7.5
750	0.1	10
750	0.25	12
750	0.5	14
750	1	16
750	1.5	18
750	2	20
750	4	22

All solutions were then analysed using the photometer. 1mL of the Fe (II)-1,10 phenanthroline complex solution was placed into the sampling well. The solution was analysed for 1 min. and then removed from the well. The well was rinsed out 3 times with deionised water before the next sample was analysed. All sample analyse was carried out in triplicate.

As previously determined the resistance of the emitting LED will have an effect on the baseline and sensitivity of the system (Figure 3-4), therefore two different

resistances were studied (1 KΩ and 4.6 KΩ). This change in resistance was achieved using a variable resistor. The resistance was measured using a HP multimeter (model 34401A). The first calibration study was conducted a resistance of 1 KΩ and the results of the responses observed are shown in Figure 3-12.

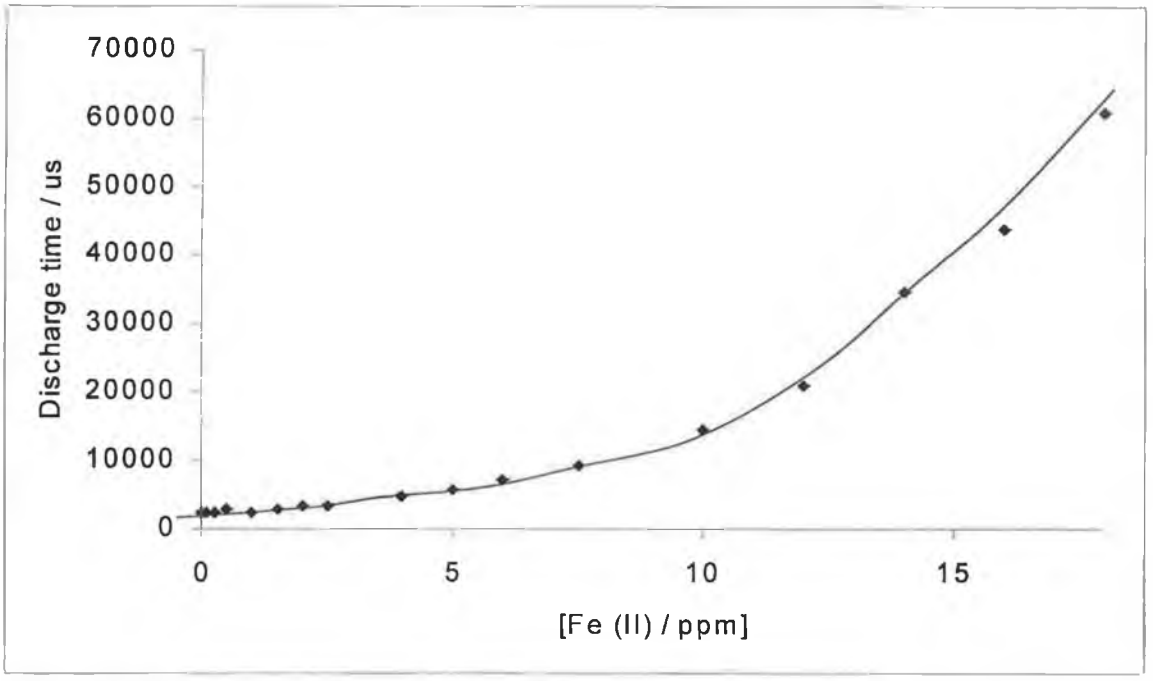

Figure 3-12: Response observed by photometer to a change in the concentration of Fe (II) while keeping 1,10 phenanthroline concentration constant at 750 ppm, at a resistance of 1 KΩ. N=3, error bars = standard deviation.

The results show a non-linear response over the concentration range investigated. However according to the proposed theory on the operation of the device (chapter 2, section 2.4) the log of the response when plotted against the concentration of Fe (II) should result in a linear plot. When the log of the response was plotted against the concentration of Fe (II) – 1,10 phenanthroline complex a linear plot was observed (Figure 3-13).

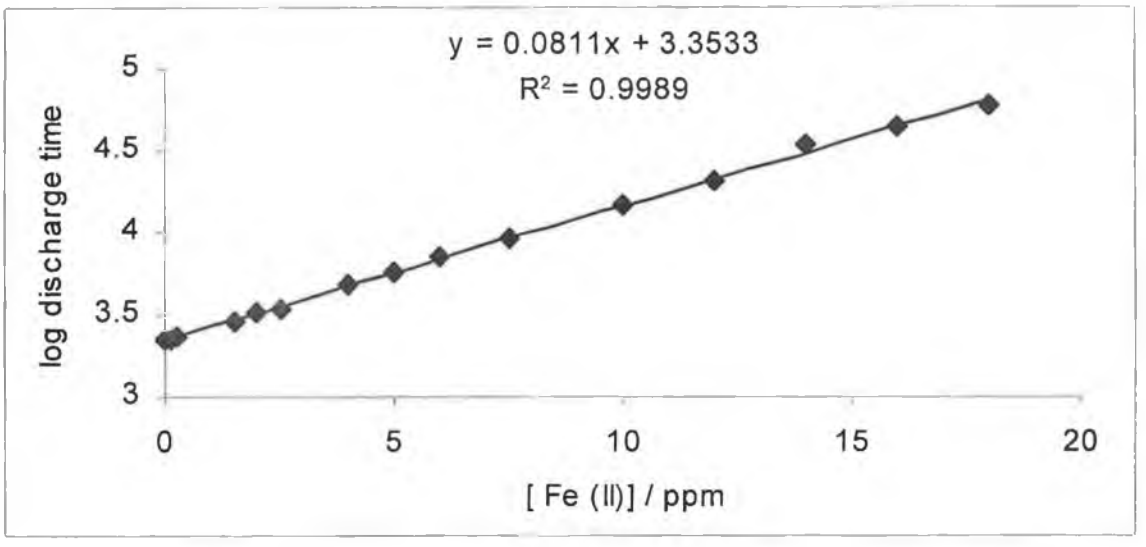

Figure 3-13: Log plot of discharge time / μS versus change in concentration of Fe (II) at 1 KΩ, N=3, error bars = standard deviation (these are small and are masked by symbols).

At a 1 KΩ resistance the working range observed was from approximately 0.1 - 18 ppm with a slope of 0.0811 ppm / au. The limit of detection found for the device was calculated as outlined in section 3.7.2 and found to be 0.04 ppm Fe (II) ± 0.001. The baseline plot observed when the blank solution (no iron) was analysed using the photometer at a 1 KΩ resistance is shown in Figure 3-14.

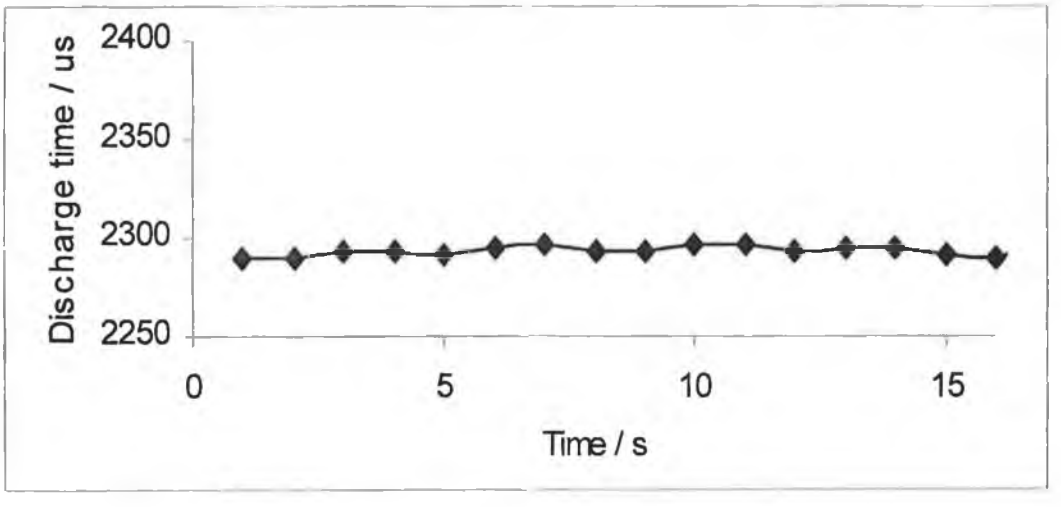

Figure 3-14: Baseline plot observed by photometer when a 1,10 phenanthroline solution containing no iron was analysed.

A weaker light intensity was obtained by changing the variable resistor from 1 KΩ to 4.6 KΩ. When the Fe (II)-1,10 phenanthroline complex concentration was plotted against the response of the photometer at a resistance of 4.6 KΩ Figure 3-15 was obtained.

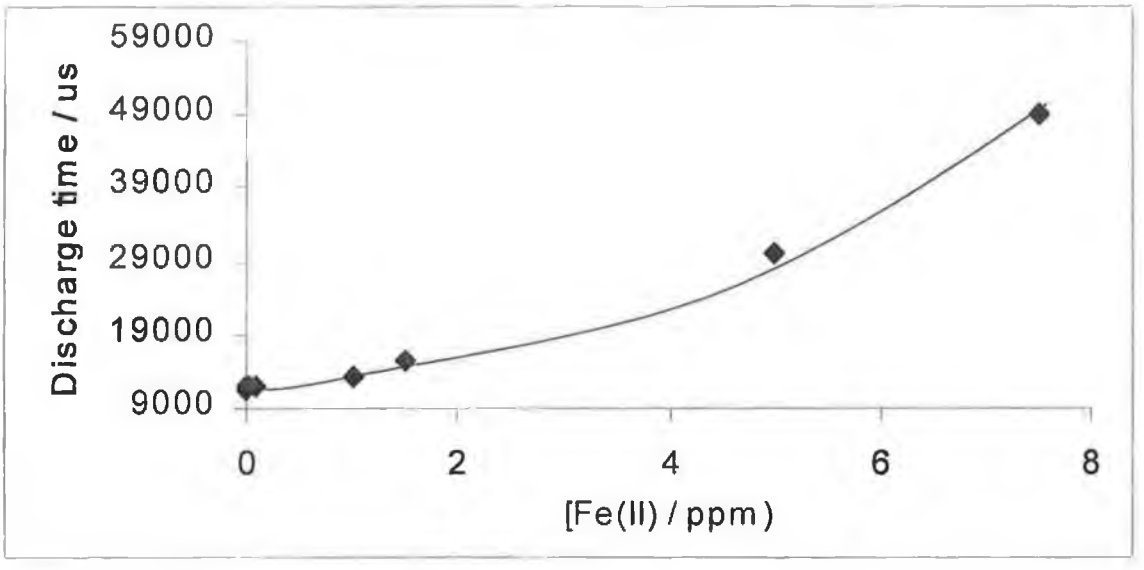

Figure 3-15: Response of optical device to a change in concentration of Fe (II) at a 4.6 KΩ resistance, N = 3, error bars = standard deviation these are small and are masked by symbols).

The plot shows that at this resistance (4.6 KΩ) a non-linear response was observed. However when the log of the response was plotted against the concentration of the Fe (II) complex a straight line was observed (Figure 3-16).

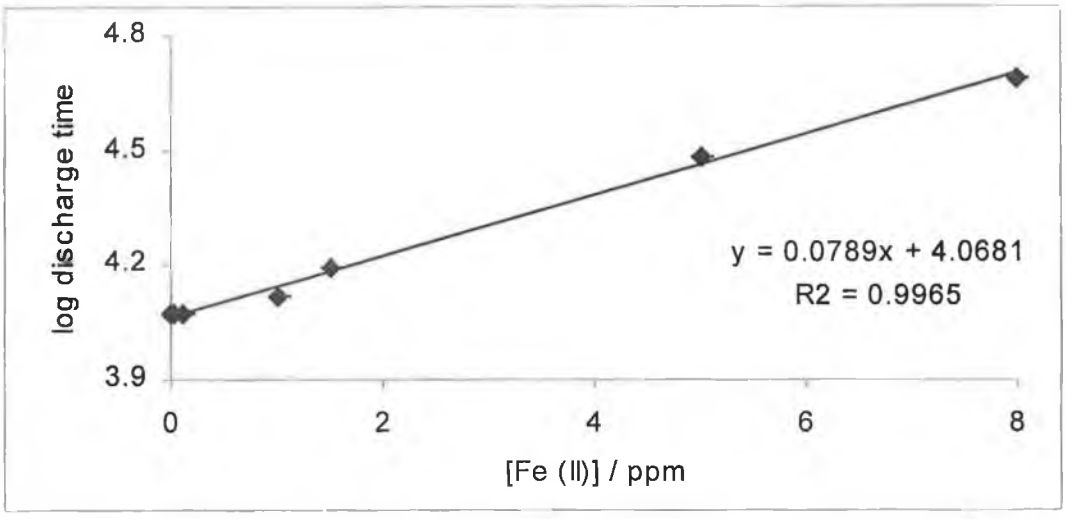

Figure 3-16: log response of the optical device to a change in concentration of Fe (II) at 4.6 KΩ, N = 3. Error bars = standard deviation

With a 4.6 KΩ resistance the working range observed was from approximately 0.1 - 8 ppm with a slope of 0.0789 ppm / au. The limit of detection was calculated to be 0.05 ppm ± 0.004 Fe (II). Figure 3-17 shows both log responses at a resistance of 1 KΩ and 4.6 KΩ when plotted together against the concentration of Fe (II) / ppm.

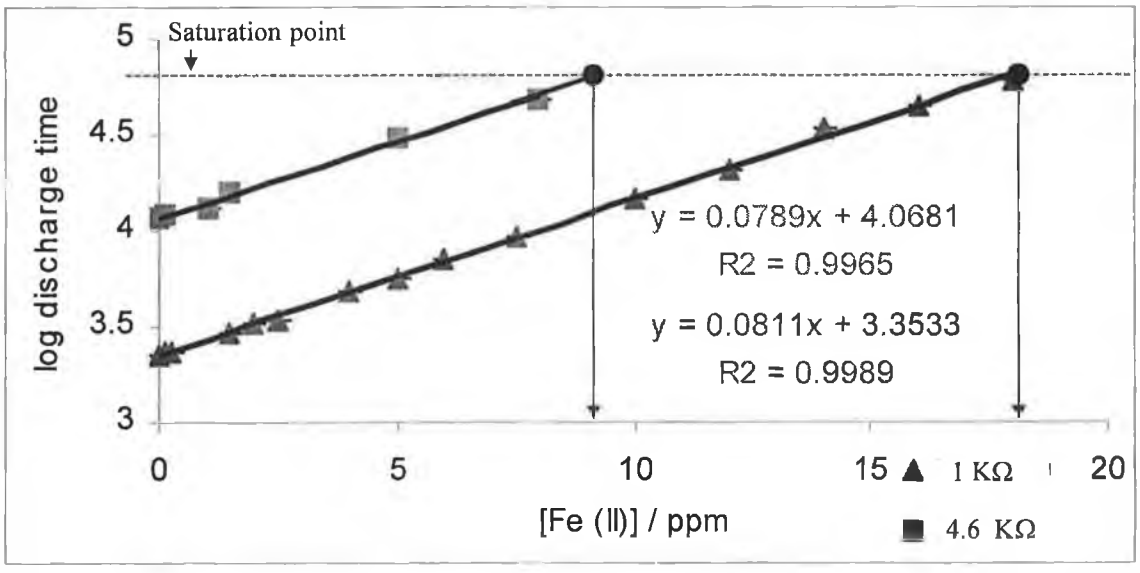

Figure 3-17: Plot of log of response against change in concentration of Fe (II) at 1KΩ and 4.6 KΩ. N = 3. Error bars = standard deviation. The dotted line show the saturation point of the photometer i.e. log (65,000).

A distinct difference between the responses is evident. Figure 3-17 indicates that changing the resistance of the system changes the baseline offset, but the slope remains the same, as does the LOD. The reason for this change in the baseline offset with a change in resistance is due to less light being emitted from the LED at a higher resistance; hence a longer discharge time is observed. The parameter most drastically affected is the linear range. At a 4.6 KΩ resistance a working range of 0.1 - 8 ppm is observed while at a 1 KΩ resistance the working range is 0.1 - 18 ppm. Therefore it can be concluded that a 1 KΩ resistor is the preferred resistance to use as it provides a broader working range then that obtainable using a 4.6 KΩ resistor but has similar LOD and sensitivity.

However, at both resistances (1 KΩ and 4.6 KΩ) a very low limit of detection (approximately 0.05 ppm Fe (II)) was found, which makes either system suitable for the use in the detection of Fe (II) as the maximum limit allowed in drinking water according to the EPA [1] is 0.2 ppm Fe (II). A table highlighting the slope, linear range and limit of detection obtained at both resistances (1 KΩ and 4.6 KΩ) is shown below (Table 3-5). The upper limit of detection found for each set up was determined by extrapolating the linear lines to the saturation point (4.821) and then substituting this value into each equation of the line.

Table 3-5: Table of comparison of results obtained from the optical device using 1 KΩ and 4.6 KΩ resistors to regulate the emitter intensity, (data generated from Figure 3-17).

Parameter	**Emitter LED with a 1KΩ resistor**	**Emitter LED with a 4.6 KΩ resistor**
Slope (log plot)	0.0811	0.0789
Linear Range	0.1 – 18 ppm	0.1-8 ppm
Lower limit of detection / ppm	0.04 ppm ± 0.001	0.05 ppm ± 0.004
Upper limit of detection / ppm	17.99	8.66

3.7.6. Comparison Study

As a comparison study the Fe (II) – 1,10 phenanthroline samples containing 750 ppm 1,10 phenanthroline and 0.05, 0.1, 0.15, 0.2, 0.25, 1.5, 2.5, 7.5, 10, 12, 14 and 14.8 ppm Fe (II) were analysed using a μQuant™ platewell reader (Biotech Instruments, USA). 200 μL of each solution was placed into a well in a 96 well plate. The samples were then scanned from 400 – 700 nm and a spectrum for each Fe (II)-1,10 phenanthroline complex obtained. The data from the platewell reader was saved in the form of a comma delimited text file. This data was then opened using Microsoft Excel and the absorbance of the complex was plotted against either the concentration of the complex (ppm) (calibration plots) or the wavelength (nm) (visible absorbance spectra). The results obtained are shown in Figure 3-18.

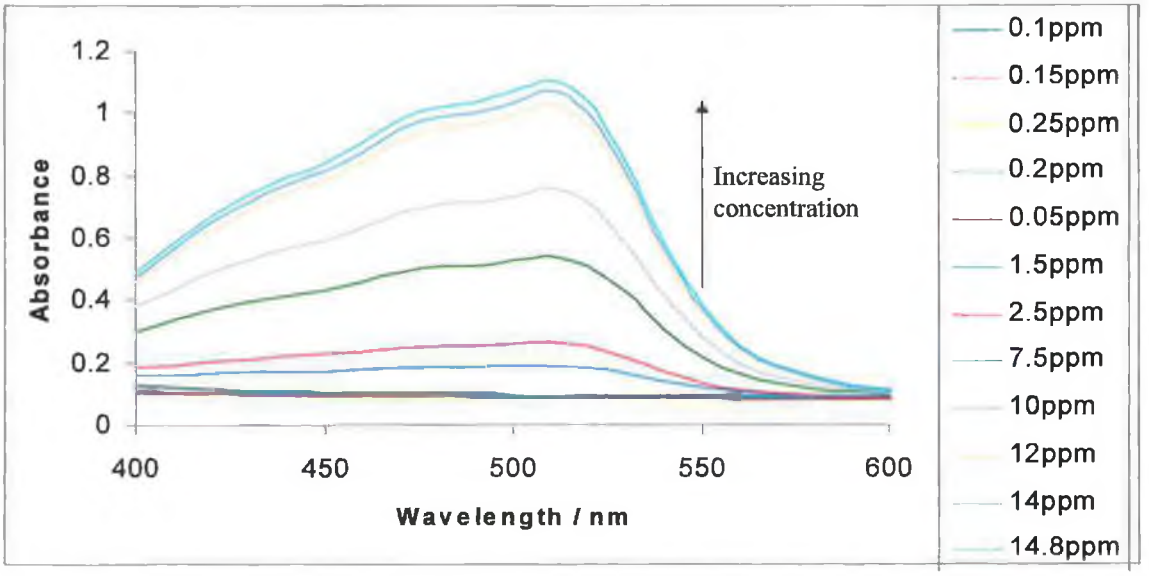

Figure 3-18: Change in concentration of Fe (II) while keeping the 1,10 phenanthroline concentration constant at 750 ppm. Results obtained using platewell reader.

The λ_{max} of the solutions were found to be at a wavelength of 510 nm. The responses obtained with a change in concentration of Fe (II) at 510 nm were

plotted against the concentration of Fe (II) / ppm and the plot observed is shown in Figure 3-19.

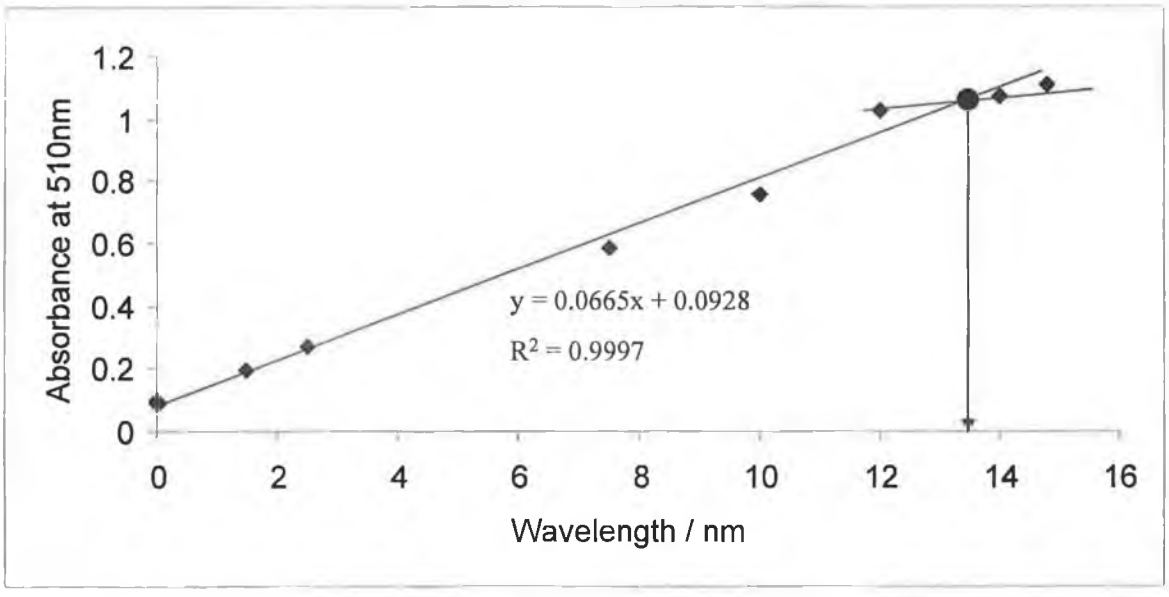

Figure 3-19: Absorbance versus concentration of Fe (II) / ppm at 510 nm

From Figure 3-19 it can be concluded that dynamic range obtainable when using the platewell reader was from approximately 1 - 12 ppm with a lower limit of detection (calculated using equation 4-3) of 0.1 ppm (as the average absorbance found for 0ppm was 0.094 ± 0.001). The upper limit of detection was calculated to be 13.64 ppm; this was obtained by substituting the value at which the two linear lines cross (see Figure 3-19) into the equation of the line. This value is equivalent to the "y" value ion the equation of the line.

The UV-Vis system gave a broader working range than that obtainable using the photometer. The limit of detection (LOD) of Fe (II) found when using the platewell reader (0.1 ppm) was higher then that found when using the LED based photometer (LOD approximately 0.05 ppm). A comparison study of the results obtained using the platewell reader and the photometer is shown in Table 3-6.

Table 3-6: Comparison of results obtained using platewell reader and novel optical device

Parameter	Optical Device @ 1 KΩ resistance	Optical Device @ 4.6 KΩ resistance	Platewell reader
Linear Range	0.1 – 18 ppm	0.1 – 8 ppm	1 – 12 ppm
Lower Limit of detection / ppm	0.04 ppm ± 0.001	0.05 ppm ± 0.004	0.1 ppm ± 0.001
Upper Limit of detection / ppm	17.99	8.66	13.64

3.7.7. Interference Study

Interferences to the study may be due to

1. The presence of cations (other than that of Fe (II)) complexing to the 1,10 phenanthroline leading to a similar colour change.

2. The presence of molecules that absorb at the same wavelength as the Fe (II) – 1,10 phenanthroline complex.

3. Molecules that form strong complexes with Fe (II) leaving it unavailable to the 1,10 phenanthroline. Some of these molecules include siderophores and hydroxamate ions.

Hydroxamate ions are powerful metal binding agents (chelators) and some are siderophores, which are compounds produced by microorganisms for the abstraction of iron from iron-deficient environments [33]. Siderophores are common products of aerobic, anaerobic bacteria and fungi [34].

The following were the common interferents that were tested to determine if they interfered with the detection of Fe (II) using the photometer, nickel (II), cadmium

(II), zinc (II) and potassium. The concentration of iron (II) used for this study was 5 ppm and the concentrations of inferences tested were the EU Maximum Admissible Concentration (MAC) for drinking water. These interferents have been proven previously not to cause any interference in the detection of Fe (II) when they are present in concentrations up to 500 ppm [35]. A list of the EU Maximum Admissible Concentration (MAC) for drinking supplied by the Environmental protection Agency (EPA) is shown in Table 3-7 [1]. These MAC values for drinking waters have not changed since 2000 [1] – (Verbal confirmation from EPA representative given on 02/02/2005). The iron was initially mixed with the interferents prior to the addition of the 1,10 phenanthroline, as if the mixing of the iron and 1,10 phenanthroline occurred first the Fe (II) – 1,10 phenanthroline complex would form.

Table 3-7: List of EU Maximum Admissible Concentration (MAC) for drinking supplied by E.P.A [1]

Parameter	**MAC values**
Aluminium	0.2 ppm
Ammonium	0.3 ppm
Chloride	250 ppm
Conductivity	2500 $\mu S\ cm^{-1}$ at 20 ^0C
Hydrogen ion concentration	$\geq$ 6.5 and $\leq$9.5 pH
Iron	0.2 ppm
Manganese	0.05 ppm
Odour	Acceptable to consumers and no abnormal change
Oxidisability	5.0 ppm O_2
Zinc	100 ppm
Potassium	12 ppm
Nickel	100 ppm
Cadmium	0.005 ppm

3 mL of zinc (300 ppm), potassium (36 ppm), cadmium (0.015 ppm) and nickel (0.15 ppm) were all individually mixed with 3 mL of 15 ppm iron (II). Following this 3 mL of 1.6 x 10^{-2} M 1,10 phenanthroline was added, and the mixtures were analysed using the platewell reader. For this analysis 200μL of each solution was placed into a 96 well plate. The plate was then scanned from 400 nm – 700 nm and a spectrum for each Fe (II)-1,10 phenanthroline complex obtained. All experiments were carried out in triplicate.

The results found from the interference study are shown in Table 3-8. The cations analysed were reported to interfere with the analysis if the average response of the blank solution (i.e. 5 ppm Fe (II) – 1,10 phenanthroline) was changed by 5 % of its initial value (6985 μS).

Table 3-8: Table of Interferents

Element	EU MAC / ppm	Conc. of interference / ppm	% Change
Zinc	100	100	None
Potassium	12	12	None
Cadmium	0.005	0.005	None
Nickel	0.05	0.05	None

From the results in Table 3-8 it can be concluded that none of these common cations interfered with the complexation of Fe (II) with 1,10 phenanthroline at the concentrations tested.

3.8. Conclusion

It has been demonstrated that the coupling two LEDs configured in forward biased and reverse biased mode gives rise to a low cost, sensitive device that can be used for absorbance based measurements in the visible region of the electromagnetic

spectrum. This device provided sensitive absorbance measurements due to the integrating nature of the measurements, which integrates the photocurrent over the measurement cycle to obtain the discharge time. The integration of a signal tends to reduce the effect of random noise. The device was reasonably resistant to small changes in the positioning of the LED laterally. When tested out by varying the distance of two LEDs (positioned in a piece of heat shrink tubing) from one another through an air gap, the intensity of the effective photons incident on the detector junction did not change significantly. The sensitivity of the photometer can be tuned using a simple variable resistor to regulate the emitter intensity. As the LED based photometer is a generic device it may be used for any form of colorimetric analysis such as in the determination of the pH of solutions with the aid of a pH indicating dye. The application chosen to present the capabilities of the photometer was in the detection of Fe (II).

The response of the photometer at two different light intensities, to a change in the concentration of Fe (II) was studied. Placing a variable resistor in line with the LED varied the light intensity of the emitter LED. The first study was carried out at a resistance of 1 KΩ. The working range achieved at this resistance was from 0.1 - 18 ppm Fe (II). The second study used a resistance of 4.6 KΩ. Changing the resistance of the system did not alter the sensitivity (slope) or the LOD obtained however it dramatically changed the working range obtainable. With a resistance of 4.6 KΩ a working range of 0.1 – 8 ppm Fe (II) was found. This is a considerably narrower working range then that obtained sung a 1 KΩ resistance (0.1 – 18 ppm).

A comparison study was conducted using a μQuant™ platewell reader (Biotech Instruments, USA). This instrument provided a working range of 1 – 12 ppm Fe (II) with a lower limit of detection of 0.1 ppm Fe (II). The photometer has an advantage over the platewell reader in that it is portable and relatively less expensive.

An interference study was carried out to determine if some of the cations that frequently interfere with the detection of Fe (II) using 1, 10 phenanthroline interfered when using the photometer. The interferents chosen were zinc, potassium, cadmium and nickel as these have previously been reported to interfere wit the complexation of Fe (II) to 1,10 phenanthroline [36]. The cations were reported to interfere with the complexation reaction if they altered the average response of the blank solution (i.e. 5 ppm Fe (II) – 1,10 phenanthroline) by 5 % of its initial value (6985 μs). None of the cations tested were found to interfere with the complexation reaction when added at their MAC levels.

3.9. References

[1] http://www.epa.ie/officeofenvironmentalenforcement/public authorityenforcement/drinkingwater
[Last accessed 28/02/2005]

[2] R.M. Liu, D.J. Liu, A.L. Sun, *Analyst*, 1992, **117**, 1767.

[3] M. Mc Garrigle, The Irish scientist year book, Swan Song and Ulster Genius, Ireland, 2002, 58.

[4] Adapted from "Iron and Manganese in Household Water," Water Treatment Notes. Fact Sheet 6, Cornell Cooperative Extension. (1989).

[5] S. Pozdniakova, A. Padarauskas, G. Schwedt, *Anal. Chim. Acta*, 1997, **35**, 41.

[6] S. Schaffer, P. Gareil, D. Dezael, *J. Chrom. A.*, 1996, **740**, 151.

[7] J. A. Sweileh, *Microchemical J.*, 2000, **65**, 87.

[8] E. Rubi, M. S. Jimenez, F. Bauza de Mirabo, R. Forteza, V. Cerda, *Talanta,* 1992, **44**, 553.

[9] B. Haghighi, A. Safavi, *Anal. Chim Acta,* 1997, **43,** 354.

[10] A.C. Lopes de Conceicas, M.T. Tena, M.M. Correia dos Santos, M.L. Simoes Goncalves, M.D. Luque de Castro, *Anal. Chim Acta*, , 1997, **191**, 343.

[11] E. P. Achterberg, Toby W. Holland, Andrew R. Bowie, R. Fauzi, C. Mantoura, P J. Worsfold, *Anal. Chim Acta*, 2001, **442**, 1.

[12] W.M. Landing, K.W. Bruland, Geochim. Cosmochim, *Anal. Chim. Acta* 1987, **29**, 51.

[13] K. Akatsuka, J.W. McLaren, J.W. Lam, S.S. Berman, *J. Anal. At. Spectrom*, 1992, **7**, 889.

[14] Z. Yi. G.S. Zhuang, P.R. brown, R.A. Duce, *Anal. Chem.*, 1992, **64**, 2826.

[15] H. Obata, H. Karantani, E. Nakayama, *Anal, Chem.*, 1993, **65**, 1524.

[16] H. Obata, H. Karantani, M. Matsui, E. Nakayama, *Mar. Chem.,* 1997, **56**, 97.

[17] S. Blain, P. Treguer, Anal. Chim. Acta, 308, (1995), 425.

[18] C.J. Measures, J. Yuan, J.A. Resing, *Mar. Chem.*, 1995, **3**, 50.

[19] R.T. Powell, D.W. King, W.M. landing, *Mar. Chem.*, 1995, **13**, 50.

[20] M. Gledhill, C.M.G. Van der Berg, *Mar. Chem.*, 1995, **1**, 51.

[21] E.L. Rue, K.W. Bruland, *Mar. Chem.*, 1995, **50**, 117.

[22] A.R. Bowie, e.P. Achterberg, R.F.C. Mantoura, P.J. worsfold, *Anal. Chim. Acta*, 1989, **361,** 189.

[23] J.F. Wu, E.A. Boyle, *Anal. Chim Acta*, 1998, **367**, 183.

[24] M.L. wells, K.W. Bruland, *Mar. Chem.*, 1998, **63**, 45.

[25] J.T.M. de Long, J. den Das, U. Bathmann, M.H.C. stoll, G. Kattner, R.F. Nolting, H.J.W. de Baar, *Anal. Chim Acta*, 1998, **337**, 113.

[26] F. O' Connor, B. Duffy, T. Champ, D. Daimond, *Intern. J. Environ. Anal. Chem.*, 2003, **83**, 713

[27] N. Demirhan, F. Tuncel Elmali, *Turk J. Chem*, 2003, 315.

[28] T.P. Lynch, N.J. Kernoghan and J.N. Wilson, *Analyst,* 1984,**109**, 298.

[29] J. Mortatti, F.J. Krug, L.C.R. passenda, E.A.G. Zagatto, S.S. Jorgensen, *Analyst*, 1982, **107**, 659.

[30] Z.O. Tesfaldet, J. F. van Staden and R. I. Stefan, *Talanta*, 2004, **64**, 1189.

[31] K. Ogura, K. Nahara and M. Ueda, *Electrochimica Acta,* 1976, **21**, 807.

[32] K.T. Lau, S. Baldwin, M. O'Toole, R. Shepherd, W. Yerazunis, S. Izuo, S. Ueyama, D. Diamond, submitted for publication, *Analyst,* ref: B412706D.

[33] http://www.irishscientist.ie/2002/contents.asp?contentxml=02p173 xml&contentxsl=is02pages.xsl
[Last accessed 28/02/2005]

[34] J.B. Neilands, *J.Biol Chem*, 1995, **45**, 26723.

[35] T.P. Lynch, N.J. Kernoghan, J.N. Wilson, *Analyst*, 1984, **109**, 845

[36] Z. Yi, G. Zhuang, P.R. Brown, R. A. Duce, Anal. Chem., 1992, **64**, 2826.

4. DEVELOPMENT OF LED-BASED REFLECTOMETER

4.1. Introduction

The aim of this work was to develop a novel, optical LED-based reflectance device (reflectometer) for the measurement of the pH of a solution. One of the LEDs used in the reflectance device was forward biased and functioned as a light emitter and the other LED was reversed biased and functioned as a light detector. Studies were carried out with this device using a pH indicating dye to monitor the pH of a solution. Studies were also conducted on a modified version of this reflectometer. The reflectometer was modified by placing a solid-state chemo-reactive sensor membrane directly in front of the LEDs. The sensor membrane changed colour proportionally with the pH of the solution and the reflectometer measured this colour change.

4.2. Laws of Reflection and Refraction

Reflection

Objects become visible due to the light they emit or, more often, due to the light they reflect. Reflected light obeys the law of reflection that states, "the angle of reflection (θ_r) equals the angle of incidence (θ_i)" (where the incident light is the light reaching the surface) [1]. A schematic of an incident and reflected ray is shown in Figure 4-1.

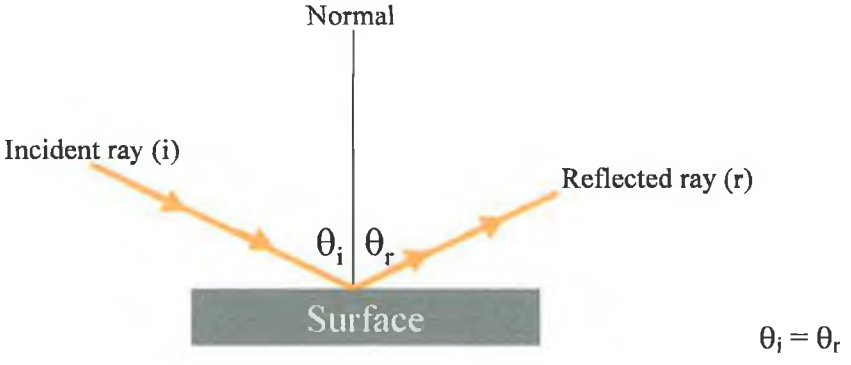

Figure 4-1: Schematic of an incident and reflected ray [1].

Refraction

The refraction of light is the bending of light as light passes from one medium to another. The degree of bending depends on the refractive index of both mediums and the angle of the incident ray and the "normal line"[2]. A schematic showing an incident light ray and refracted light ray is shown in Figure 4-2.

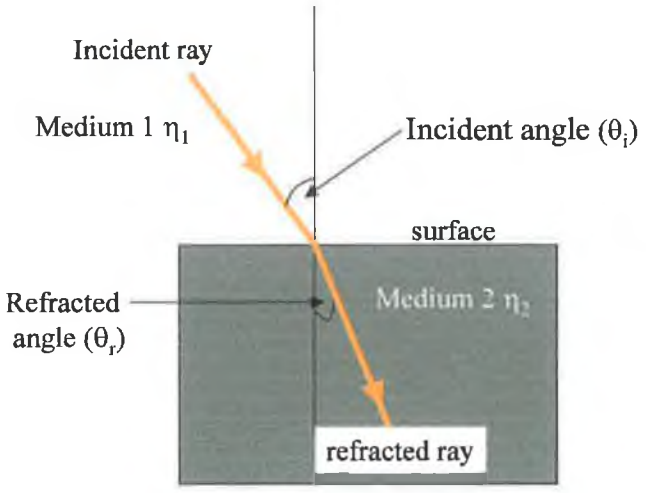

Figure 4-2: Schematic of an incident and refracted ray [2].

By definition the refractive index of a vacuum is 1. In practise, air makes little difference to the refraction of light with a refractive index of 1.0008. Table 4-1 highlights the refractive indexes of common materials [3].

Table 4-1: Table of values for common refractive indexes

Material	Air	Water	Glass, soda – lime	Diamond
Refractive Index	1.0008	1.330	1.510	2.417

In 1621, a Dutch physicist named William Snell derived the relationship between the different angles of light as it propagates through one medium to another. As light passes from one medium to another it bends according to Snell's Law that states [3],

$$\eta_1 \, x \, \sin(\vartheta_i) = \eta_2 \, x \sin(\vartheta_r)$$ **Equation 4-1**

Where η_1 = index of refraction of the incident medium and η_2 = index of refraction of the refractive medium

Total internal reflection

When the angle of incidence is equal to the critical angle then the angle of refraction is 90 degrees and when the angle of incidence is greater then the critical angle then all of the light undergoes reflection and this is known as total internal reflection Figure 4-3 shows schematics of when the angle of incidence is equal to the critical angle (1) and when the angle of incidence is greater then the critical angle (2).

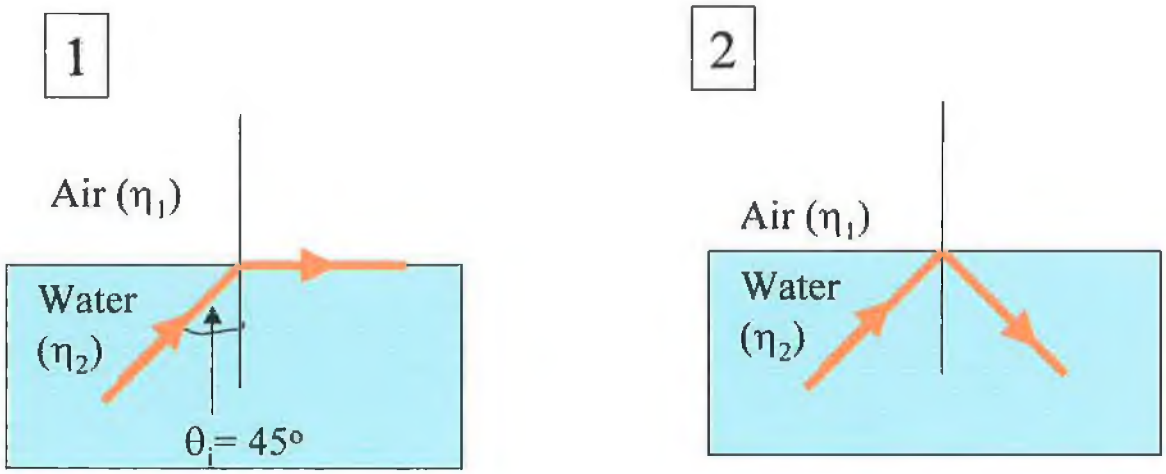

Figure 4-3: (1) Schematic of angle of incidence equal to the critical angle and (2) angle of incidence when greater than the critical angle

The refractive index for air (η_1) and water (η_2) is 1.0008 and 1.330 respectively, therefore by substituting these values into Equation 4-1 θ_r can be calculated. This value was calculated to be 32.1 degrees.

4.2.1. pH optodes

pH optodes are commonly used for the determination of the pH of a solution. They are usually made from a polymer along with a composite of dyes with pH dependant optical properties. It is essential that the dyes are successfully incorporated into the polymer. The following are the two most common methods used to incorporate the dyes into a polymer matrix.

1. Physicochemical adsorption - physical entrapment of reagent into a polymer membrane.
2. Covalent chemical binding - binding of a dye to the surface of the polymer membrane.

Throughout this work the physiochemical method of entrapment was used to incorporate the dye into the polymer membrane. A sol-gel matrix is an example of a matrix that is commonly used for physiochemical adsorption entrapment of dyes for the optical sensing of pH [4 7]. They offer a very versatile platform for the deposition of films onto various kinds of substrates such as glass, ceramics or polymers. In a sol-gel process, a silica gel is made by hydrolysis of an alkoxide precursor followed by the condensation of silanol [8, 9]. The solvent and alcohol are evaporated during the hydrolysis step and "xerogel" is formed. This is highly porous and can be cast into thin films that are optically transparent and provide a stable and inert matrix for immobilisation of molecules [10].

Nivens *et al.* [10] have developed a pH sensor using a sol-gel matrix. The sol-gel was prepared by co-polymerising polydimethylsiloxane (PDMS) and a coupling reagent aminopropyltriethoxysilane (APTES) with tetraethylorthosilicate (TEOS). APTES covalently attaches to the dye through an amino group [11 13], therefore preventing the dye from leaching. These sol-gel based sensors were reported to have a shelf life of 12 weeks, when stored dry. However in a buffer solution, they had a lifetime of 6 months. The drawback of using a sol-gel based matrix is that a lot of preparation is needed. Each step in the preparation of the sol-gel takes time

(hours) and once the gel is formed it needs to be coated onto the substrate, which then can take up to a further 24 hours to dry.

Lobnik *et al.* [14] worked on the development of an optical pH sensor. This sensor was based on the absorption of antenna generated europium (Eu^{+3}) luminescence by bromothymol blue (BTB) in a sol-gel membrane. The Eu (III) complex is shown in Figure 4-4.

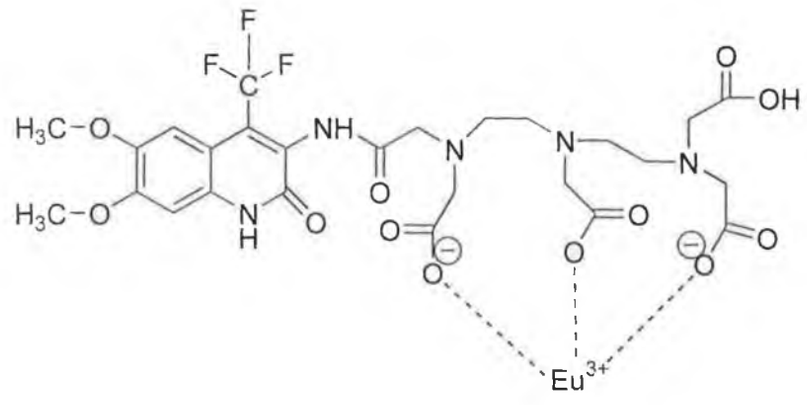

Figure 4-4: Structure of europium complex [14].

They studied the influence and pH response of BTB as a co-immobilized, non-fluorescence indicator. A europium (III) complex was synthesised, this was then entrapped into various sol-gel matrices. The optimum matrix found for pH sensing (from pH 5 – pH 9) was a tetramethoxysilane (TMOS) doped with an Eu^{+3} complex and approximately 3 equivalents of BTB. This sensor detected a pH change from 9.15 - 5.13 and back to pH 9.15 in approximately 1000 s (16.66 min.). This is an extremely long response time and would not be suitable for real time applications, where the pH of the solution is required almost instantaneously. Optical fibres may be adapted for chemical sensing (for more on fibre optic sensors see Appendix Section. Ammonia sensors, based on the use of optical fibres, have been described in the literature. These sensors use pH indicator dyes as the sensing agent [15, 16]. M.R. Shahriari *et al.* [20] describe a reversible highly sensitive, porous fibre-optic sensor for the detection of ammonia gas (Figure 4-5).

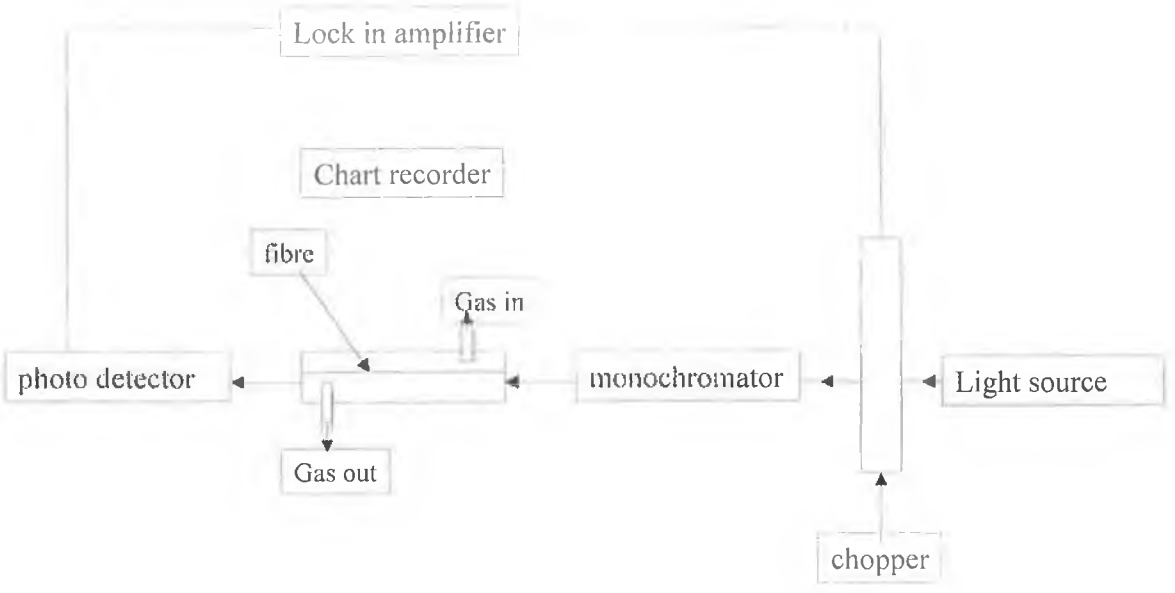

Figure 4-5: Schematic diagram of optical sensing system used by Shahriair [15].

In this approach a section of borosilicate glass fibre was sensitised by exposing it to a colorimetric chemical agent or indicator, in this case, bromocresol purple, BCP. A change in the response of the sensor was observed as a colour change of the BCP, which correlated to the concentration of ammonia gas present in the sample. The system was capable of detecting ammonia concentrations of less than 7 ppm. The two major disadvantages of this system are that it has a very slow response time (8 – 9 min. to respond to a concentration of 7 ppm ammonia gas) and the system is relatively large and bulky in size.

Another form of a physiochemical method, often used in the detection of pH, incorporates a cellulose-based derivative. Here the indicator dyes are entrapped in the polymer membrane. There are usually other components contained in the formulation along with the polymer and pH indicating dye, which are present to enhance the properties of the sensor membrane, these components are listed below.

Polymer

The polymer, most commonly used in the fabrication of optically based pH sensor membranes, is cellulose acetate or a cellulose acetate derivative. This is primarily due to the polymer's high permeability for water and ions and also due to the stability of the polymer under both basic and acidic conditions.

Indicator dye

When a pH indicating dye is placed into a solution with a pK_a higher than that of the dye itself, a proton is removed from the dye and it becomes deprotonated. This displacement of the proton causes a change in the electronic distribution within the molecule and is seen as a colour change (this is the basis of a pH indicating dye, e.g. bromocresol purple BCP). BCP has a pK_a of 6.3, [17] is yellow in its protonated form and purple in its deprotonated form. The chemical structures of bromocresol purple in both its protonated and deprotonated form are shown in Figure 4-6.

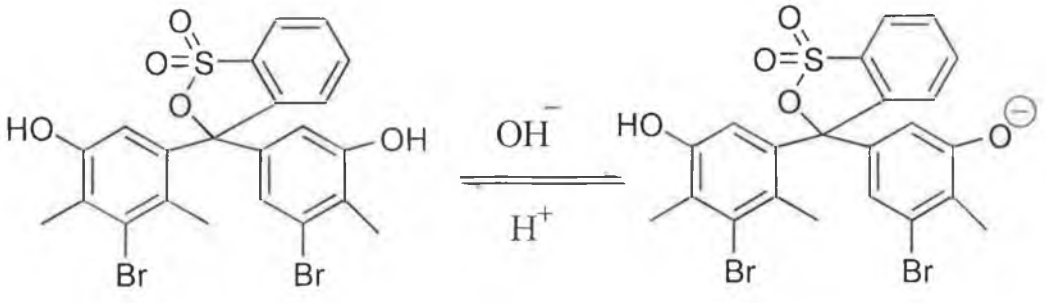

Protonated form of bromocresol purple (yellow)

deprotonated form of bromocresol purple (purple)

λ_{max} = 430 nm

λ_{max} = 590 nm

Figure 4-6: Chemical structures of the pH indicating dye bromocresol purple in both its protonated and deprotonated form.

Plasticizer

A plasticizer is used in the formulation to add flexibility and workability to the sensor membrane. A common plasticizer used is dibutyl phthalate. The chemical structure of dibutyl phthalate is shown in Figure 4-7.

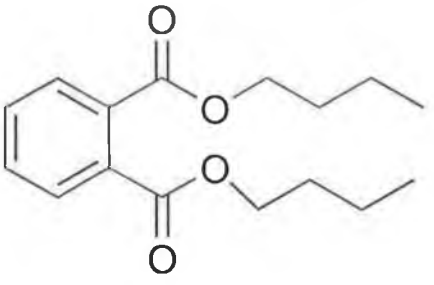

Figure 4-7: Chemical structure of dibutyl phthalate

Ethylene glycol

Ethylene glycol is a wetting agent used to enhance the hydrophilicity of the sensor. If water is retained, then the response time decreases [18]. The chemical structure of ethylene glycol is shown in Figure 4-8.

Figure 4-8: Chemical structure of ethylene glycol

Ion-pairing

Due to the hydrophilic properties of the ionic form of the indicator dye, leaching of the dye out of the polymer membrane into the solution maybe observed, which becomes a major problem. A method to overcome this problem of leaching and to improve the efficiency of the immobilisation of the dye into the polymer membrane is to introduce a lipophilic ion-pair [19]. This is successfully achieved by using an appropriate cationic or anionic salt e.g. tetraoctylammonium bromide.

Safavi *et al.* [20] developed an optical sensor that is used in the determination of uranium. The indicator dye used in this sensor was alizarin red, which is a water-soluble indicator. In its lipophilized state it formed an ion pair with tetraoctylammonium bromide, which was immobilized onto a triacetyl cellulose membrane. Figure 4-9 shows a schematic of the ion pair.

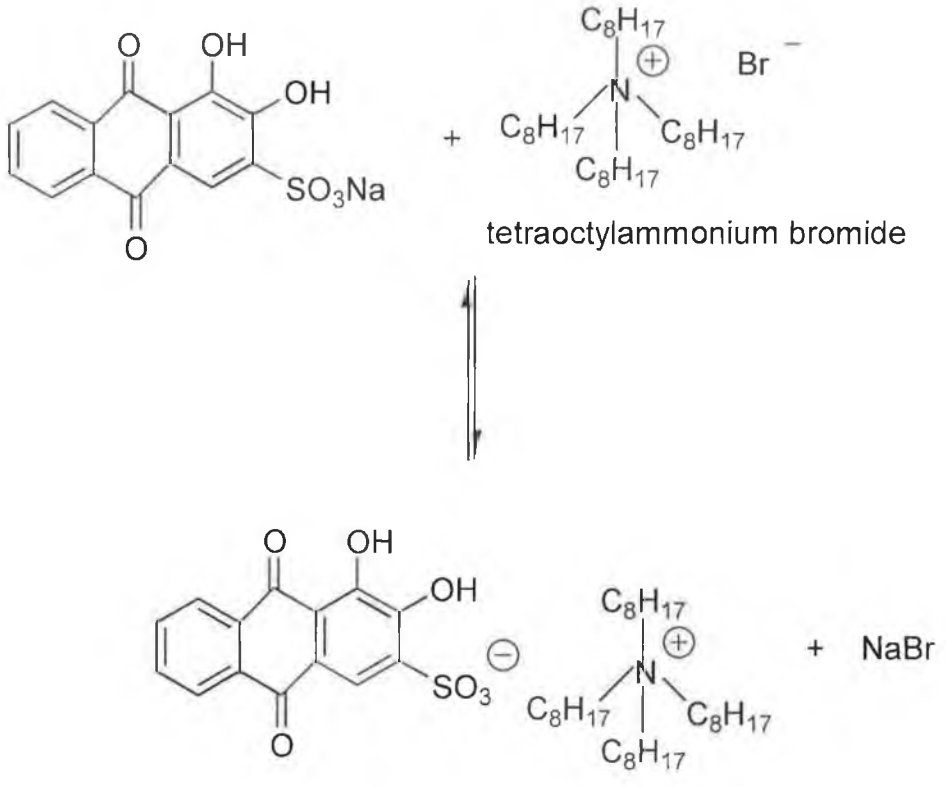

Figure 4-9: (1) Chemical structure of alizarin red and (2) alizarin red S-tetraoctylammonium ion pair

The indicator dye was successfully immobilised onto the triacetylcellulose membrane by exposing the membrane to a solution of alizarin for 7 min., next the membrane was washed with water and ethylene diamine to remove any loosely bound molecules. The sensors were stored in water to keep them hydrolysed. The linear range obtained using the optode was from 1.70×10^{-5} M – 1.87×10^{-4} M uranium. The sensor responded in 6 min. to a solution containing 1.70×10^{-5} M uranium. This is quite a long response time for such a concentration of uranium.

Wroblewski *et al.* [21] developed a cellulose acetate based fibre-optic chemical sensor (FOCS) for the determination of the pH of a solution. This sensor was based on the physical entrapment of a dye (congo red) into a polymer membrane. A range of plasticizers were tested out and the most hydrophilic plasticizer was found to be dibutyl phthalate. The response time of the pH sensor was found to be less than 1 min. A linear range from pH 2.5 to pH 5.5 was observed. This sensor had a fast response time but a narrow working range, due to the limitation of the pH indicator dye (congo red).

In our research the pH sensing membrane used in conjunction with the reflectometer incorporated the pH indicating dye (bromocresol purple, BCP) into the sensor membrane.

4.3. Experimental Reagents

All of the chemicals and reagents were of analytical grade (Sigma Aldrich, Dublin, Ireland). Bromocresol purple (BCP) was chosen as the pH indicator. A stock solution of 9.26×10^{-5} M BCP was prepared by dissolving 50 mg of BCP in 1 L in a buffered pH 7 solution. The buffered solution was made from pH 4 buffer tablets obtained from BDH Laboratories (Poole, England). Two solutions of 4 M HCl and 4 M NaOH were prepared by adding 33 mL of concentrated (12 M) HCL in 100 mL of water and 16 g of sodium hydroxide pellets in 100 mL of water, respectively, which were used to alter the pH of the solutions. Cellulose acetate, cyclohexanone, dibutylsebecate, ethylene glycol and tetraoctylammonium bromide were all used in the fabrication of the polymer-based sensor membrane. These chemicals were of analytical grade and were also obtained from Sigma Aldrich, Dublin, Ireland.

4.4. Results and Discussion

4.4.1. Choice of LEDs

In order to obtain the maximum sensitivity from the device the emitting LED used needed to have a similar emission band to the absorption band of the sample. When BCP is in it's deprotonated form, it has a λ_{max} of 590 nm and when protonated, it has a λ_{max} of 430 nm. Using the μQuant™ reader (Bio-Tek Instruments, Vermont, USA), the absorption spectrum of a 5.7 x 10^{-6} M BCP solution was taken. This was then compared to the emission spectra of a red LED (LTL-2V3SRKW), yellow LED (LTL – 2V3SKS), green LED (LTL – 2T3TGK6), and blue LED –(LTL – 2R3CBK5) taken using the OceanOptics S2000 (OceanOptics Inc., UK) (Figure 4-10). All LEDs were obtained from LiteOn, USA. The LED with an emission band that overlaps with the absorption band of the complex was chosen as the optimum LED to be used as the light emitter.

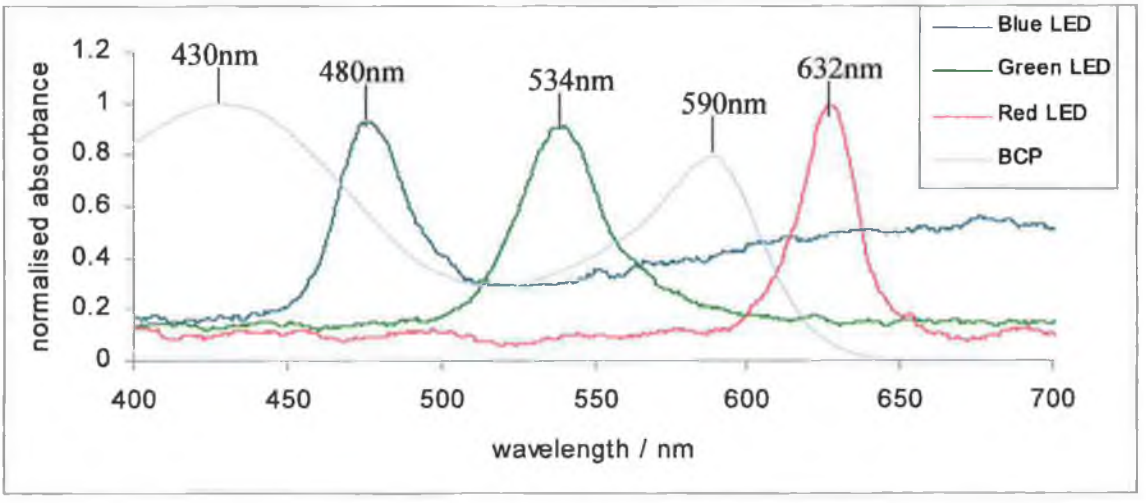

Figure 4-10: Emission spectra of LEDs obtained using OceanOptics spectrometer, red LED – LTL-2V3SRKW, green LED – LTL – 2T3TGK6, blue LED – LTL – 2R3CBK5 and the absorption spectrum of a 5.7 x 10–6 M BCP at pH 7. All of the LEDs were obtained from LiteOn, USA.

This plot shows that the deprotonated form of the dye (BCP) absorbed at a λ_{max} of 430 nm while the protonated form of the dye absorbed at a λ_{max} of 590 nm. The red LED (λ_{max} 632 nm) was chosen as the emitter LED. Although this was not the optimum LED, it was found to emit in the same region as the BCP absorbed. The red LED was an ultra bright LED (3200 mcd) with an emission band ranging from approximately 600 nm to 650 nm. The absorption band of the dye ranged from approximately 560 nm to 630 nm so it is evident that there was partial overlap between the absorption spectrum of the BCP solution and the emission spectrum of the red LED. The optimum LED (dominant λ_{max} of 590 nm) was not readily available at the time of analysis so a prototype device was constructed using the red LED. If repeated an emitter LED with a dominant wavelength of 590 nm would be used to compare the sensitivity of the device using this LED as opposed to using the red LED.

4.4.2. Fabrication of the Reflectometer

Two identical 5 mm LEDs (LTL-2V3SRKW, LiteOn, USA) were used to fabricate the reflectometer. These LEDs were filed down by hand at a 7.6° angle to one another using abrasive fine grade sand paper (Homebase, Dublin, Ireland). Next the rounded tips of the LEDs were sanded down a distance of 10 mm using abrasive fine grade sand paper (Homebase, Dublin, Ireland). The LEDs were then polished using 3 μm polishing paper (Radionics, Dublin, Ireland). Black heat shrink tubing (diameter 5 mm, Radionics, Dublin, Ireland) was placed around the diameter of the LEDs to eliminate light escaping, the LEDs were then merged using Araldite glue (Radionics, Dublin, Ireland) and left to dry for 2 hours. Once fully dried electrical wire was soldered onto the legs of the LEDs and the device was put into 8 cm plastic cylindrical tubing, leaving the plastic dome of the LEDs exposed at the end of the tubing and 3 cm of the electrical wire exposed at the top of the tubing. This wire was then connected to the circuit board that controlled the illumination and detection of the LEDs.

The sample chamber was fabricated using a polypropylene (PP) plastic tube of dimension 11 cm (width) x 3 cm (height) with orifices to allow the sample to enter and exit the chamber. A mirror (11 cm in length) was placed at the bottom of the chamber to act as a reflecting surface. The mirror was attached to the PP tubing using the Araldite glue and left to dry for 1 hour. Once fully dried the sample chamber was attached to the probe again using Araldite glue and left to dry for a further 2 hours. A schematic of the design for the reflectometer is shown in Figure 4-11.

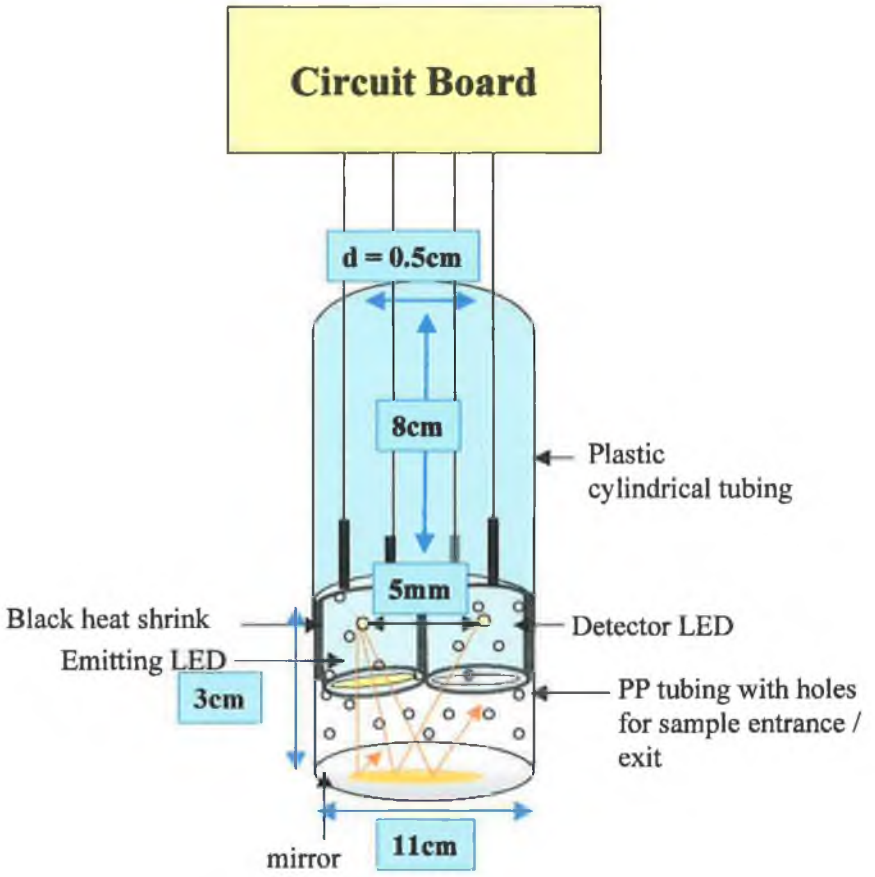

Figure 4-11: Schematic of LED based reflectometer

4.4.3. Data Capture

The microcontroller was set to collect 16 data points per second (8 ambient readings and 8 readings with LED ON). The data was then averaged to n=32

resulting in a new averaged data point being printed every 2 seconds. The data was exported to the PC via an RS232 cable (an interface connection between a PC and an electronic circuit board). After being exported from HyperTerminal, the data was saved as a text file, opened with Microsoft Excel© and comma delimited. A more detailed description of the data capture procedure is outlined in Chapter 2, Section 2.6.

4.4.4. Data normalisation

The data was normalised between 0 and 1 using the following equation,

$$\frac{R - R_{\min}}{R_{\max} - R_{\min}}$$ **Equation 4-2**

Where R is the signal response, and R_{max} and R_{min}, the maximum and minimum responses observed, respectively.

4.4.5. Data Extrapolation using Theoretical data points

Idealized data points from the theoretical equation were obtained using the Solver tool in Microsoft Excel©. The experimental data points were fitted to a best-fit logistic sigmoidal curve equation [22], the equation of which is shown in equation 4-3.

$$x(pH) = \left[\frac{a}{(1+\exp[b(pH-c)]^{r}}\right] + d$$ **Equation 4-3**

Where $x\ (pH)$ = sigmoidal response at a defined pH

a = Height of absorbance peak

b = Slope coefficient

c = pH units from baseline to point of inflection

d = Baseline offset

e= Symmetry parameter

The pK_a of the solution was obtained by plotting the first differentiation of the predicted value against the corresponding pH values. A Gaussian curve was observed and the maximum point of this curve is equal to the pK_a of the sample solution.

4.4.6. Optimisation of the device

The optimum distance of the LEDs from the reflecting surface was calculated theoretically using the Sine formula [23].

$$\frac{a}{SinA} = \frac{b}{SinB} = \frac{c}{SinC}$$ **Equation 4-4**

Where the parameters a, b, c, A, B, and C are equal to the following;

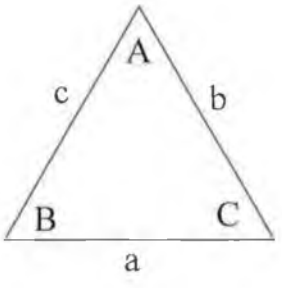

The LEDs were positioned at a 7.6° angle to one another with the dies of each LEDs (centre of LED) 5 mm apart. By inserting these values into Equation 4-4, the optimum distance of the LEDs from the mirror to obtain maximum reflection was calculated to be 1 cm. A set of images of the reflection behaviour of the emitted light at various distances from a reflecting surface (white filter paper) was recorded. The photographs were taken in a dark room at distances of 5 cm, 3 cm, 1 cm and 0.5 cm from the reflecting surface using the following set up (Figure 4-12) and can be seen in Figure 4-13.

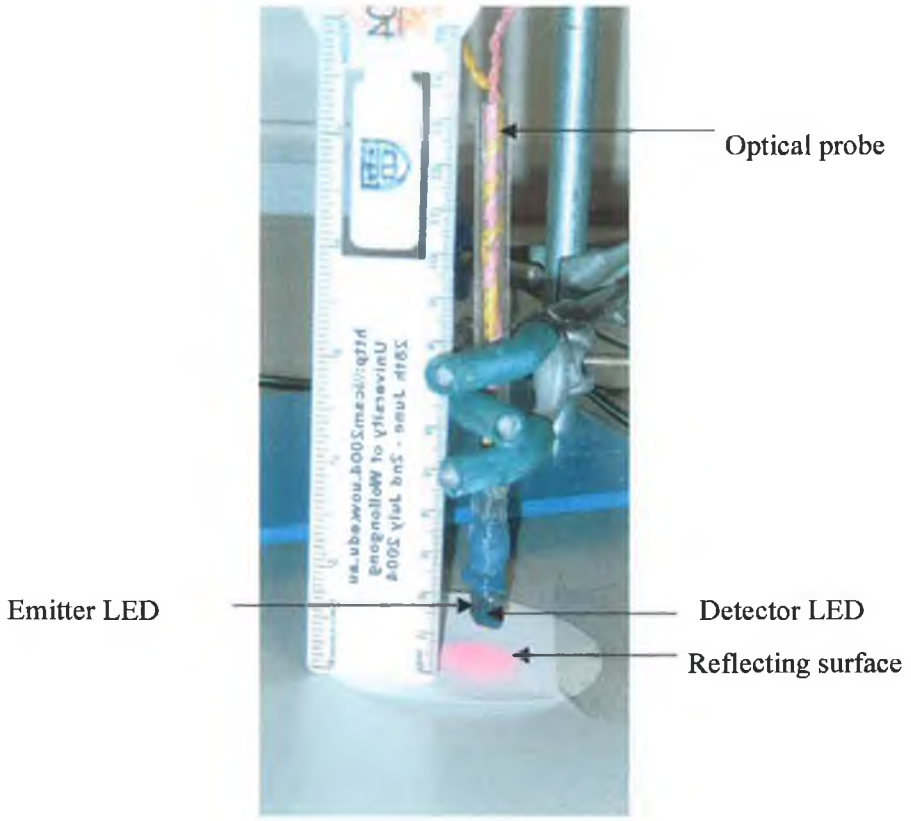

Figure 4-12: Photograph of experimental set up used to take photographs of light emitted from reflectometer when positioned at different distances above a reflecting surface.

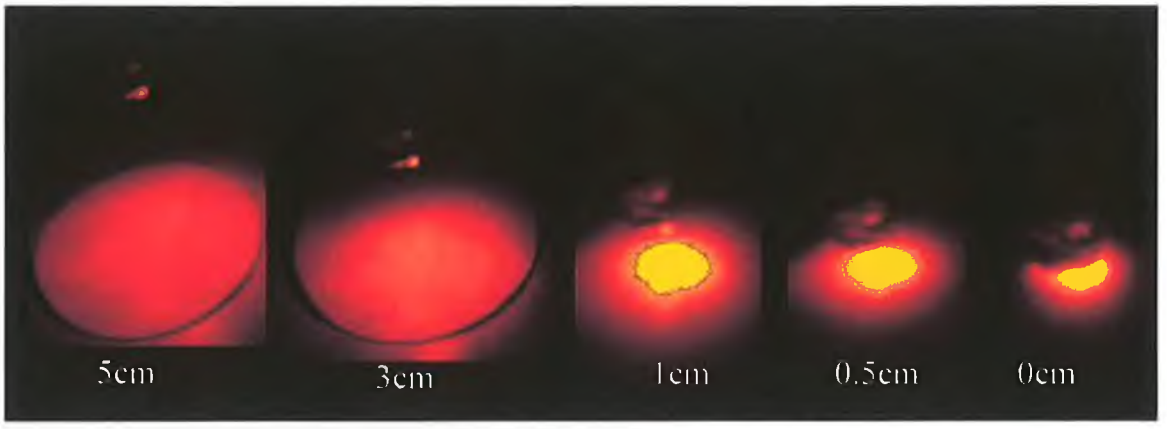

Figure 4-13: Set of photographs obtained when reflectometer was positioned 5 cm, 3 cm, 1 cm and 0.5 cm away from a reflecting surface.

From the images it can be seen that the light emitted from the reflectometer was diffusely reflected off the white surface. When the reflectometer was positioned 5 cm away from the reflecting surface, the light was not focussed on any particular

point but instead was dispersed. As the distance of the mirror from the LED decreased, the light emitted from the LED largely became more concentrated, i.e. at a fixed distance from the surface the light was focused.

4.4.7. Unmodified reflectometer

The aim of this experiment was to determine if the reflectometer could detect a change in the pH of a 9.26 x 10^{-5} M BCP solution, when the pH of the solution was changed from acidic form (approximately pH 3) to basic form (approximately pH 10) by addition of 200 μL of 4 M NaOH. The response of the reflectometer, when exposed to the 9.26 x 10^{-5} M BCP solution at pH 3 was monitored initially. Once the 4 M NAOH was added the pH of the solution was measured using a Metrohm pH probe (Metrohm, UK) and the response of the reflectance probe was monitored.

The pH of the solution was then reverted back to a pH of 3 (200 μL of 4M HCl) and this response measured. All experiments were carried out in a 250 mL beaker and covered with a black cloth to exclude any ambient light. A schematic of the experimental set up excluding the black cloth is shown in Figure 4-14.

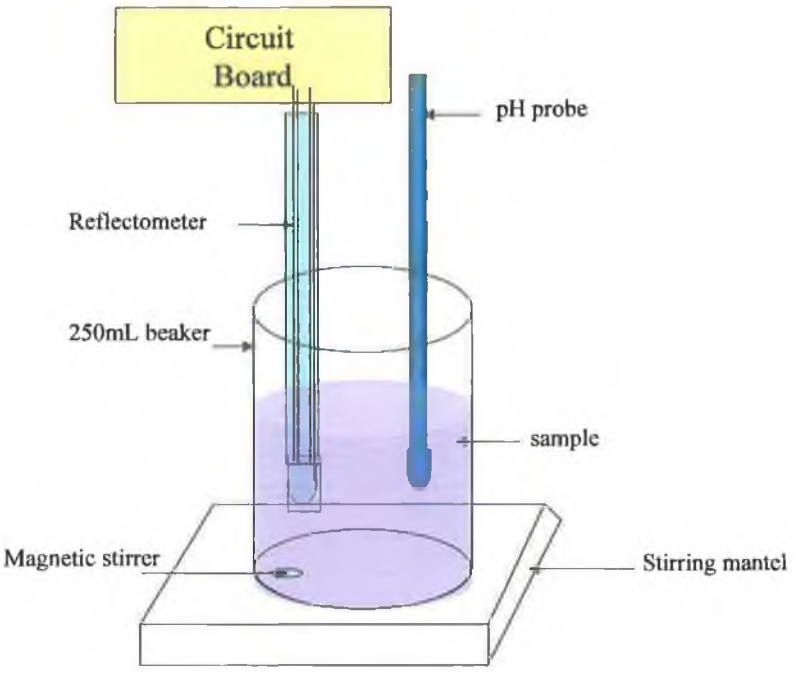

Figure 4-14: Schematic of experimental set up used for pH measurements made with the unmodified reflectometer.

The plot observed, when the reflectometer was exposed to a change in the pH of a 9.26 x 10^{-5} M BCP from pH 3 (A) to pH 10 (B) and back to pH 3 (C), is shown in Figure 4-15. The solid black line at 65,536 μs indicates the saturation point of the device.

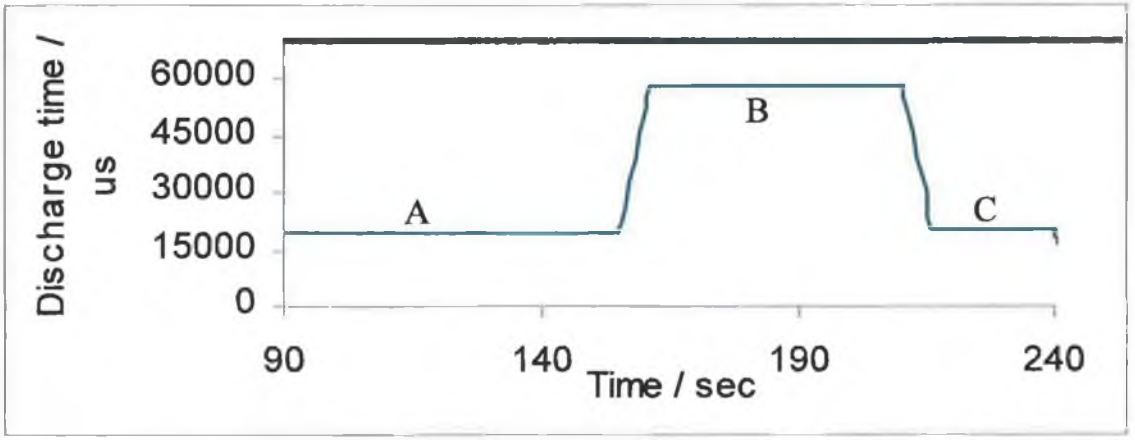

Figure 4-15: Real time trace observed using the reflectometer with a change in pH, from pH 3 (A) – 10 (B) and back to pH 3 (C) of a 9.26 x 10^{-5} M BCP solution.

Figure 4-15 shows that there was a large change in the response (approximately 40,000 μs) observed by the reflectometer in a 9.26 x 10^{-5} M BCP solution with a change in the pH of the solution (pH 3 – 10). There was no apparent drift associated with the change in the pH, as the initial average response of the reflectometer to the BCP solution at pH 3 was 19981 μs ± 8.59 μs, and after the pH was changed to pH 10 and reverted back to pH 3, the average response was 19776 μs ± 7.49 μs (n=3).

The response time of the unmodified probe to a change in the pH of a 9.26 x 10^{-5} M BCP solution from pH 3 to pH 10 was found to be approximately 1 s (Figure 4-16).

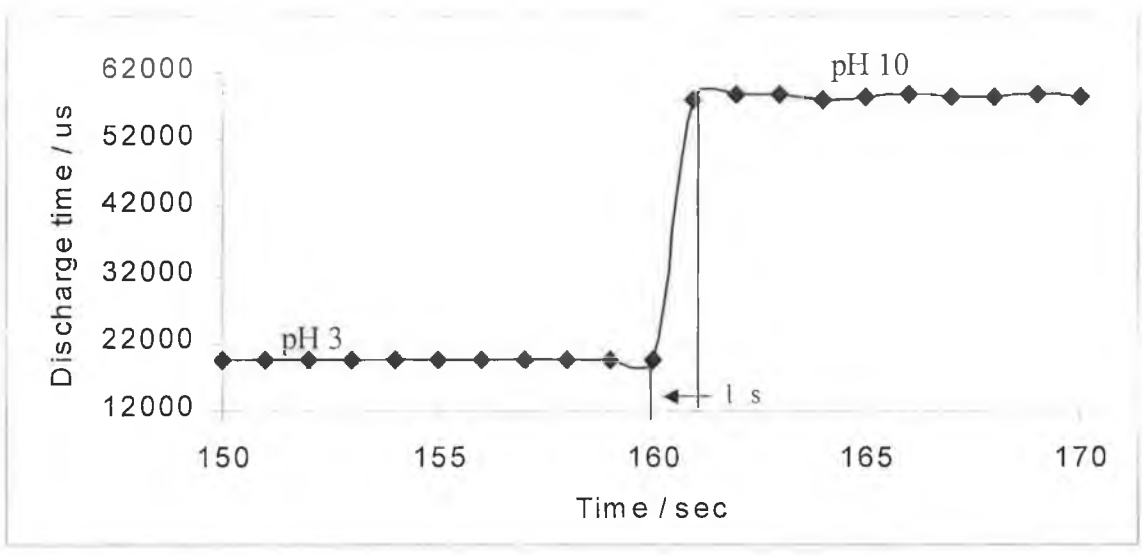

Figure 4-16: Zoomed in plot of real time trace observed using the reflectometer which enables the determination of the response time of the sensing device.

4.4.7.1. Calibration of unmodified reflectometer

A calibration study of the response of the reflectometer to a change in the pH of a 9.26 x 10^{-5} M BCP solution was carried out. The starting pH of the sample solution was pH 4.07. This pH was increased in small increments by the addition

of 4 M NaOH and the response observed at each pH monitored. The pH of the solution at the different pH values was measured using both a Metrohm pH probe and the reflectometer. All experiments were carried out in triplicate and the data obtained from the 3 individual calibrations were normalised using Equation 4-2. The R_{max} and R_{min} (maximum and minimum response, respectively) found for the reflectometer at a pH of 3.55 were 59197 μs and 20163 μs respectively. The response of the unmodified probe to a change in the pH of a 9.26 x 10^{-5} M BCP solution is shown in Figure 4-17.

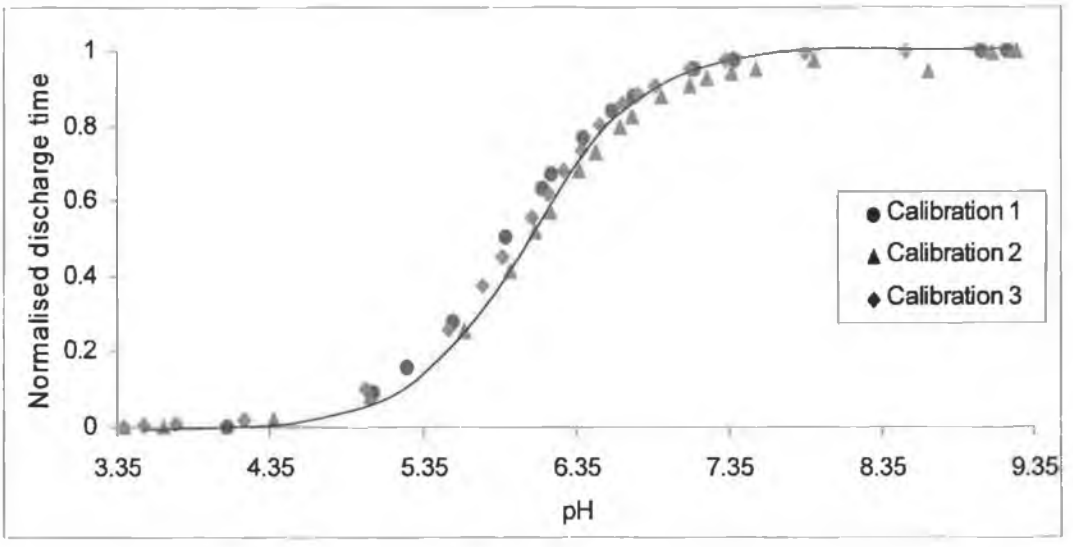

Figure 4-17: Response of the unmodified probe to a change in the pH of a 9.26 x 10^{-5} M BCP solution. The solid line acts as a visual aid.

It can be concluded that the sensor has good reproducibility over the pH range of 3.35 – 9.35, as the results suggest. A sigmoidal shaped plot was observed with an average slope of the device of 20238 and an average linear range of pH 4.43 - 7.1 (as seen in Figure 4-17). Table 4-2 outlines the working range and slope found for each of the 3 calibration runs, assuming a linear response for the region of pH 5.3 – pH 7.

Table 4-2: Table highlighting working range and slope found for each calibration curve.

RUN #	Working range / pH	Slope
Run 1	5.35 – 6.39	19448
Run 2	5.40 – 6.63	20573
Run 3	5.35 – 6.65	20693
Average	5.37 – 6.56	20238
Std. Dev.	0.134	686.78

The pK_a of the solution was calculated by using two different methods of calculation

(1) **Method 1**: This method took into consideration the experimental data values obtained using the reflectometer. Assuming that, at a normalised response of 1, the solution is 100 % in its deprotonated form, and at a normalised response of 0, the solution is 100 % in its protonated form; therefore at a normalised response of 0.5, there is a ratio of 50:50 (protonated: deprotonated form) present, i.e. the pH, at which the response equals 0.5, is the pK_a of the solution

(2) **Method 2**: This method took into consideration the predicated data points. The dy/dx (first differentiation) of the predicted values obtained using Equation 4-3 were plotted against the pH of the solution. This resulted in an extrapolated plot as 100's more points were obtained based on theoretical data.

Figure 4-18 shows the plot observed when the first differential data, the theoretical data and the actual data were plotted against the pH of the solution. The data was normalised between 0 and 1 using Equation 4-2.

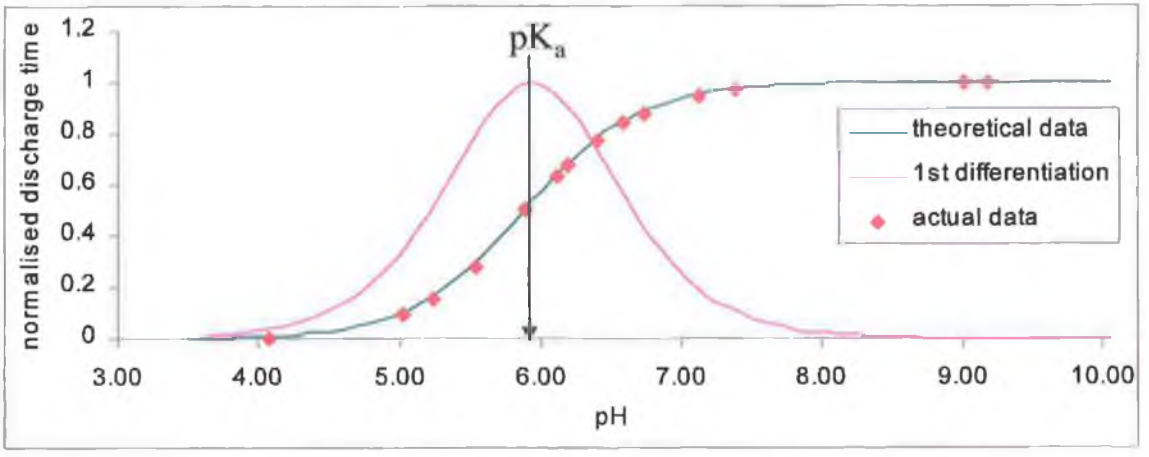

Figure 4-18: Sigmoidal plot of the real data, the predicted data and the first differential of the predicted data.

The pK_a values observed for each of the three runs using both methods of pK_a determination are shown in Table 4-3.

Table 4-3: Unmodified reflectometer, summary of pK_a values obtained using two different methods of pK_a determination

Parameter	**(1) Obtained from Experimental data**	**(2) Obtained from First differential data from the best fit model**
pK_a calibration 1	5.88	6.01
pK_a calibration 2	6.07	6.03
pK_a calibration 3	6.02	5.88
Average pK_a	5.99	5.97
Std. Dev.	0.098	0.08
% RSD	1.64	1.35

The pK_a values for the BCP dye solution calculated from both methods of determination were highly comparable. With the first method the pK_a of the BCP solution was found to be 5.99 ± 0.098. While the second method found the pK_a to be 5.97 ± 0.08. The actual pK_a value quoted for BCP in the literature is 6.3 [22].

4.4.8. Modified Reflectometer

The reflectometer was modified by attachment of a pH polymer-based membrane (Figure 4-19).

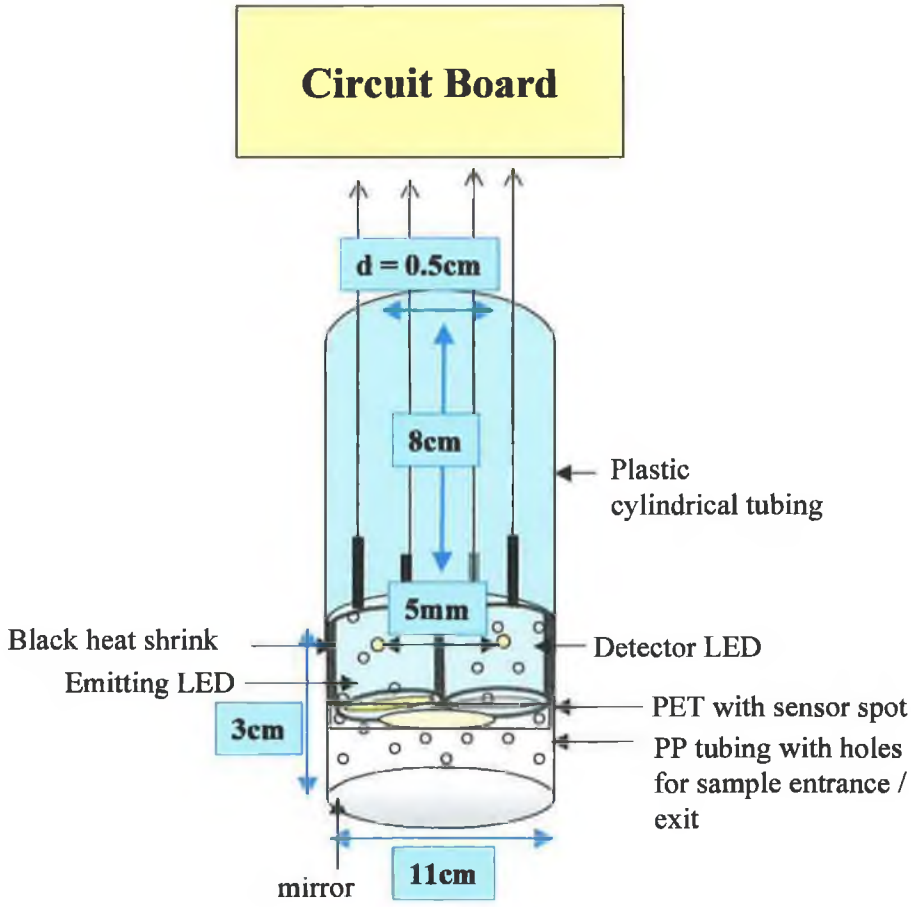

Figure 4-19: Schematic of modified reflectometer.

The preparation of the sensor membrane is outlined in Section 4.4.8.1. The advantage of using this type of design is that it is a stand-alone sensing device.

No indicating dye needs to be added to the sample, leaving it untreated and suitable for further analysis.

4.4.8.1. Preparation of the Polymer Based Sensor Membrane

A lot of work within the research group has been carried out on the optimisation of the polymer-based sensor membrane [24, 25, 26]. Figure 4-4 outlines the formulation previously used for this sensor membrane. This formulation was based on that used by Pacquet *et al.* [27].

Table 4-4: Formulation for polymer based pH sensor membrane

Reagent	**% m/m Reagent added**
Tetraoctylammonium bromide	3.04
Bromocresol purple	1.41
Cellulose acetate	48.01
Ethylene glycol	23.53
Dibutylsebecate	24.01
Cyclohexanone	8 mL

The formulation was prepared by mixing all of the dry reagents together; this included the cellulose acetate, the pH indicating dye (bromocresol purple) and the tetraoctylammonium bromide. Next the ethylene glycol was added, followed by the dibutylsebecate. The mixture was shaken vigorously before addition of the cyclohexanone. All of the reagents were then mixed vigorously for a further 10 min. and placed into an ultrasonic bath and left to sonicate until all of the solid particles had dissolved.

Polyethylene Terephthalate (PET) of dimension 11 cm (width) x 12 cm (height) was pre-treated by washing it with deionised water followed by ethanol. The PET was then placed into an oven to dry at 60° C for 20 min. Once fully dry, 3 μL of

the sensor formulation (Table 4-4) was spotted onto the PET using a micropipette. The spot was left to dry in air for 24 hours. Figure 4-20 shows an image of the BCP polymer based sensor spot.

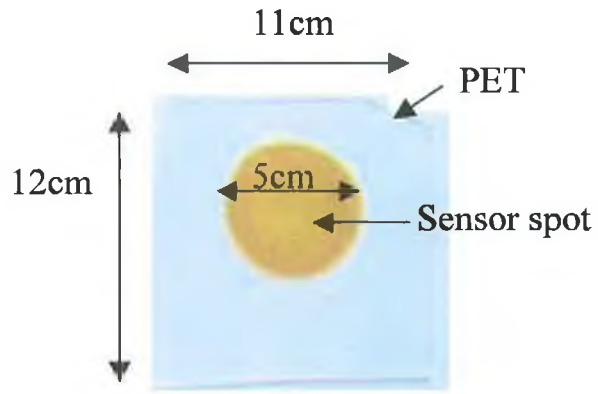

Figure 4-20: Photograph of BCP polymer based sensor spot.

Once the sensor membrane had fully dried it was attached to the sensing end of the LEDs using Araldite glue prior to attaching the sample chamber.

To determine whether a detectable response for a change in pH from pH 3 to pH 10 using the reflectometer was possible, 100 mL H_2O buffered at pH 3 was placed in a 250 mL beaker. The reflectometer and the Metrohm pH probe were placed into the solution along with a magnetic stirrer bar and the beaker was covered with a black cloth to exclude any ambient light. The response of the reflectometer to the water sample at pH 3 was measured. The pH of the solution was then changed to pH 10 by the addition of 200 µL of 4 M NaOH, as before, and the response of the reflectometer to this pH measured (Figure 4-21).

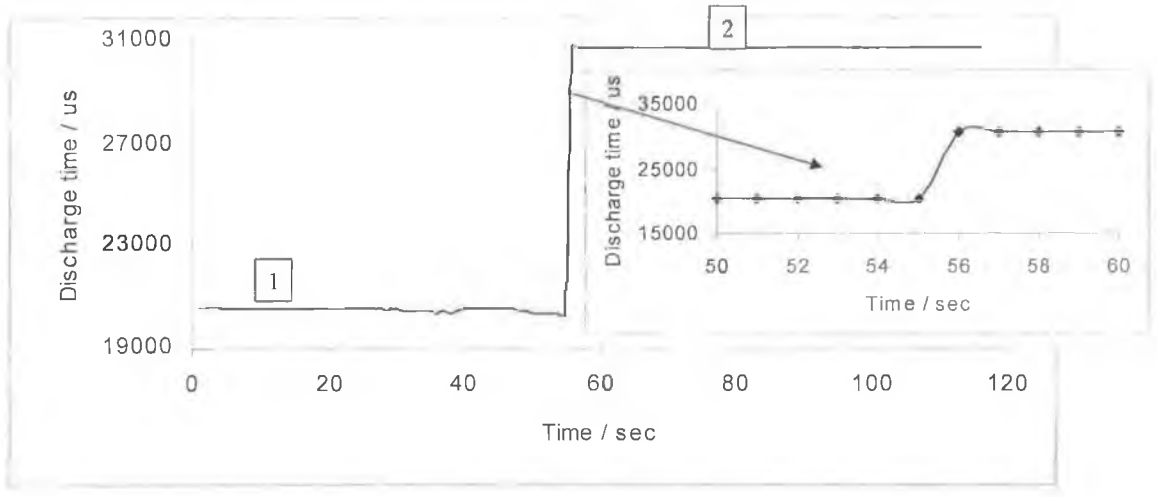

Figure 4-21: Real time trace observed using the modified reflectometer with a change in pH, from (1) pH 3 to (2) pH 10 of a 9.26 x 10^{-5} M BCP solution. The inset shows a blown-up version of the plot, which allows the response time of the sensing device to be determined.

The response time of the reflectometer to a change in the pH of a 9.26 x 10^{-5} M BCP solution was extremely fast. This was determined to be approximately 1 s. There was an approximate 10,000 μs change in response observed with a change in the pH of the BCP solution from pH 3 to pH 10. This produced a very stable baseline; and had an average discharge time of 20572.36 μs ± 28.77 μs at pH 3. The response observed at pH 10 resulted in an average discharge time of 30742.52 μs ± 6.84 μs. Overall this proves that the device when modified is capable of detecting a change in the pH of a BCP solution and that the modification carried out on the device does not interfere with the stability of the reflectometer.

4.4.8.2. Calibration of Modified Reflectometer

A full calibration study was carried out by gradually increasing the pH of the water sample from pH 4.8 to pH 8 by dropwise addition of 4 M NaOH and the response observed at each pH was monitored. All experiments were carried out in triplicate. The response of the reflectometer to each pH was normalised using

Equation 4-2 where R_{max} and R_{min} equal 34186.89 μs and 22893.73 μs respectively. Figure 4-22 shows the normalised response curve.

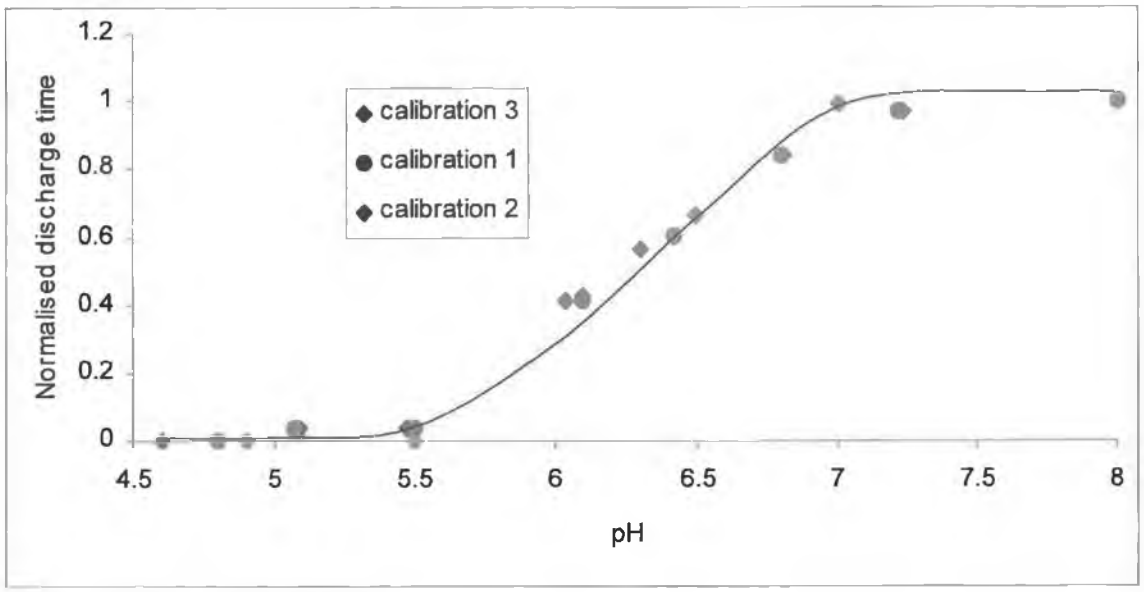

Figure 4-22: Use of modified probe to detect a change in the pH of a 9.26 x 10^5 M BCP solution. The solid line acts as a visual aid only.

The pK_a of the 9.26 x 10^{-5} M BCP solution was calculated for each of the three runs using the two methods of pKa determination outlined in section 4.4.8.1. Figure 4-23 shows the plot observed when the first differential data, the theoretical data and the actual data were plotted against the pH of the solution. The data was normalised between 0 and 1 using Equation 4-2.

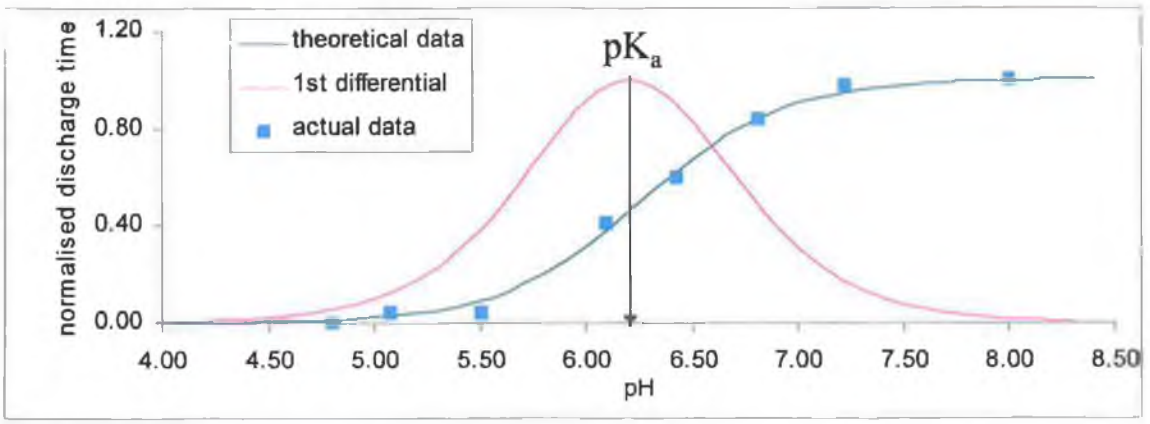

Figure 4-23: Sigmoidal plot of real data and theoretical calculated using the Microsoft Solver tool

The pK_a values for the BCP using both methods of determination along with the average pK_a values are shown in Table 4-5, where the pK_a values were calculated using (1) the actual experimental data and (2) by means of first differential plot. The true pK_a value for BCP is 6.3 [17].

Table 4-5: pK_a data obtained using modified reflectometer for a 9.26 x 10^{-5} M BCP solution.

Parameter	**(1) Obtained from Experimental data**	**(2) Obtained from First differential data from the best fit model**
pK_a calibration 1	6.3	6.25
pK_a calibration 2	6.23	6.21
pK_a calibration 3	6.29	6.22
Average pK_a	6.27	6.23
Std. Dev	0.03	0.02
% RSD	0.49	0.32

The average (n=3) pK_a found, using the experimental data (pK_a = 6.27), was very similar to that obtained when using the first differential data (pK_a = 6.23). As BCP is known to have a pK_a of 6.3 [22], both methods of calculation have resulted in very similar values to that of the actual value. The modified reflectometer had an average working range of pH 5.5 – pH 7 (n=3) with a slope of 5746.27. This shows that the immobilisation has had no effect on the response.

4.5. Conclusion

A reflection based optical device (reflectometer) has been successfully designed and developed. The reflectometer is a generic platform for colorimetric analysis and to highlight its capabilities the use of the reflectometer for the determination of the pH of a solution was investigated. The device was based upon the use of two LEDs, which were positioned at a 7.6° angle to one another. One LED functioned as the light source and the other as the light detector. A mirror was placed beneath the LEDs, which acted as a reflecting surface. The optimum distance of the LEDs from the reflecting surface was calculated to be approximately 1 cm. Hence the LEDs were placed 1 cm away from the reflecting surface for all analytical measurements. The reflectometer was optimised by choosing the appropriate waveband LED for the pH determination study and an appropriate focal distance for the LEDs in order to obtain maximum sensitivity. Bromocresol purple (BCP) was the pH indicator dye used for this study. This dye was found to have an absorption band ranging from 560 - 630 nm and the red LED had an emission band ranging from 600 - 650 nm, therefore the ultra bright red LED was chosen as the emitter LED because there was partial overlap between the absorption spectrum of the BCP solution and the emission spectrum of the LED.

Unmodified and modified versions of the reflectometer were developed. The modification of the reflectometer entailed placing a BCP doped polymer membrane in contact with the LEDs. The studies undertaken using the unmodified version of the reflectometer involved placing the reflectometer into a 9.26×10^{-5} M BCP solution and observing its response to a change in the pH of

the solution from pH 3 to pH 10. A 40,000 μs difference in discharge time was observed. This was a large change in response considering that the baseline had an average discharge at pH 3 of 19981 μs ± 8.59 μs. The baseline recovery of the system was remarkable, as when the solution was reverted back to pH 3 the average response was 19776 μs ± 7.49 μs.

A calibration study was carried out at using the 9.26 x 10^{-5} M BCP solution and the unmodified reflectometer, whereby a sigmoidal plot was observed. The average (n=3) slope of this device was found to be 20238 with an average working range of pH 5.37 – pH 6.56 ± 3.39 %.

The pK_a of the bromocresol purple solution was determined using the unmodified reflectometer. This was calculated using two different methods of determination. The first method took into consideration the experimental data obtained by the reflectometer while the second method used the theoretical experimental data obtained from the Solver equation in Microsoft Excel. Both methods of calculation resulted in very similar pK_a values for the BCP dye. Method one calculated the average pK_a (n=3) of the BCP to be 5.99 ± 1.64 %, while method two calculated the pK_a to be an average of 5.97 ± 1.35 %. The actual pK_a of BCP quoted in the literature is 6.3 [17]. The response time of the unmodified reflectometer was found to be approximately 1 s.

The reflectometer was modified by attaching a piece of PET with a polymer membrane containing the BCP dye to the LEDs. The change in colour of the membrane due to a change in the pH of the solution was measured using the reflectometer. The first experiment carried out with this modified probe was to determine if the reflectometer was capable of detecting a change in the colour of the sensor membrane with a change in the pH of the solution. A large change (10,000 μs) in the discharge time was observed with a change in the pH of the solution (pH 3 – 10). This confirms that the modification of the reflectometer did not have an effect on the sensitivity of the device. Using the modified version of the reflectometer the response of both the protonated and deprotonated form of the dye were very stable.

The modified reflectometer resulted in an average (n=3) pK_a for the BCP dye of 6.27 ± 0.49 % and 6.23 ± 0.32 % when calculated using the first method of determination (incorporating experimental data points) and the second method of determination (incorporating theoretical data points), respectively. These values are very similar to the actual pK_a value of BCP, which has a pK_a of 6.3. The response time of this device to a change in the pH of a BCP solution from pH 3 to pH 10 was extremely fast (~ 1 s).

Overall it can be concluded that this generic reflectometer is an inexpensive, easy to use optical device that can be used in the rapid and accurate determination of the pH of a solution. The emitter LED used (dominant wavelength 632 nm) was not the optimum LED. If a LED with a dominant wavelength of 590 nm was chosen as the emitter LED a more sensitive response should be observed. At the time of analysis this LED was not readily available, however the red LED (dominant wavelength 632 nm) although not optimum still provided very sensitive and accurate results in a very short time (1 s).

During analyses using the modified reflectometer no dye leaching was observed however further studies needs to be carried out on the optical device to ensure that dye leaching and photo bleaching are not an issue.

4.6. References

[1] J. Warrwn Blaker, William M. Rosenblum, *Optics an introduction for students of Engineering,* Robert Mc Connin, 1993, 8.

[2] F.L. Pedrotti, Leno S. Pedrotti, *Introduction to Optics,* Kathleen M. Lafferty, 1987, 32.

[3] W. H.A. Fincham, M.H. Freeman, *Optics,* Butterworths, 1980, 467.

[4] M.H. Noire, L. Coustin, E. Douvaire, D. Pouyat, *J. Sol-Gel Sci. Technol.*, 2000, **17**, 131.

[5] S.C. Kraus, R. Czolk, J. Reichert, H.J. Ache, *Sens. and Actuators A*, 1993, **15**, 199.

[6] O. B. David, E. Shafir, I. Gilath, Y. Prior, D. Avnir, *Proc. SPIE*, 1997, **104**, 3136,.

[7] D.D. Gupta, S. Sharma, *Opt. Commun.*, 1998, **154**, 282.

[8] L. Yang, S.S. Saevedra, N.R. Armstrong, J. Hayes, *Anal. Chemistry*, 1994, **66**, 1254.

[9] K.T.V. Grattan, G.E. Badini, A.W. Palmer, A.C.C. Tseung, *Sens. and Actuators B*, 1991, **25-27**, 483.

[10] D.A. Nivens, M.V. Schiza, S.M. Angel, *Talanta*, 2002, **58**, 543.

[11] J.W. Parker, O. Laskin, C. Yu, M. Lau, S. Kilima, R. Fisher, I. Scott, B.W. Atwater, *Anal. Chem.*, 1993, **65**, 2329.

[12] M.D. Degrandpre, *Anal. Chem.*, 1993, 65, 331.

[13] A. Mills, L. Monag, *Analyst*, 1996, **121**, 535.

[14] A. Lobnik, N. Majka, K. Niederrecter, G. Uray, *Sens. and Actuators B*, 2000, **74**, 200.

[15] M.R. Shahriari, Q. Zhou, G.H. Sigel, JR., *Optic Lett.*, **13**, 407

[16] Q. Zhou, D. Kritz, L. Bonnell, G.H. Sigel Jr., *Applied Optics*, 1989, **28**, 2022.

[17] W.R. Orndorff, A.C. Purdy, *J. Am. Chem. Soc.*, 1926, **48**, 2216.

[18] T.J. Cardwell, R.W. Cattrall, L.W Deady, M. Dorkos, G.R. O'Connell, *Talanta*, 1993, **40**, 765.

[19] M. Trinkel, W. Trettnak, F. Reininger, R. Benes, P. O' Leary, W.O. Wolfbeis, *Anal. Chim. Acta*, 1994, **292**, 41.

[20] A. Safavi, M. Bagher, *Anal. Chim. Acta*, 2004, Article in press.

[21] W. Wroblewski, E. Roznіecka, A. Dybko, Z. Brzozka, *Sens. and Actuators B*, 1998, **48**, 471.

[22] D. Diamond, V.C.A. Hanratty, *Spreadsheet Applications in Chemistry using Microsoft Excel*, J. Wiley and Sons, 1997, 197.

[23] Conducted by the department of education and the civil service commissioners, Mathematics tables.

[24] L. Byrne, K.T. Lau, D. Diamond, *The Irish Journal of Agricultural and Food Research*, 2003, **42**, 119.

[26] L. Byrne, K.T. Lau, D. Diamond, *Analyst*, 2002, **127**, 1338.

[27] A. Pacquit, J. Frisby, K.T. Lau and D. Diamond, submitted for publication January 2005.

5. DEVELOPMENT OF PEDD DEVICE

5.1. Introduction

This chapter describes the development of a novel optical device based on two fused LEDs. As with the photometer and reflectometer one LED functioned as a light source and the other as a light emitter. The optical device was known as a PEDD device i.e. *Paired Emitter Detector Diode* device, and worked in reflectance mode. The difference between the PEDD and that of the reflectometer was the angle at which the LEDs were fused together. In the reflectometer the LEDs were fused together at a 7.6° angle. This chapter investigated three different angles of fusion (i) 30°, (ii) 45°, (iii) 60° and determined a possible mechanism for the PEDD device.

The angle of fusion needed in order for the emitted light to be totally internally reflected (TIR, i.e. a bound ray) is calculated using Snell's law (Equation 5-1). This gives the relationship between the refraction of light travelling between media of two different refractive index (η_1 and η_2).

$$Sin\ \vartheta_{critical} = \frac{\eta_2}{\eta_1} \qquad \textbf{Equation 5-1}$$

Where η_1 = refractive index of material 1

η_2 = refractive index of material 2

The media used in this study was

- The epoxy casing of the LED
- Water

The manufacturer of the LEDs (LiteOn, USA) confirmed on 25th April 2002 that the refractive index of the epoxy (LTL2F3VAKNT) used was 1.53 ± 0.01. The following was the reply received "The epoxy used in LTL2F3VAKNT is 12E088/089". Therefore the critical angle for TIR to happen was calculated by substituting this value and the refractive index for water (1.33) into equation 5-1

i.e. $\sin^{-1}$ (1.33/1.53). This angle was found to be 60.37°, which implied that when the LEDs were fused together at approximately a 60° angle all of the light emitted from the emitter LED would be totally internally reflected, resulting in the device being non-sensitive to activity happening in the surrounding solution. In order for the emitted light to come into contact with the sample solution the angle of fusion needed to be less then this critical angle.

In this study a 60° angle (critical angle) was investigated along with narrower angles, 45° and 30°. The optimum angle was found and used in the PEDD device for the pH determination of a solution.

5.2. Experimental Reagents

All of the reagents used were analytical grade. The dyes used were bromocresol purple (BCP), nitrazine yellow (NY) and rhodamine B (RB). All of these dyes were water-soluble and were obtained from Sigma Aldrich, Dublin, Ireland. All samples were made from ultra pure water and pH 4 and 9 buffer solutions were prepared by dissolving the relevant buffer tablet obtained from BDH Laboratories, (Poole, England) in 100 mL of water. Stock solutions of 4 mM NY and RB were prepared by dissolving 0.21 g and 0.19 g respectively in 100 mL of pH 9 buffer solutions. A 9.2 mM BCP stock solution was prepared in 100 mL of pH 9 buffer solution. From this stock solution a 0.92 mM and 1.85 μM BCP solution was prepared. Ethylene glycol (Sigma Aldrich, Dublin, Ireland) was also used.

5.3. Results and Discussion

5.3.1. Fabrication of PEDD Device

The fused LEDs were fabricated using two identical LEDs (LTL2F3VAKNT, LiteOn, USA). The epoxy housing of the LEDs was ground down at a 45° angle

(to the base of the LED) so that the two LEDs when joined together formed a 90° angle. Figure 5-1 shows a schematic of the LEDs fused together at a 45° angle.

Figure 5-1: Schematic of LEDs fused together at a 45° angle (to the base of the LED).

The ground surface was polished with increasing fine grades of silicon carbide abrasive paper up to # 400 to smooth the surface of the LEDs prior to bonding. The LEDs were then fused together using UV curable epoxy glue (Edmund Scientific: Orland 81 extra fast curing, USA) and placed under UV light (280 nm) for 30 min.

The 60° and 30° fused LEDs were fabricated in the same manner as the 45° fused LEDs the only difference being that the epoxy housing of the LEDs were ground down at a 60° and 30° angle (to the base of the LED), rather then at a 45° angle. A schematic of the 60° and 30° fused LEDs are shown in Figure 5-2 and Figure 5-3 respectively.

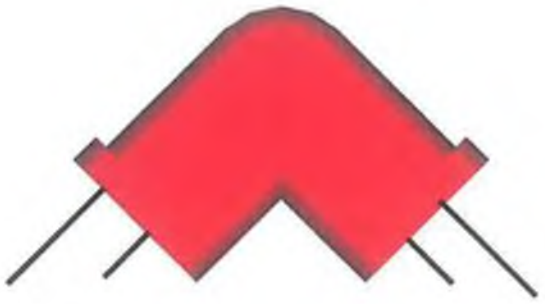

Figure 5-2: Schematic of LEDs fused together at 60° (to the base of the LED).

Figure 5-3: Schematic of LEDs fused together at 30° (to the base of the LED).

Electrical insulating wire (20 cm) was soldered onto the legs of the LEDs, which was later attached to the circuitry. The fused LEDs were then placed into an opaque polypropylene tubing (L: 10 cm x d: 1 cm), (Atlantic Homecare, Dublin, Ireland) so that the tips of the LEDs were exposed at one end of the tubing and the leads at the other end. The tube was filled with fast curing epoxy (Lennahans, Dublin, Ireland), leaving approximately 2 mm of the LEDs exposed. A schematic of the PEDD device is shown in Figure 5-4. This configuration allowed the sensor to operate in solution while restricting the amount of ambient light reaching the detector.

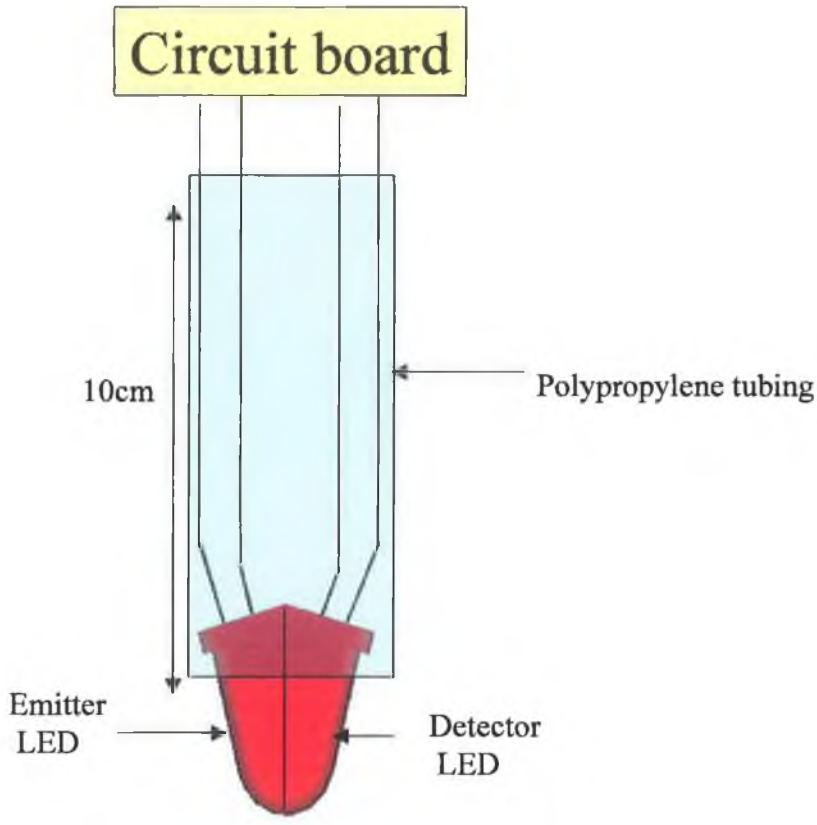

Figure 5-4: Schematic of PEDD device.

5.3.2. Measurement Rationale

The measurement rationale for the PEDD device was the same as that for the photometer and reflectomer i.e. a photon emitted from the light emitting LED hit the detector (reversed biased LED) and produced a small photocurrent. Instead of measuring this small current the internal parasitic capacitance of the LED was measured. Due to the configurations of the fused LEDs a significant amount of light reached the detector LED, some angles resulted in more light then others reaching the detector. The signal was measured in units of time, typically μs. A more detailed description of the measurement rationale can be found in chapter 2, section 2.4.

5.3.3. Data Capture and Analysis

5.3.3.1. Data capture

The data was captured via the PC serial port using HyperTerminal. The microcontroller on the circuit board (which controls the data capturing) was programmed to capture 16 data points per second. The data was then averaged every 2 seconds (n = 32) and printed to Hyper Terminal from where it was exported to Microsoft Excel where it was further analysed. For more on how to transfer the data to Microsoft Excel and obtain a text file refer to chapter 2, section 2.6.

5.3.3.2. Data analysis

Normalisation

The data was normalised between 0 and 1 using the following equation,

$$\frac{R - R_{\min}}{R_{\max} - R_{\min}}$$ **Equation 5-2**

Where R, represents the response and R_{max} and R_{min} are the maximum and minimum response observed respectively.

5.3.3.3. Data Extrapolation using Theoretical data points

Idealized data points from the theoretical equation were obtained using the Solver tool in Microsoft Excel©. The experimental data points were fitted to a best-fit logistic sigmoidal curve equation [1], outlined in Equation 5-3.

$$x(pH) = \left[\frac{a}{(1+\exp[b(pH-c)]^e}\right] + d \qquad \textbf{Equation 5-3}$$

Where x (pH) = sigmoidal response at a defined pH

a = Height of absorbance peak /au

b = Slope coefficient

c = pH units from baseline to point of inflection

d = Baseline offset

e = Symmetry parameter

The pK_a of the solution was obtained by plotting the first differentiation of each data point against the corresponding pH values. A Gaussian curve was observed and the maximum point of this curve was equal to the pK_a of the sample solution.

5.3.4. Choice of LEDs

In order to achieve the optimum sensitivity for the PEDD device, the appropriate emitting LED had to be used. The basic requirement for the LED was that its emission band had to overlap with the absorption spectrum of the dye. Therefore using an Ocean Optics 2000 spectrometer (Ocean Optics Inc., UK) the emission spectra of LED LTL2F3VAKNT was taken and compared to the absorption band of a 4.25 x 10^{-5} M NY solution, 3.5x10^{-5} M RB solution and 8.26x10^{-4} M BCP solution (Figure 5-5). The LED with the emission band most similar to the absorption band of the complex was chosen as the optimum LED.

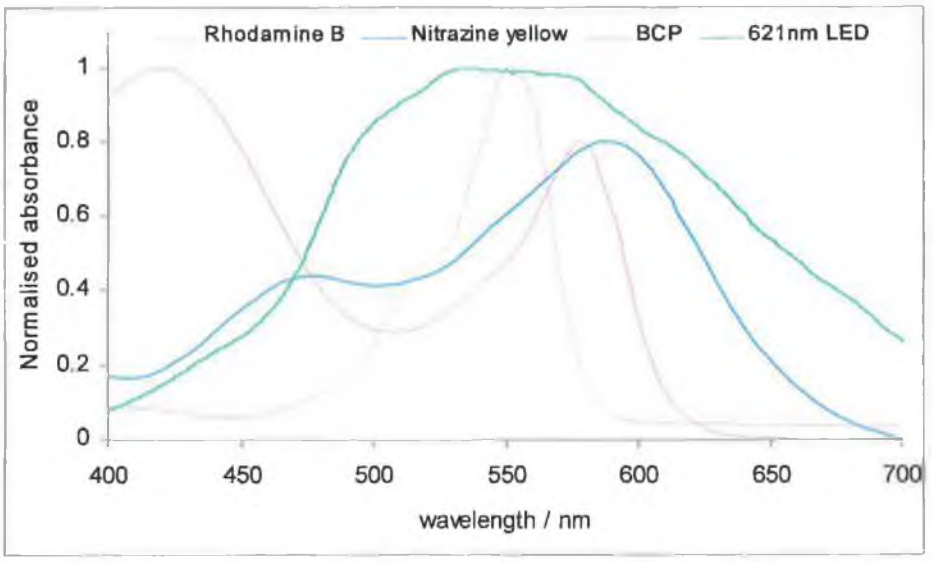

Figure 5-5: Comparison of emission band of LED (LTL2F3VAKNT) with absorption spectra of a 4.25×10^{-5} M NY, 3.5×10^{-5} M RB and 8.26×10^{-4} M BCP solution.

The emission band for the LED was very broad covering the wavelength range 500 – 700 nm. Therefore the 2F3VAKNT LED was a suitable emitter to be used in conjunction with the RB, NY, and BCP dyes as these dyes absorbed within the same region as the emission band of the LED.

5.3.5. PEDD to monitor colour changes

The aim of this experiment was to determine the response of all three angles (30°, 45° and 60°) to a change in the pH of a 9.26×10^{-5} M BCP solution with a change in pH from pH 9 - 2. The angle that gave the maximum change in discharge time with a change in pH was said to be the optimum angle. According to the theory outlined in section 5.1 when using the 60° angle most of the light is totally internally reflected within the device hence the 30° or 45° angle should result in a larger change in response with a change in pH.

100 mL of a 9.26 x 10^{-5} M BCP solution at pH 9 was placed into a 250 mL beaker. The PEDD probe (LEDs fused together at 30°) and a Metrohm pH probe (Metrohm, UK) were placed into the BCP solution. The beaker was covered with a black cloth to exclude ambient light. The pH of the solution was changed from pH 9 - 2 with the addition of a miniscule amount of 4 M HCl, (taking care not to change the concentration of dye present) and the response measured. The experiment was repeated using the PEDD probe fabricated with LEDs fused together at 45° and 60°. All experiments are carried out in triplicate. The probe, which gave the largest change in response with a change in the pH of the BCP solution, was chosen as the optimum configuration.

The response of the 30°, 45° and 60° PEDD devices when exposed to a change in the pH of a BCP solution from pH 9 - 2 are shown in Figure 5-6.

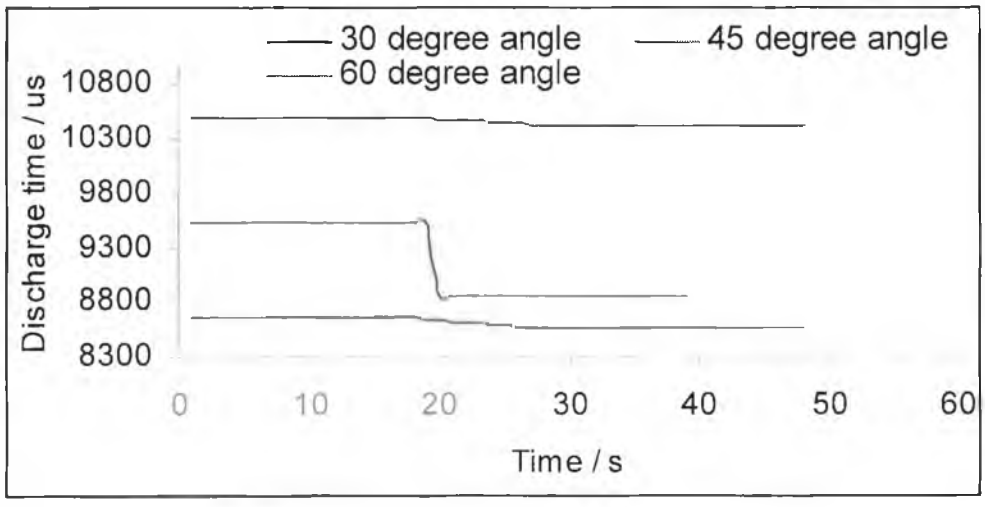

Figure 5-6: Response of PEDD device (LEDs fused together at a 30, 45 and 60 -degree angle to base of the LED) to a change in pH of 9.26 x 10^{-5} M BCP solution from pH 9 – 2.

A summary of the results obtained is shown in Table 5-1.

Table 5-1: Summary of results obtained from 30°, 45° and 60° fused LEDs in a 9.26 x 10^{-5} M BCP solution with a change in the pH of the solution from 9 – 2.

Angle	30°	45°	60°
Average deprotonated response / μs (n=3)	10509	9487	8668
Average protonated response / μs (n=3)	10436	8818	8537
Difference / μs	73	669	95
STDEV	1.15	0.57	3.1
% RSD	0.03	0.02	0.13

The response time of the device when the LEDs were fused together at a 45° angle was investigated and found to be approximately 2 s, shown in Figure 5-7.

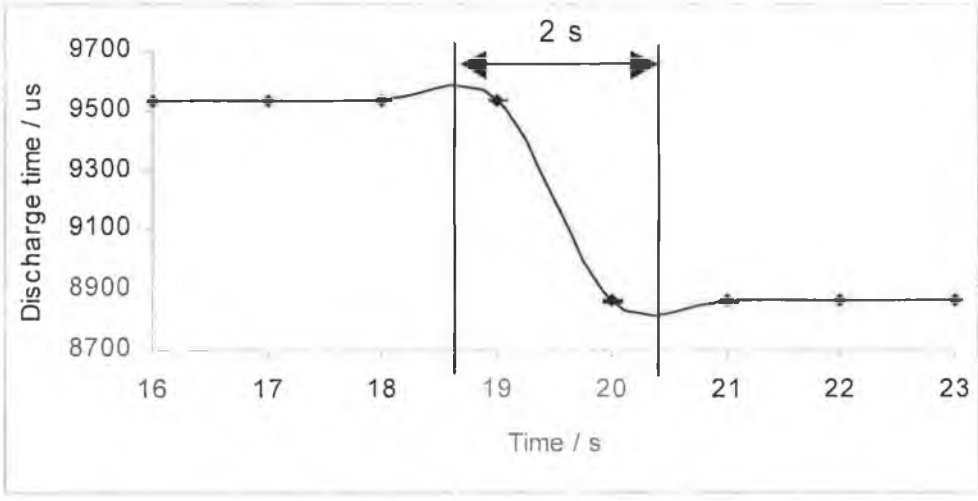

Figure 5-7: Response of PEDD device (fused at a 45° angle), to a change in the pH of a 9.26 x 10^{-5} M BCP solution from pH 9 – 2, highlighting the response time of the device to be approximately 2 s.

The angle of fusion, which gave the largest change in response with a change in the pH of the solution from (pH 9 – 2), was the 45° angle. This angle resulted in a 669 μs change in the discharge time compared to a change of 73 μs and 95 μs for

the 30° and 60° angles respectively. This adhered to the theory of the device that suggested that with the 60° angle most of the light would be totally internally reflected. This was the case as the 60° angle had the fastest discharge time, i.e. the most light reaching the detector. With the 30° angle most of the light was lost to the surrounding solution, which resulted in the longest discharge time observed by the probe as not much light was being reflected back to the detector. Therefore the LEDs when fused together at 45° angle to the base of the LEDs was chosen as the optimum configuration to use for experimental studies as this angle gave the most sensitive results.

5.3.6. Control experiment

Using the optimum configuration (LEDs fused together at 45°) a control experiment was carried out to investigate if a change in the pH of a solution altered the refractive index of the PEDD device. The following procedure was used, 30 mL of pH 4 buffered solution was added to a clean beaker. The dominant wavelength of the emitter LED was 621 nm. The beaker was placed onto a stirring mantel and a magnetic stirring bar was added. A Metrohm pH probe (UK) (used to measure the pH of the solution), and the PEDD device were placed into the solution. The PEDD device was positioned in the water so that the tips of the LEDs were fully immersed into the water. A schematic of the experimental set up is shown in Figure 5-8.

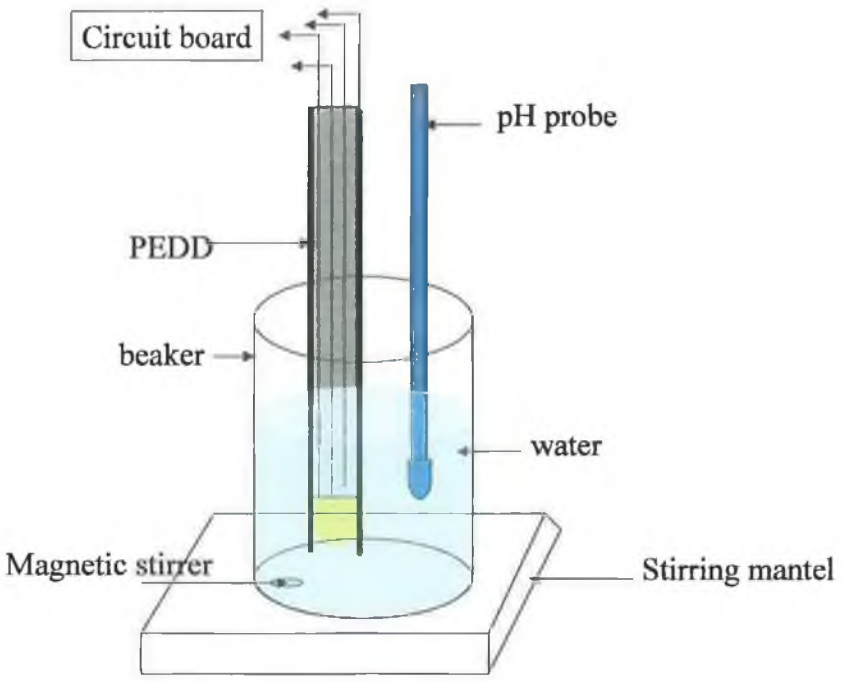

Figure 5-8: Experimental set up used to evaluate the LED based PEDD device. Schematic emits black cloth used to emit ambient light.

The pH of the solution was varied by the addition of approximately 50 μL of 4 M NaOH and was constantly monitored with the use of the Metrohm pH meter. The pH range investigated was from pH 4.5 - 6.7. After the addition of acid or base, the solution was left to stir for 1 min. The measuring time was 10 s. The data was captured as outlined in section 5.3.3.1. All experiments were carried out in triplicate. The results observed are shown in Figure 5-9.

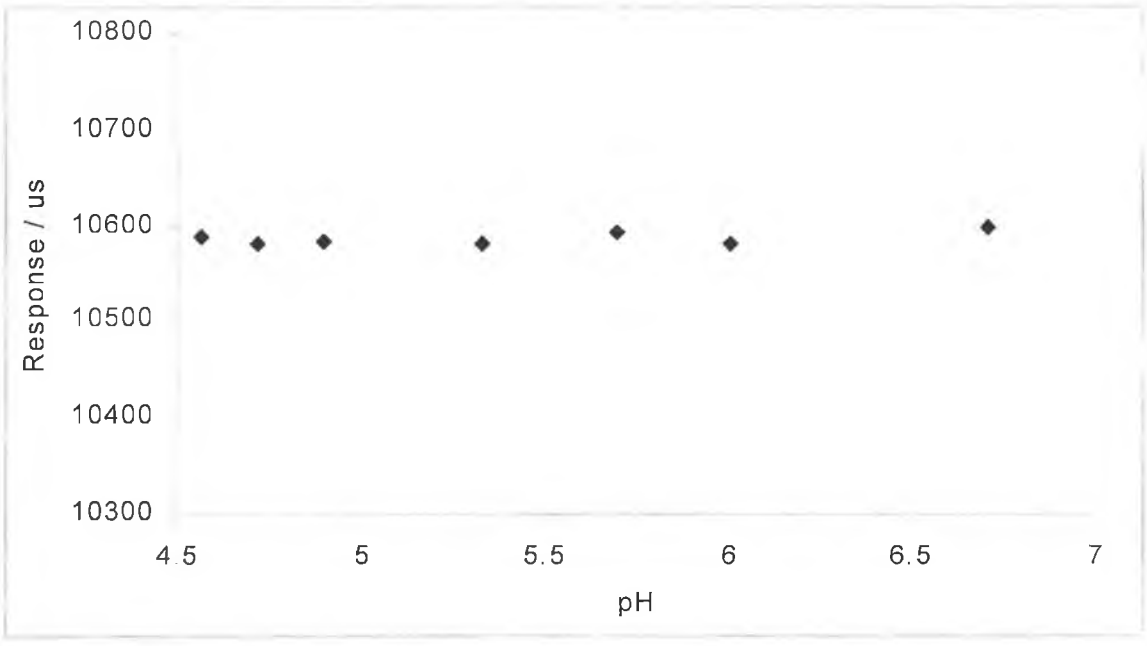

Figure 5-9: Response of PEDD device (fused at 45°) to a change in pH of water from pH 4.5 – 6.7. Points as mean of n = 3 measurements, error bars = standard deviation.

Figure 5-9 shows a very small random change in the discharge time when the pH of the water was changed. This small change of ± 20 μs was possibly due to noise rather than to a change in pH. The fact that the PEDD device observed no change in response with a change in the pH of water indicates that the refractive index of the device was not altered with a change in pH. If there were an interaction between the surface of the device and the change in pH of the water then a change in response would have been observed.

5.3.7. Response of PEDD to an increase in dye concentration

This experiment involved the use of RB, NY and BCP. The concentrations of these dyes were varied to determine if the PEDD device could detect a change in dye concentration. The following was the procedures for each individual dye.

20 mL of deionised water was added to a 100 mL beaker. The concentration range examined for RB was 0.4 – 63.38 μM, 14.35 – 291.49 μM for NY and 0.12 – 14 μM for BCP. Once the dye was added, the solution was stirred for 1 min. and the data was captured as outlined in section 5.2.3.1. All data was recorded in triplicate.

5.3.7.1. Rhodamine B

This experiment examined the response of the PEDD device (dominant wavelength, 590 nm) to an increase in concentration of RB, (absorption band $\lambda_{max,}$ 560 nm).

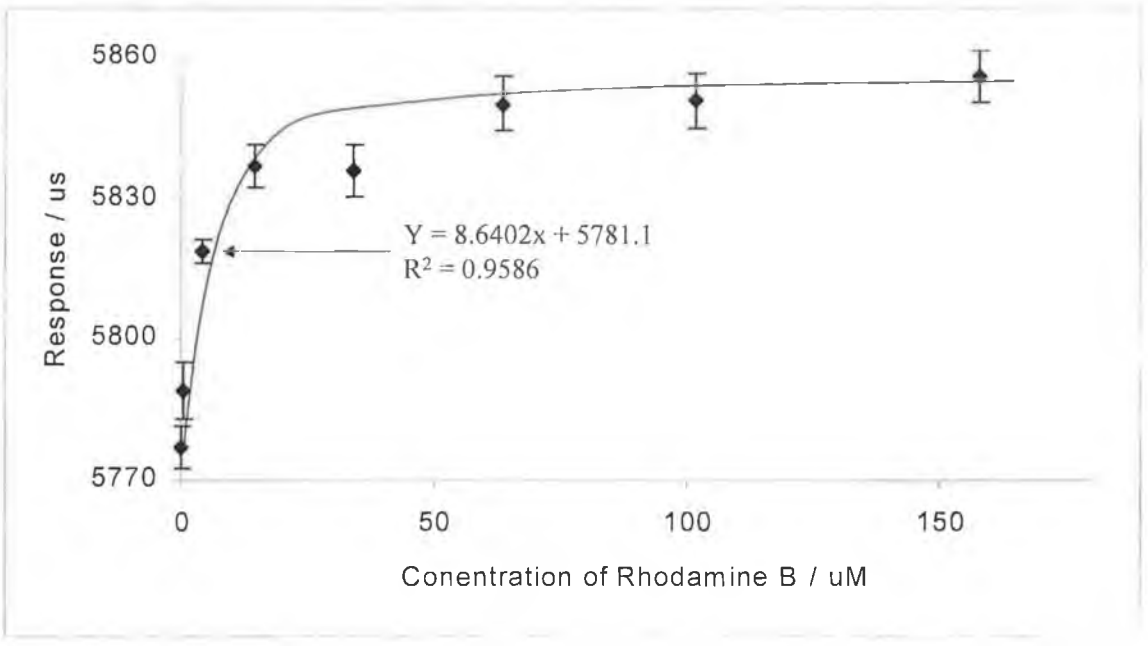

Figure 5-10: Response of 45° PEDD device to a change in concentration of RB from 0.4 - 63.38 μM. The dotted line serves as a visual aid only. Points as mean of n = 3 measurements, error bars = standard deviation.

The concentration range examined was from 0.4 - 63.38 μM RB. All RB solutions were made up in pH 9 buffer solutions. From Figure 5-10 it is clear that

the PEDD device did respond to a change in concentration of RB at pH 7. The working range observed is from 0.4 - 4.4 μM RB with a slope of 8.6402.

5.3.7.2. Nitrazine yellow

A different dye (nitrazine yellow $\lambda_{max,}$ 586 nm) was investigated. The result from the response of the PEDD device to a change in the concentration of this dye is shown in Figure 5-11.

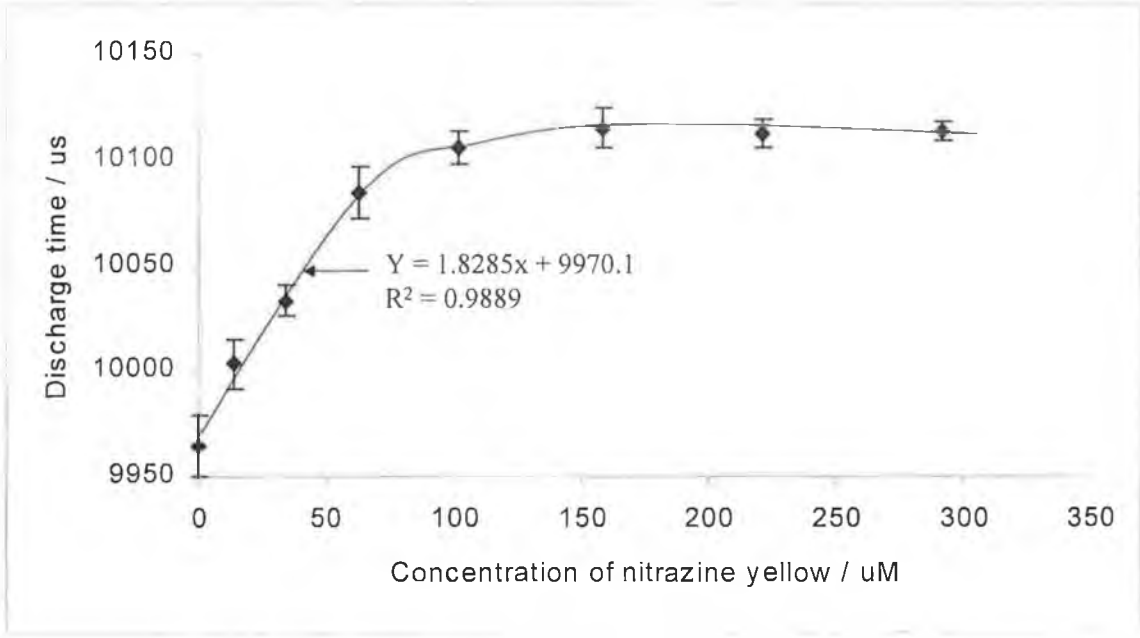

Figure 5-11: Response of 45° PEDD device with an emitter LED of λ_{max} 621 nm to a change in concentration of nitrazine yellow from 14.35 - 291.49 μM, n=3. The fitted line acts as a visual aid. Points as mean of n = 3 measurements, error bars = standard deviation.

The range of concentrations used in this experiment was from 14.35 - 291.49 μM NY. The linear range observed was from circa 0.4 - 101.74 μM NY. An upper limit of detection of 125 μM NY was found with a slope of 1.1727.

5.3.7.3. Bromocresol purple

The third dye investigated was the pH indicating dye bromocresol purple. This dye in the deprotonated form (λ_{max}, 590 nm) was more similar in wavelength to the dominant wavelength of the LED ($\lambda_{max,}$ 621 nm) than when present in the protonated form ($\lambda_{max,}$ 430 nm). The BCP solutions were made up in pH 9 buffer so that the dye was present in the deprotonated form. Figure 5-12 outlines the response of the PEDD device to a change in BCP concentration at pH 9. The concentration range investigated was between 0.12 - 14 μM BCP.

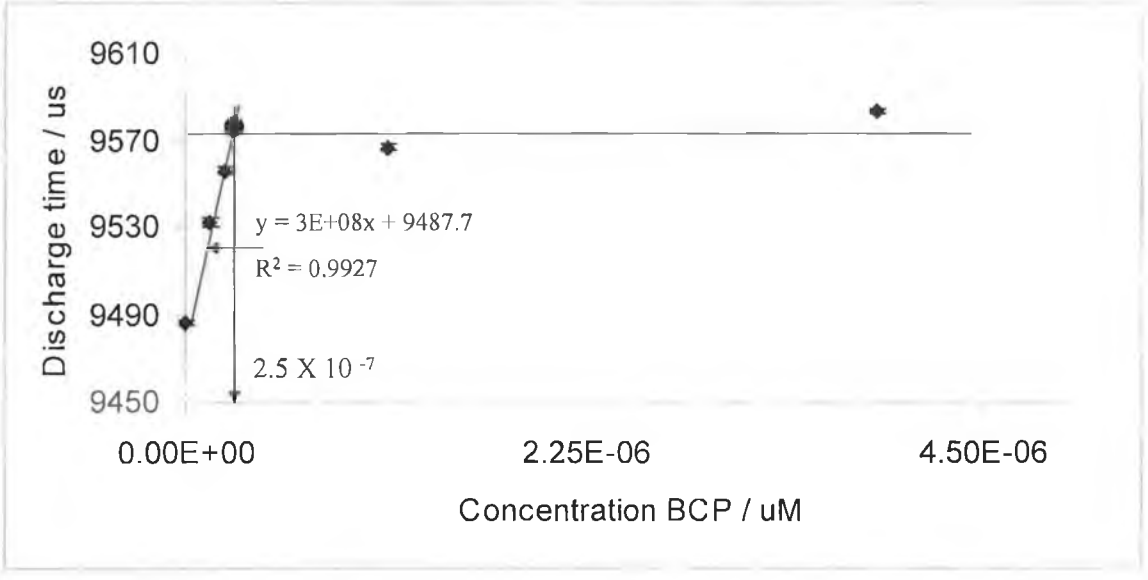

Figure 5-12: Response of 45° PEDD device with an emitter LED of λ_{max} 621 nm to a change in concentration of bromocresol purple from 0.12 - 14 μM BCP, Points as mean of n = 3 measurements, error bars = standard deviation.

The plot observed had a linear range from approximately 0.12 - 2 μM. With a minimum limit of detect of 2.5 x 10^{-7} μM and a slope of 3 x 10^{8}.

The above findings prove that the device can be used to detect changes in colour of pH sensitive dyes in a sample solution.

5.3.8. Application Of PEDD device

The application chosen to highlight the capabilities of the device was the use of the PEDD device for the determination of the pH of a solution. This was achieved with the aid of a pH indicating dye, bromocresol purple, (BCP). The calibration of the PEDD device was carried out in relation to a change in the pH of a BCP solution. The PEDD probe (dominant emission wavelength 621 nm) was placed into 40 mL of a 1.85 μM BCP solution. The minimum amount of 4M HCl or 4 M NaOH was added to alter the pH of the solution. The solution was stirred for 1 min. and the response of the probe at each pH was recorded. The data was captured as described in section 5.2.3.1. The pH of BCP solution was varied and the procedure was repeated. The sampling time at each pH was 10 s.

5.3.9. Calibration of PEDD using bromocresol purple

From previous experiments carried out using the PEDD device and bromocresol purple (Figure 5-12) it was clear that a low concentration of BCP could be detected. A 1.85 μM BCP solution was chosen as the concentration of BCP used for the calibration study, as the device can detect within this concentration region. The results observed from this experiment are shown in Figure 5-13.

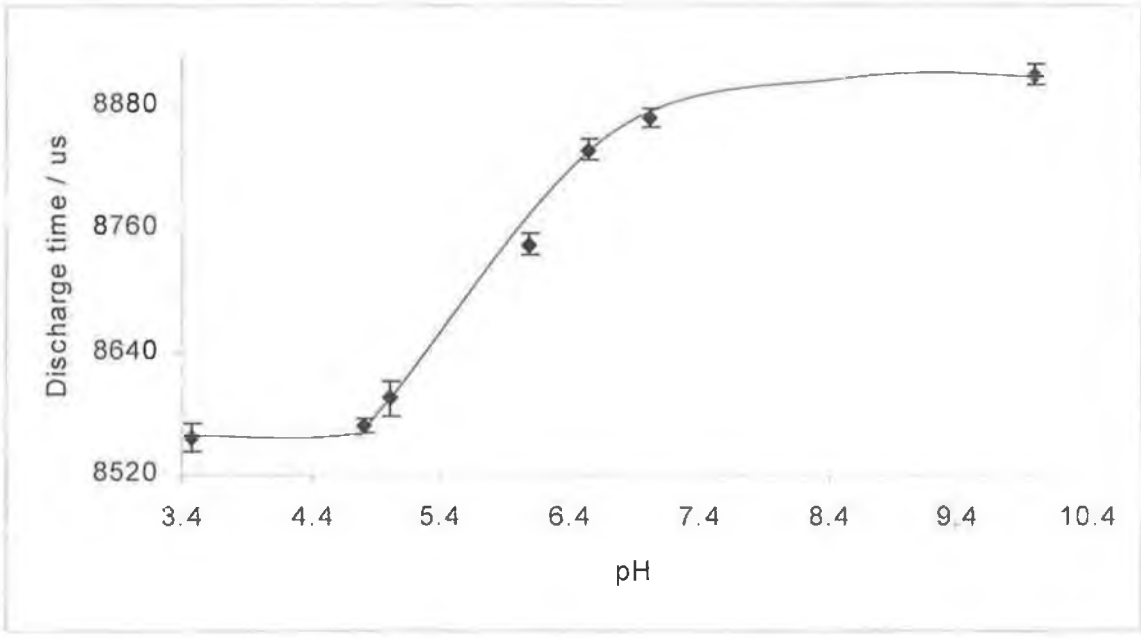

Figure 5-13: Response of fused LED (λ_{max} 621 nm) to a solution of 1.85 μM BCP with a change in pH. Line acts as visual aid only. Points as mean of n = 3 measurements, error bars = standard deviation.

The plot resulted in a sigmoidal shaped curve with a linear range of pH 4.8 - 7.2 and a slope of 150.83. The average pK_a of the solution was calculated using Equation 5-3. Figure 5-14 shows the plot observed when the first differential data, the theoretical data and the actual data were plotted against the pH of the solution. The data was normalised between 0 and 1 using equation 5-2.

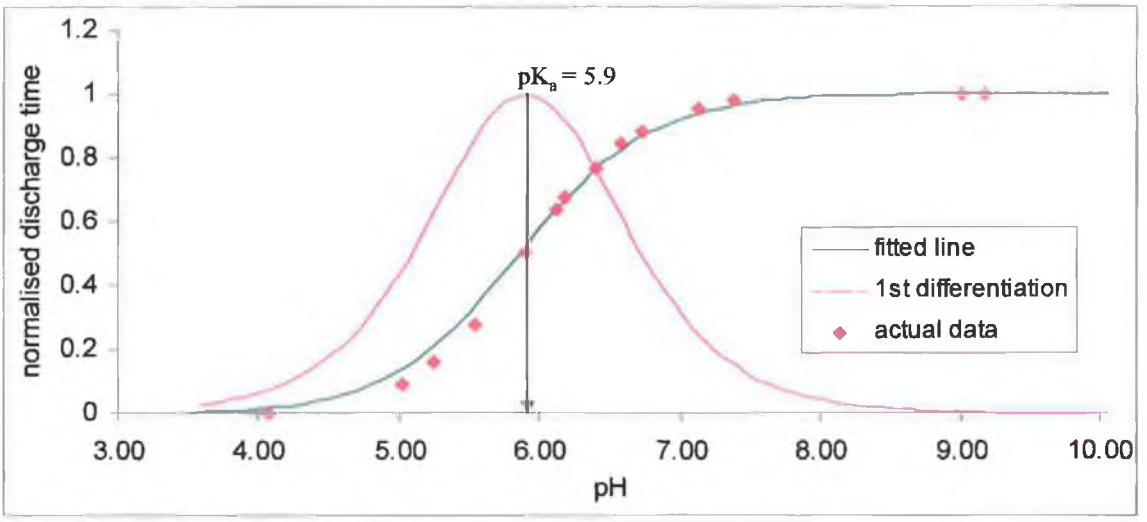

Figure 5-14: Sigmoidal plot of actual data obtained with 45° PEDD device, the theoretical plot obtained using solver (equation 5-3) and the first differential of this theoretical data.

The pK_a of the BCP solution obtained using the PEDD device was found to be 5.9. This is similar to the literature value for the pK_a of BCP, which is 6.3 [2].

As a comparison study the pK_a of bromocresol purple was determined using a μQuant platewell reader™ (Bio-Tek Instruments, USA). Ranges of different BCP solutions varying in pH were prepared. The pH range investigated was from pH 1.94 - 8.88). 200 μL of each solution was placed into each well of a 96 well plate and an absorption spectrum was obtained. The results were plotted in Excel and the pK_a of the dye was obtained with the aid of the solver tool in excel (refer to section 5.2.3.3). Once the best-fit model was obtained the first differentiation of the data was taken which resulted in a Gaussian shaped curve. The maximum point of this curve equalled to the pK_a of the dye. As a model was obtained extra data points could be added to result in a more accurate estimation of the pK_a (Figure 5-15).

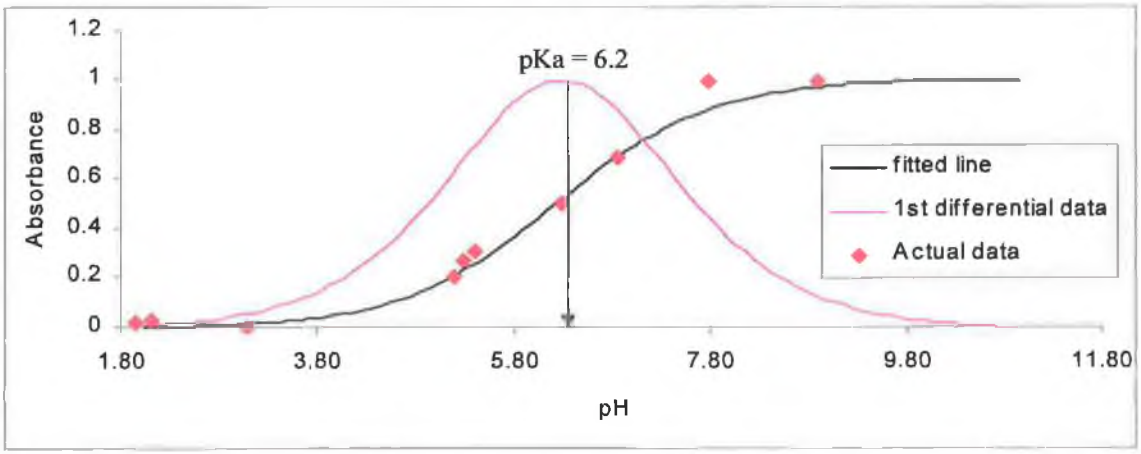

Figure 5-15: Chart of model data and first differential of model at 22°C. The red line indicates the first differential data and the blue line is the best-fit line (platewell reader).

The pK_a of bromocresol purple was found to be 6.2 using the platewell reader. This is very close to the pK_a found when using the fused LEDs. The literature value for BCP is 6.3 [5].

5.3.10. Determination of response mechanism of PEDD device

Experiments were carried out using the PEDD device to determine the effect of a surfactant to a change in the pH of a bromocresol purple solution. The surfactant was used to investigate if it would bind to the surface of the fused LEDs replacing the dye. The expected results from this experiment were;

(1) A suppressed response of the PEDD device due to the presence of the surfactant at the surface of the interface.

Or

(2) No response of the PEDD device to a change in pH of the dye and ethylene glycol solution.

These experiments aided in the clarification of the detection mechanism for the fused LEDs. The following procedures were used to carry out the different experiments.

A Response of PEDD device to a change in pH of a BCP solution.

The PEDD probe (dominant emission wavelength 621 nm) was placed into a solution of 1.85 μM BCP. The pH of this solution was varied using 4 M HCL and 4 M NaOH, once the pH was varied the solution was stirred for 1 min. and the response at each pH was measured. The data collected was captured as per section 5.2.3.1. Note: The pH of the BCP solution was monitored using a Metrohm pH meter, UK.

B Response of PEDD device to a change in pH of an Ethylene glycol and dye solution.

The PEDD probe (dominant emission wavelength 621 nm) was placed into a solution of 1.85 μM BCP. 10 μL of ethylene glycol was added to the dye solution. The solution was stirred for 1 min. and the response of the probe to the change in pH was measured. A Metrohm pH probe was used to control the pH of the solution. The data was captured as per 5.2.3.1.

C Response of the PEDD device to a change in pH of an ethylene glycol solution.

The PEDD probe (dominant emission wavelength 621 nm) was placed into 20 mL of deionised water. 10 μL of ethylene glycol was added to the water, the pH of the solution was varied using 4 M HCL and 4 M NaOH and the response of probe to the solution was measured. The pH of this solution was controlled using a pH Metrohm pH probe, UK. The data collected was captured as per section 5.2.3.1.

The sampling time for each experiment was 10 s.

Proposed mechanism 1

If the mechanism for the PEDD device was based on diffuse reflection then with dye and surfactant present in solution, the response of the PEDD device should not have changed with the presence of surfactant. The light from the LED would have been emitted into the bulk dye solution. This would have then been reflected back to the detector from a reflecting surface and the presence of a surfactant would not have interfered with the measurement. Figure 5-16 shows the proposed mechanism 1: diffuse reflection.

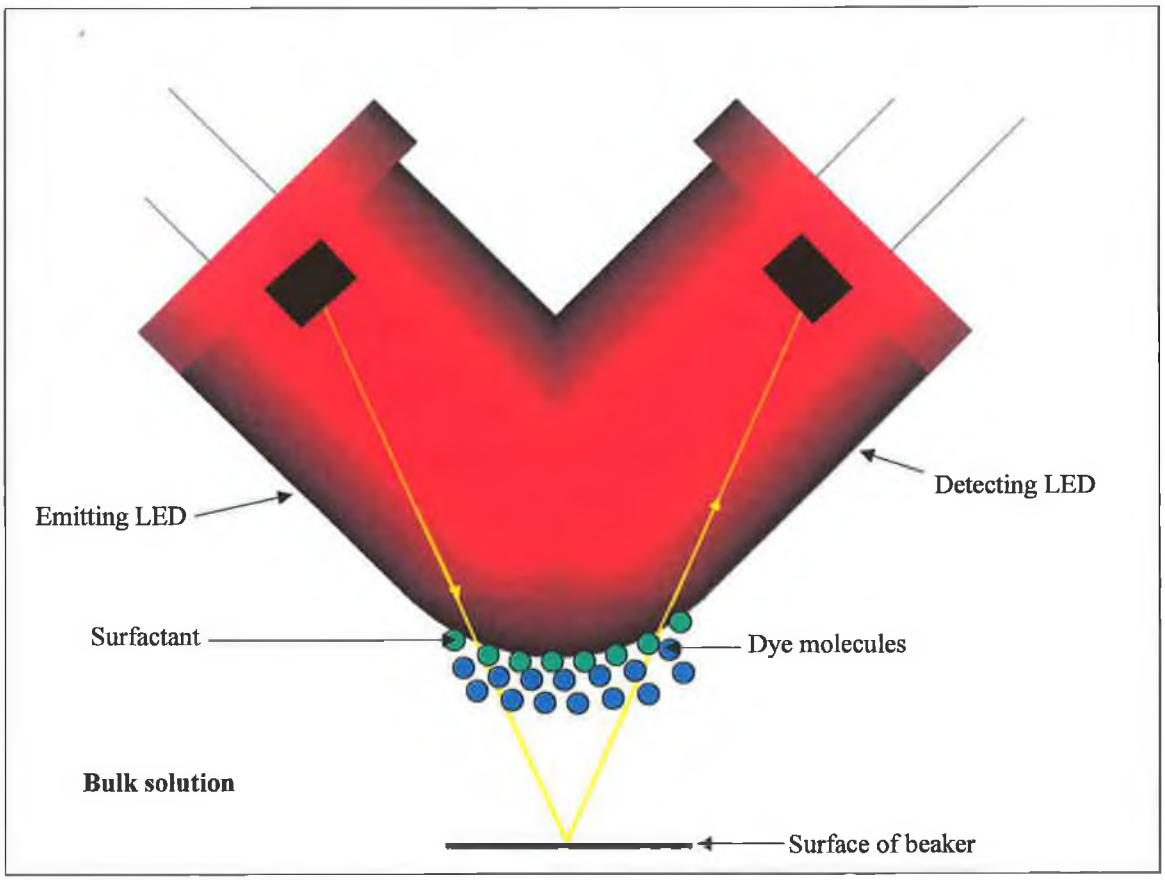

Figure 5-16: Proposed mechanism 1: Diffuse reflection.

Proposed mechanism 2

The second proposed mechanism outlined in Figure 5-17 is based on the theory of an evanescent wave. If the fused LEDs were based on an evanescent wave principle, then some of the light emitted will have escaped out into the dye layer and then have been reflected back to the detector. With a surfactant present the light must firstly pass into the surfactant layer and then into the dye layer, hence if there was a suppressed response observed with the presence of a surfactant then it can be concluded that the fused LEDs mechanism was based on the evanescent wave principle of detection. A schematic of the proposed mechanism is outlined in Figure 5-17.

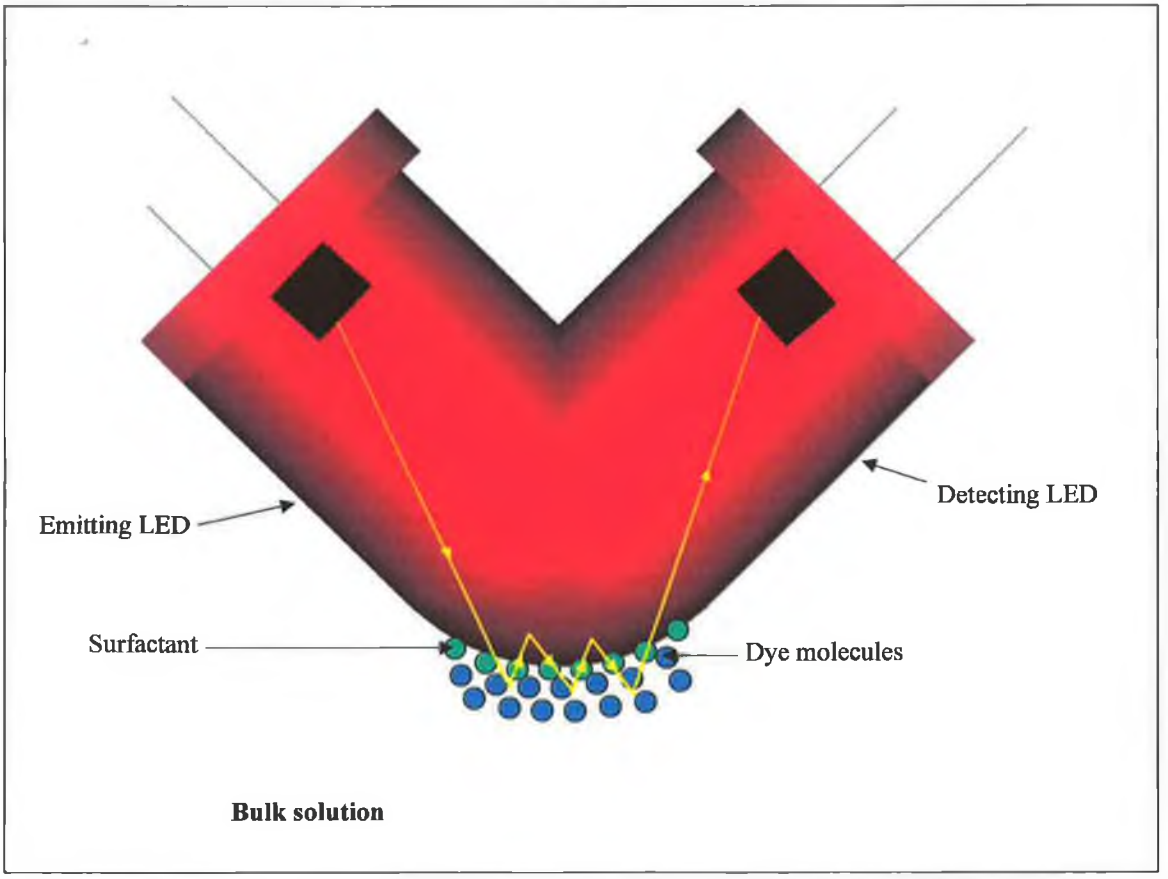

Figure 5-17: Proposed mechanism for 2: Evanescent wave principle.

A. The change in the pH of a solution of bromocresol purple (1.85μM BCP) was analysed. The resulting plot is shown in Figure 5-18A. A sigmoidal curve was observed. A slope of 56.962 was found with a linear range of pH 4.78 - 7.56. The upper limit of detection observed was pH 7.56 and the pK_a of this dye was 5.9.

B When bromocresol purple and ethylene glycol were present in solution a sigmoidal curve resulted, but the response of the PEDD device to this solution was suppressed (Figure 5-18B). The linear region of this plot was from pH 5.246 - 5.56 with a slope of 113.13. The pK_a of the dye was estimated to be ~ 5.3. This demonstrates that the presence of a surfactant suppresses the response of the PEDD device to a change in the pH of a BCP solution. The pH at which the BCP is fully deprotonated when a surfactant is present is equal to the pK_a of the dye when there is no surfactant present. This indicates that when a dye is in the basic form it is more strongly attracted to the surfactant hence the PEDD device will be able to detect the presence of the BCP.

C The response of the PEDD device to a change in the pH of a solution containing water and ethylene glycol was investigated. The results are shown in Figure 5-18C. From the results observed it is clear that the PEDD device did not respond to an increase in the pH of the ethylene glycol and water solution. This confirmed that the presence of a surfactant did not alter the refractive index of the solution.

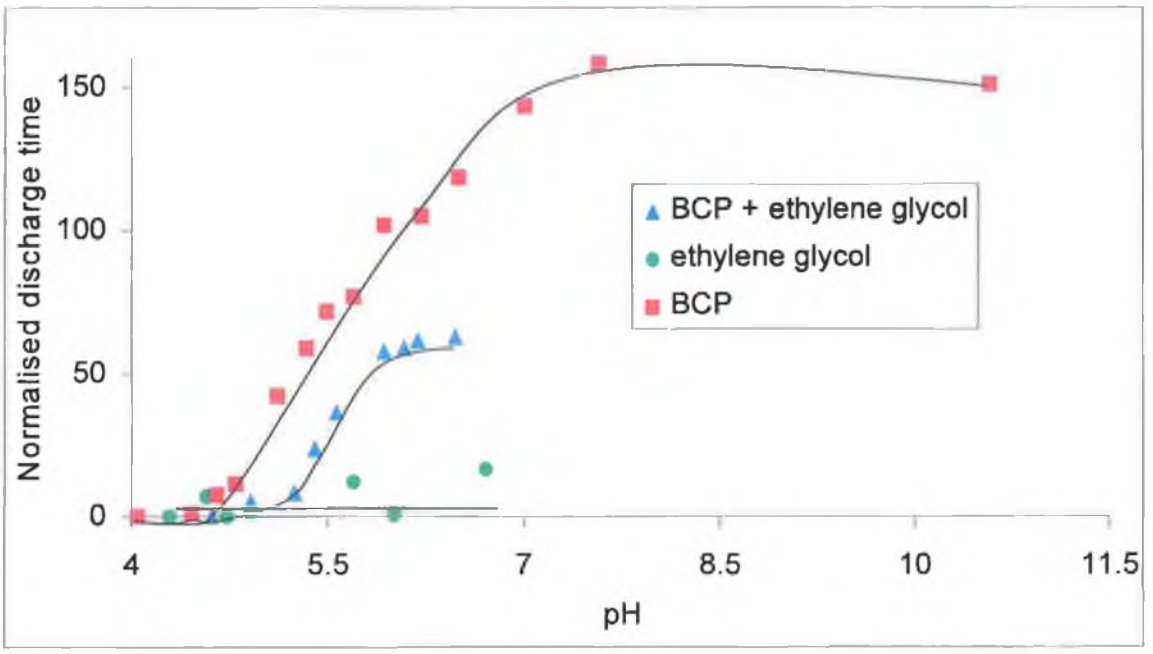

Figure 5-18: Plot of effect of surfactant on PEDD device

Figure 5-18 demonstrates that the presence of ethylene glycol suppressed the response of the PEDD device to a change in the pH of the BCP solution. Ethylene glycol alone did not respond to a change in pH of a solution therefore the presence of ethylene glycol did not alter the refractive index of the solution. Due to the presence of ethylene glycol the PEDD device was "observing" less dye and a suppressed response was observed. Therefore it can be concluded that mechanism two is unlikely to be the sole mechanism of operation for the fused LEDs.

The mechanism most likely to be taking place is mechanism number 2. The light emitted from the LED penetrated past the interface of the fused LED and into the solution. Some of the light passed through the surfactant layer and into the dye layer, getting reflected back to the detector. The reason why a suppressed signal was observed may have been due to the presence of the surfactant layer, hence not as much of the emitted light was penetrated into the dye layer. The evanescent energy decreases exponentially with distance from the boundary, so if the dye molecules were displaced by a surfactant then a suppressed response will be observed.

Diffuse reflectance may also play a part in the detection mechanism but not to such an extent as the evanescent wave mechanism because if the detection mechanism was purely diffuse reflectance this would be predominantly based on the activities in the bulk solution and the presence of a surfactant would have little or no effect on the detector response. As studies show that the surfactant does suppress the response observed, therefore it is very probable that the dominant mechanism is that of an evanescent wave principle but diffuse reflectance also plays a part in the detection mechanism.

5.4. Conclusion

A generic Paired Emitter Detector Diode (PEDD) device has been developed for the use in colorimetric based sensing. Inexpensive optical and electronic components were used to construct the PEDD device that operated from a 9 V battery, leading to an overall low cost sensing device.

Snell's law was used to calculate the critical angle of fusion for the two LEDs to be in order for the light emitted to be totally internally reflected. This angle was calculated taking into consideration the refractive index of water (1.33) and the refractive index of the epoxy casing of the LED (1.53). This angle was found to be approximately 60° (i.e. $\sin^{-1}$ (1.33/1.53)). This applied that in order for the light to come into contact with the sample and get reflected back to the detector an angle narrower then 60° was required. After studying three different angles of fusion (30°. 45° and 60°) the 45° angle was found to result in the largest change in response with a change in the pH of a BCP solution. A control experiment was designed to determine if the refractive index of the PEDD device, which used a solution of changing pH values. The results from this experiment indicated that a change in the pH of the solution did not alter the refractive index of the device. The response of the PEDD device to three different dye solutions was examined. The dye solutions studied were RB, NY and BCP. A working range of 0.4 – 4.4 μM RB was observed with a slope of 8.6402, with NY a working range of 0.4 –

101.74 μM was found with a slope of 1.1727 and with BCP a working range of 0.12 - 2μM was observed.

The optical device was validated for the pH determination using BCP. The linear range observed was from pH 4.8 - 7.02 with a slope of 150.53.

The pK_a of the BCP solution obtained using the PEDD device was calculated to be 5.9 this is very similar to the literature value for the pK_a of BCP, which is 6.3. A comparison study was conducted using a μQuant platewell reader™ (Bio-Tek Instruments, USA). The pKa of BCP using this instrument was found to be 6.2.

A series of studies were conducted to determine the detection mechanism of the fused LEDs. The results proved that the dominant mechanism for the PEDD device was based on an evanescent wave principle as the presence of a surfactant was found to suppress the response observed by the fused LEDs. Therefore a very low cost optical platform for performing analytical measurements based on an evanescent wave principle has been developed.

5.5. References

[1] D. Diamond, V.C.A. Hanratty, *Spreadsheet Applications in Chemistry using Microsoft Excel,* J. Wiley and Sons, 1997, 197.

[2] W.R. Orndorff, A.C. Purdy, *J. Am. Chem. Soc.*, 1926, **48**, 2216.

6. Conclusion & Future work

Three different prototype LED based devices have been developed that can obtain information on the molecular status of the devices environment due to the change in the light intensity of the emitting LED. The designs of the devices (sensors and circuitry) are neat, compact and inexpensive (<$10). Each device consists of a sensor linked to simple a microcontroller-based circuit, offering the possibility of using the devices as a basic building block for wireless chemical sensing.

Communication through computer networking has vastly improved over the past decade but traditionally this requires a physical wire to be connected to the network. The use of wireless communication offers flexibility and mobility allowing us to live and work in ways that were never before possible. One question posed by many is "how can the digital world sense and respond to changes in the real world"? [1]. The answer is through networks of wireless sensing devices. Low power wireless sensor networks provide a new monitoring and control capability for civil and military applications in transportation, manufacturing, biomedical, environmental management and safety and security systems [2]. Network sensing devices combine distributed sensing, computation and wireless communication, therefore this area is of great interest to computer science and engineering researchers worldwide e.g. the WWRF (Wireless World Research Forum), a global organisation was founded in 2001 to develop and maintain a consistent vision of the Wireless World. This area of research is also of great interest to chemists as the core of these devices is the sensor. Chemical and / or biosensors can be deployed in the environment to provide this vital link between the digital world and the real world. The devices developed in this thesis are generic optical sensing platforms that can be incorporated into a networked sensing system to generate a selective response due to a specific analyte. Some of the applications explored include the use of the devices for the detection of Fe (II) and the determination of the pH of a solution. The sensing devices may be used to sense any analyte that will result in the colour change of a chemical reagent. This provides a very usefully and inexpensive device with endless colorimetric sensing applications. Another application that could be explored is the use of the optical device for the detection of phosphate in water. Previous research has been carried out on the detection of orthophosphates in water using the yellow method or molbdovanadophosphoric method of detection [3]. This method of detection forms a yellow coloured complex (which absorbs at λ_{max} 380 nm) in the presence of

orthophosphates. By using a blue LED as a light emitter any of the optical devices developed can be altered to sense for phosphates in water.

All of the devices use a reagent-based method of detection. This implies that a reagent needs to be added to the sample in order for the sensor to successfully detect the presence of a particular analyte. A point that must be considered with this method of detection is the amount of reagent that will be consumed annually. For example if one device requires 0.5 L of reagent annually and there are thousands of devices used, then this network of sensors requires a lot of reagent also the cost for the disposal of the reagent would be very significant. A method to over come this problem is to use an immobilised sensing system. This method of detection was explored using the reflectometer. Here a colorimetric reagent was physically entrapped into a polymer membrane and the sensor membrane changed colour in the presence of a specific analytic without the need for an additional reagent. This method of determination eliminates the excess cost of reagent disposal. With this method of detection the sensor is highly reproducibly and robust. It must be safely protected from external environmental factors that may in return result in the sensor not functioning e.g. excess moisture or photo-fading. Further studies need to be carried out into the optimisation of the reagent concentration and also into the automation of the addition of the reagent. Work into the packaging of these devices also needs to be done so that they can be deployed safely in the environment. For example if the devices are required to monitor seawater they need to be fully sealed to protect them from any water coming into contact with the circuitry.

The advantage of the optical devices developed is that the appropriate configuration may be chosen depending on the users application. The devices are configured in (1) transmission mode; (2) reflection mode or (3) the chemochromic reagent may be coated onto the LEDs

Current levels of sampling locations and frequency of analysis are insufficient to provide enough information for geographical mapping of distribution. With a networked sensing system multiple sensors can be distributed which can continuously monitor any activity happening in the surrounding environment. A simple schematic

of a networked sensing system is shown below in Figure 6-1. The main components needed are (1) the sensor, (2) a signal processor and (3) a network interface.

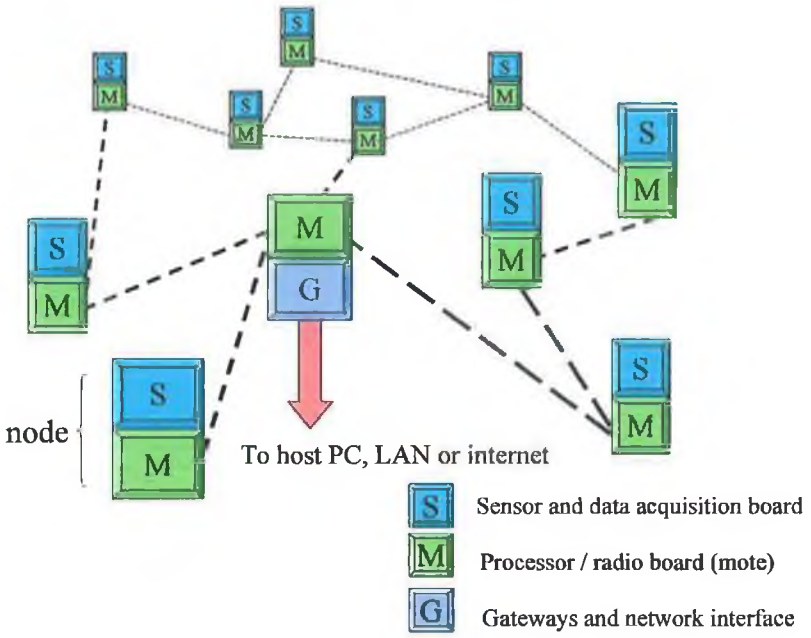

Figure 6-1: Schematic of network sensing system set up.

Ideally the system should use a simple flexible programme, be power efficient, have a robust sensor, have a built in self-check, be able to self-organize, repair themselves and manage their power consumption, allowing the sensors to be deployed long-term. This enables continuous monitoring of the world around them. These low-cost, low-power sensors can be deployed in large numbers, expanding the area under observation providing early, accurate information.

For example they can provide advance warning to the presence of a large oil spill and also highlight the extent of the oil spill. If a network of sensors were not in place a single sensor may not be in the right place at the right time to detect the spillage.

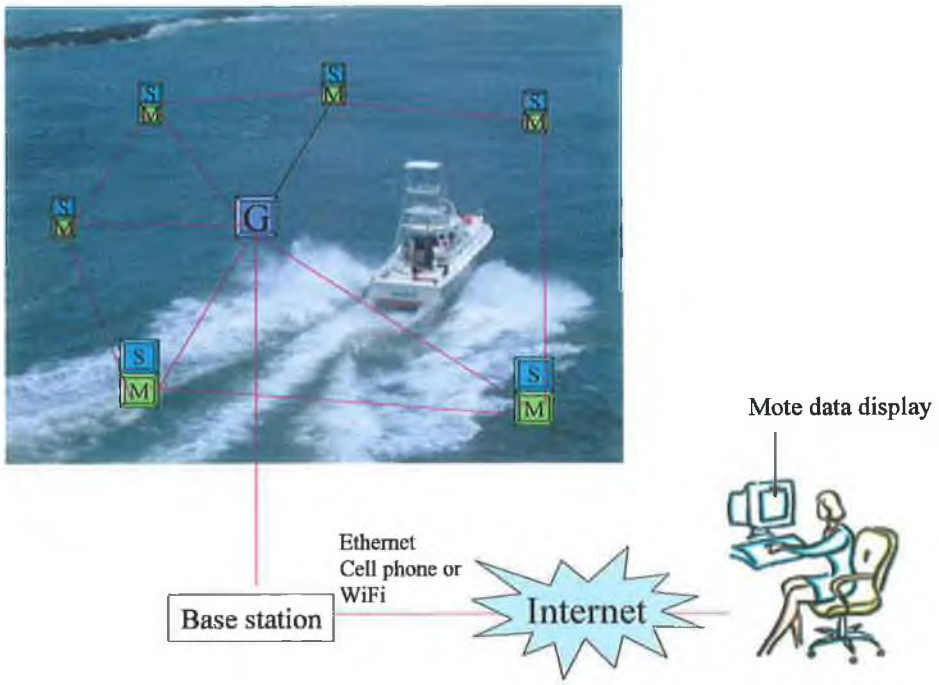

Figure 6-2: Schematic of the application of a networked sensor

Paradiso et al. have carried out research into the development of a RF random access integrated node [4]. This node contains an RF transceiver and a microcontroller in one package. This device can be used as a stand-alone wireless sensing device. Another device developed by Paradiso *et al.* is the pushpin computing system [5,6]. These devices can be updated or altered easily by replacing any of the modules making up the device. The modules used are a power module, a communication module, a processing module and an expansion module

The Tyndall National Institute in Cork, Ireland are also working on developing autonomous transducer nodes. They have currently developed nodes of size 25 mm^3, and 10mm^3 [7] (see Figure 6-3) and aim to achieve sensor nodes of size 5 mm^3 and 1 mm^3 in the near future!!!

Figure 6-3: Photograph of 10 mm^3 sensor node designed by the Tyndall Institute [7].

This area of networked chemical sensors is very popular as it provides a means of continuous sample monitoring. The success of sensing depends on the robustness of the miniaturized devices and the ability of the devices to operate from low powered devices. Considerable challenges still remain within the area.

---

[1] D. Diamond, *Anal. Chem.*, 2004, **76**, 286A.

[2] K. Bult, A. Burstein, D. Chang, M. Dong, M. Fielding, E. Kruglick, J. Ho, F. Lin, T.H. Lin, W.J. Kaiser, H. Marcy, R. Mukai, P. Nelson, F. Newberg, K.S.J. Pister, G. Pottie, H. Sanchez, O.M. Stafsudd, K.B. Tan, C.M. Ward, S. Xue, J. Yao. Proceedings of the 1996 International Symposium on Low Power Electronics and Design. Monterey, CA, USA, 12-14 Aug. 1996,17.

[3] Towards Autonomous Environmental Monitoring Systems, M. Sequeira, M. Bowden, E. Minogue, D. Diamond, *Talanta*, 2002, **56**, 355.

[4] http://www.media.mit.edu/resenv/rfrain/info.html
Last accessed 5/04/05

[5] J.A. Paradiso, J. Lifton, M.Broxton, *BT Technology Journal*, 2004, **22**, 32.

[6] J. Lifton, D. Seetharam, M. Broxton, J. Paradiso, Proceedings of the Pervasive Computing Conference, Zurich Switzerland, 26-28 August 2002, Springer Verlag, Berlin Heidelberg,139.

[7] http://www.tyndall.ie/research/mai-group/10cube_mai.html
Last accessed 5/04/05

7.0 APPENDIX

pH Sensors

Optical pH sensors (optodes) are required to be small, mechanically stable, have fast response times, inexpensive, accurate and reproducible. The pH response of most glass electrodes is imperfect at both ends of the pH scale and therefore the optical sensor is advantageous for safety, remote sensing and the removal of electrical interference. Optical pH sensors are based on pH dependant changes of the optical properties of thin and proton permeable layers, in which a pH indicator has been chemically or physically immobilised. The ideal immobilisation technique should produce a highly stable assembly of molecules that remain accessible to the dissolved pH indicator dye [1]. As the pH of the solution changes, the colour of the pH indicating dye also changes. Most pH sensors have a narrow working range and dyes are only sensitive to changes over 2 - 4 pH units [2]. A considerable amount of work has dealt with poly (vinyl chloride) (i.e. PVC) based membranes [3]. However these membranes tend to suffer from a slow response time (in the order of seconds to minutes) [4]. This has lead to the use of cellulose acetate based membranes, as they generally tend to have a much faster response time than the PVC membranes. Recently Liu *et al.* [5] have developed an optical pH sensor based on the immobilisation of phenolphthalein into a cellulose membrane. The phenolphthalein was first reacted with formaldehyde to produce a series of pre-polymers with numerous hydroxymethyl groups; these pre-polymers were abbreviated to phenolphthalein formaldehyde (PPF). The PPF was covalently immobilised to the diacetyl cellulose membrane via the hydroxymethyl groups. The results obtained by an absorbance measurement to (A) a change in the pH of a phenolphthalein solution at a wavelength of 553nm and (B) a change in the pH of a buffer solution containing the phenolphthalein in an immobilised PPF membrane at a wavelength of 572 nm are shown in Figure 1.

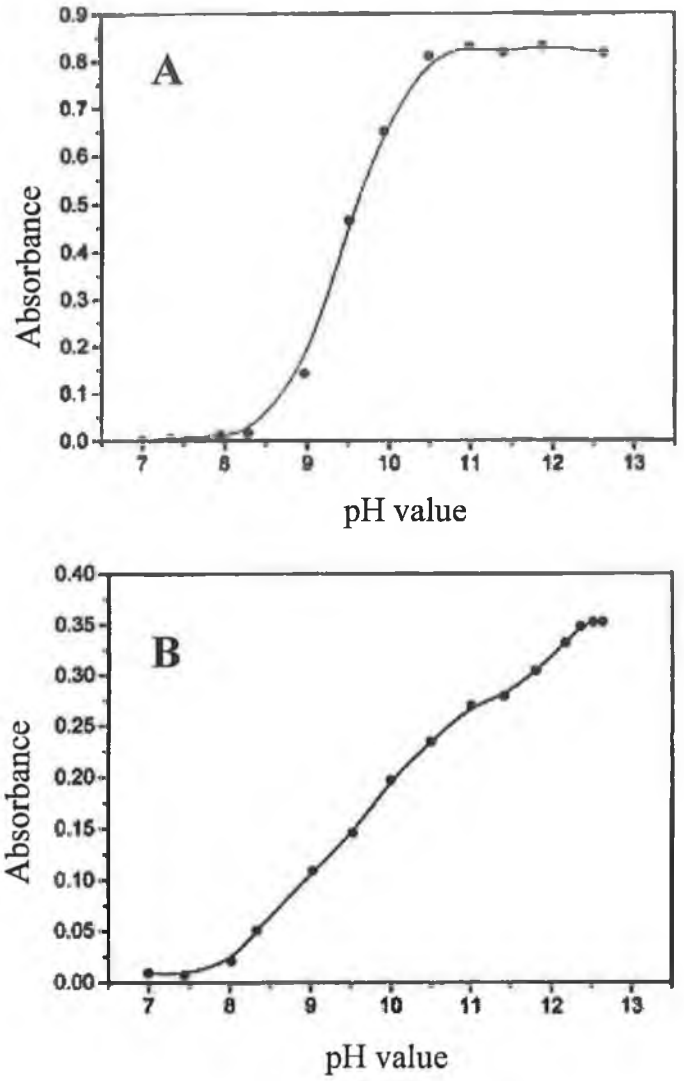

Figure 1: Absorbance as a function of pH values (A) phenolphthalein in solution at 553 nm, (B) immobilised PPF in the membrane at 572 nm [5].

The immobilised PPF had a broader dynamic range then that observed for the free phenolphthalein (pH 8 - 12.5 and pH 8 – 11, respectively), and the response time of the immobilised optical sensor was approximately 30 s. This sensor was capable of detecting a change in pH but could only be used to detect a change in the pH of very basic solutions i.e. between pH 8 and 12. This is a drawback and cannot be used for many sensing applications including biological samples and drinking water samples as these are not present at such high pH values, e.g. the pH of blood is 7.5 and the pH of drinking water is usually between pH 6.5 and 7.5.

Safavi *et al.* [6] developed an optical pH sensor that can measure a wide pH range. This was based on the immobilisation of a mixture of two dyes onto a triacetylcellulose membrane. The dyes were dipicrylamine (DPA) and victoria blue (VB). The detection method used was a spectrometer measurement in transmittance mode. The response curve observed with a change in pH at (A) λ_{max} 437 nm and (B) λ_{max} 621 nm is shown in Figure 2.

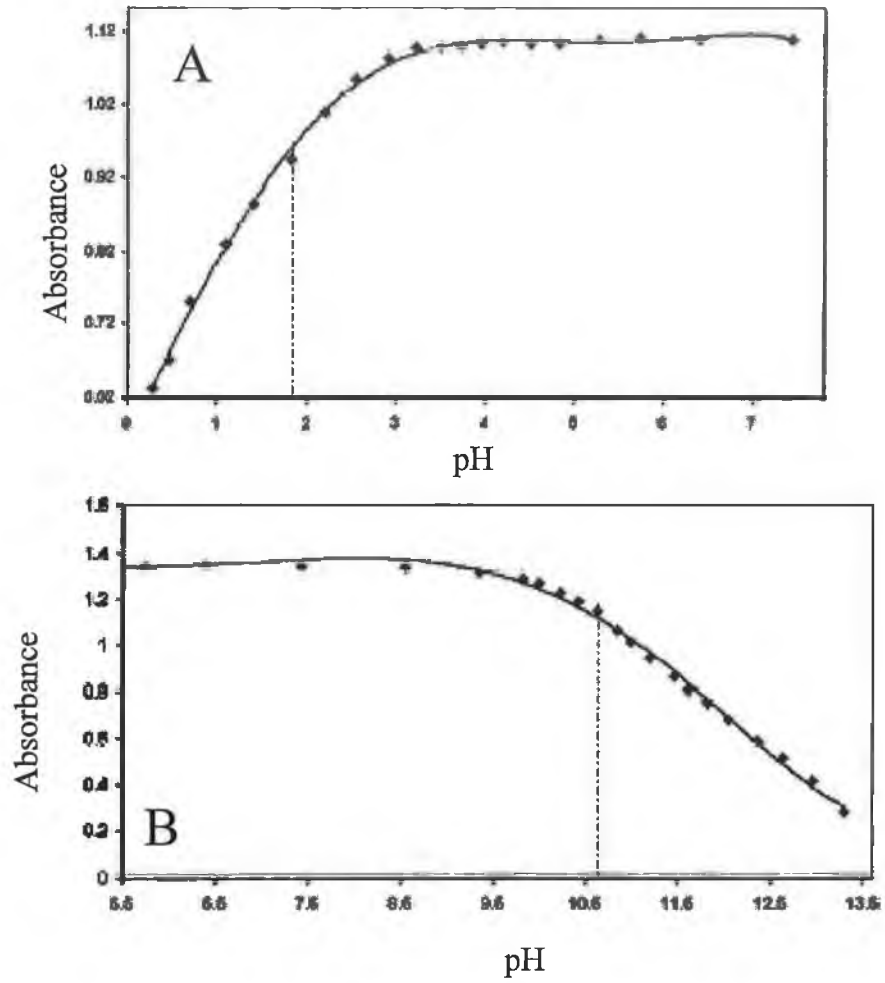

Figure 2: (A) Response of optode to a change in pH (λ_{max} 437 nm), (B) response of optode to a change in pH (λ_{max} 621 nm) [6].

It is clear from the plot obtained by Safavi *et al.* that this method can detect two linear ranges. The lower range is from circa pH 0.3 - pH 2 and the higher range is between approximately pH 10 and pH 13. The advantage of this method of pH

determination over that developed by Liu *et al.* [5] is that the optode has the ability to measure pH at both high and low pH ranges. However a rough estimation of the pH of the sample must be known before analysis, this is due to the fact that if an absorbance reading of example 0.7 is observed this could mean a pH of 12 or 0.8. The drawback is the response time of this method is a lot longer then that obtained by Liu *et al.* The response time observed by Safavi *et al.* to a change in pH from 7.12 - 12.63 was 90 s, whereas the response time observed by Liu for a change in pH from pH 8 - 12 was 30 s.

Ammonia (NH_3) Sensors

Recently there has been a large interest in the monitoring of NH_3 gas. This is mainly due to an increase in environmental awareness and stricter regulations for pollution control. NH_3 monitoring is an important part of industrial, environmental, food and clinical analysis [7]. Optical sensing methods used for the determination of NH_3 are based on either the intrinsic infra-red (IR) absorption of gaseous NH_3 [8, 9] or the selective reaction of a reagent with NH_3 to give a detectable colour [10, 11]. Most of these tests work irreversibly. Reversible sensing has been achieved by incorporating pH sensitive chromophores into an internal buffer placed inside or behind a gas permeable membrane. Changes in pH are reversible as a result of the diffusion of NH_3 in and out of the buffer solution [12].

Werner *et al.* [12] developed an NH_3 sensor that consists of a pH indicator, which is made polymer soluble by converting it into an ionic ion pair contained in a thin silicon membrane and then spread onto a transparent polyester support. The indicator dyes studied were bromophenol blue and bromocresol green, these dyes were selected for the sensing of NH_3 as they have the appropriate pK_a values (3.9 and 4.8 at 20°C, respectively), are water soluble, commercially available and stable. The response times (for 90 % of the total signal change to occur) ranged from 2 - 20 min. depending on a number of factors. These factors included

- The concentration of NH_3 present. At low levels of NH_3 the response time was extremely slow and could extend to 24 hours or more.

- The thickness of the membrane. A 10 μm membrane was found to respond at a third of the rate for a 3 - 5 μm membrane. This was due to a slow diffusion rate of the gas through the membrane.

- The dye loading. At low concentrations of indicator the response time increased. The dynamic range of the sensor is affected by the pK_a of the dye. Therefore by changing the dye, the dynamic range is easily altered. The dynamic range found for the bromophenol blue (pK_a 3.9) was from 0.017 – 17 ppm NH_3 while the dynamic range found for bromocresol green (pK_a 4.8) was from 0.04 to 24 ppm NH_3.

The sensors developed by Werner *et al.* [12] are based on a visual colour change. If a blue decolourisation occurs then this indicates unacceptably high levels of NH_3. This method of NH_3 detection works effectively in the presence of high levels of NH_3 gas but if there are low levels present then the sensor takes a lot longer to result in a colour change resulting in this method of detection being very slow.

CO_2 Sensors

Carbon dioxide is released to the atmosphere when solid waste, fossil fuels (oil, natural gas, and coal), and wood and wood products are burned. CO_2 sensing is required in various fields, such as chemical, clinical and environmental monitoring in order to maintain an appropriate level of CO_2 gas, as CO_2 is known to contribute to about 50 % of the greenhouse effect. Research focused on plasticized and unplasticized ethyl cellulose based CO_2 colorimetric sensors has been carried out by Mills *et al.* [13]. The dye used in these sensors was *m*-cresol purple. The structure of this conjugated compound is shown in Figure 3. A more detailed discussion on conjugated compounds can be found in Chapter 1.

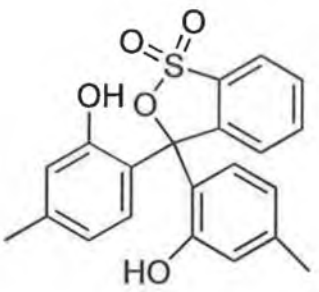

Figure 3: Chemical structure of *m* cresol purple.

This dye is blue in its protonated form and yellow in its deprotonated form. The rate of deprotonation increases with an increase in the ionic strength of the liquid. Mills *et al.* [13] found that the plasticized sensor, when exposed to an aqueous solution, developed a measurable degree of opacity, while the unplasticized sensor film remained clear. However the lack of plasticizer did restrict the rate of diffusion of the CO_2 gas in and out of the sensor membrane. The response time and recovery time of the unplasticized sensor membrane were approximately, 2 s and 23 s, respectively while the response time and recovery time of the plasticized sensor membrane were approximately, 0.5 s and 7 s, respectively.

In 2004 Amao *et al.* [14] developed a CO_2 sensor based on the overlay of the CO_2 induced absorbance change of pH indicating dye α - naphtholphthalein with the fluorescence of tetraphenylporphyrin (TTP) and containing a plasticizer. The CO_2 sensing film was made up of different layers including a CO_2 indicator dye, a phase transfer reagent, a polymer, a plasticizer, a solid support, a reference luminescence dye, another polymer, i.e. α - naphtholphthalein, tetraoctyl ammonium hydroxide, ethyl cellulose, tributyl phosphate, a non luminescent glass slide, TPP, and polystyrene. The instrument used to measure the changes in the film due to the presence of CO_2 was an RF5300-PC fluorescence spectrometer [14]. Different CO_2 standard samples were prepared by controlling the flow rates of CO_2 and nitrogen gas entering the sampling chamber. Using an excitation wavelength of 350 nm and an emission wavelength of 655 nm, it was found that the observed luminescence intensity from TPP increased with increasing CO_2 concentration (see Figure 4).

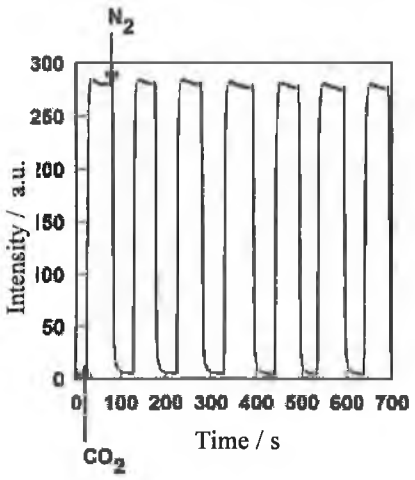

Figure 4: Response time and relative intensity change for CO_2 sensing film switching between 100 % nitrogen and 100 % CO_2 [14].

The response time and recovery time from switching from 100 % nitrogen to 100 % CO_2 was 5 s.

Both methods [13 & 14] for the determination of CO_2 proved to be successful, a more transparent membrane was observed when there was no plasticizer present in the membrane formulation, however the lack of plasticizer resulted in a longer response time and recovery time being observed.

Fibre Optic Sensors

Optical fibres have been adapted for chemical sensing. They were initially designed and developed for the communications industries but are synonymous with optical detection for chemical sensing [15, 16, 17]. The majority of these optical sensors are prepared by immobilising a dye onto the surface of the fibre [18].

pH Determination

Fibre optic pH sensors form one of the major classes of fibre optic chemical sensors [19, 20]. They are extensively used for in-vivo and in-vitro applications, especially in ground water analysis and in blood pH measurements [21, 22]. They make use of a colorimetric based technique, where a pH sensitive dye is coated onto a portion of the optical fibre; a dye colour change corresponds to a change in the pH of the sample. An example of the light path taken in a fibre optic is shown in Figure 5 [23].

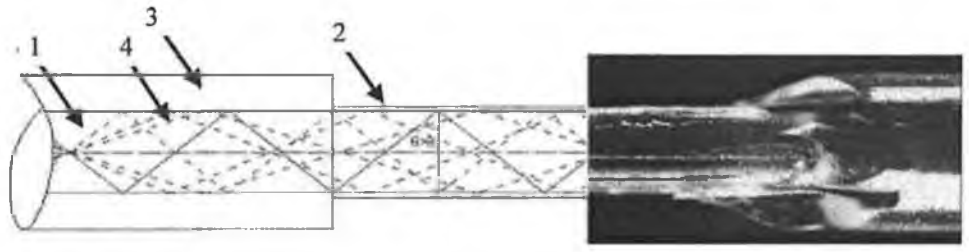

Figure 5: Optical fibre with cladding removed- schematic and picture (1) fibre core, (2) original cladding, (3) buffer, (4) typical propagation modes. Picture is actual fibre with cladding removed [23].

Sotomayor *et al.* [24] developed optical sensors for the measurement of pH. These sensors worked by measuring the diffuse reflectance of a conductive polymer in the visible region of the spectrum. The pH sensitive material used was poly (o-methoxyaniline) doped with *p*-toluene sulfonic acid (PoAnis / TSA), which was immobilised, either on, or within a polymeric structure. Two configurations of the optode were studied. The first optode was assembled using a bifurcated (splits into two parts) bundle of borosilicate optical fibres. The sensing phase was made from PoAnis/TSA and cellulose acetate, which was affixed at the end of the bundle of fibres. The second optode was built using two cables of optical fibres, each having a single-phase fibre with 1.0 mm diameter. The two cables were placed into the Perspex box, together with a pH sensitive layer. In

this case the sensing phase of the optode was a film of PoAnis/TSA absorbed on polyethylene. Figure 6 shows a schematic of the pH optode.

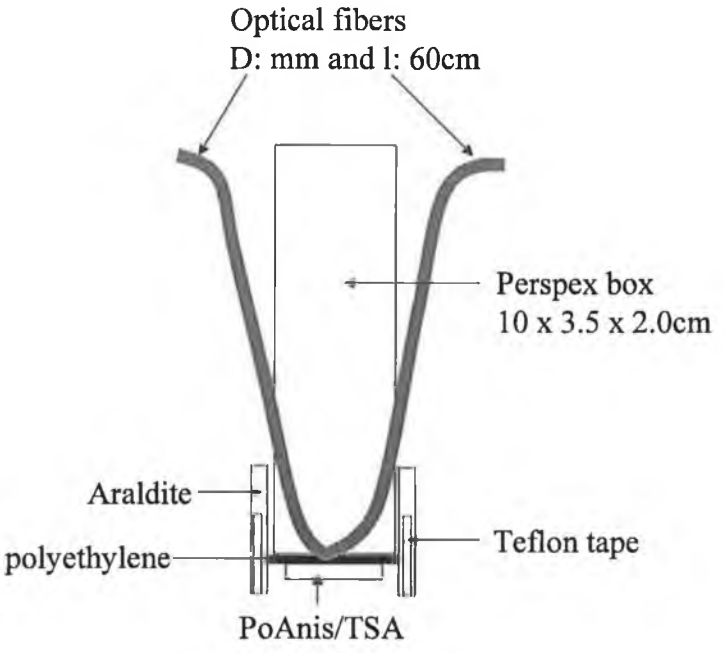

Figure 6: Schematic of pH optode based on PoAnis/TSA adsorbed on polyethylene [24].

The first optode resulted in a dynamic range of pH 4.9 - 10.5 with a precision of ± 0.01. The response time (for a 90 % change from acid to base) was 5 min. and the recovery time was 22 min. Using the second optode configuration the dynamic range was found to be pH 2 - 10 and the response time (for 90 % change) was also 5 min. The optode with the PoAnis / TSA absorbed in the polyethylene resulted in a broader dynamic range then that of the PoAnis / TSA and cellulose acetate affixed at the end of the bundle of fibres. However both configurations had a comparatively long response time (5 min.) to a change in the pH of a solution (acid to base).

Jones *et al.* [17] developed a pH sensor, which incorporated congo red in a porous cellulose film. A flow cell (Figure 7) was designed for the analysis of the pH.

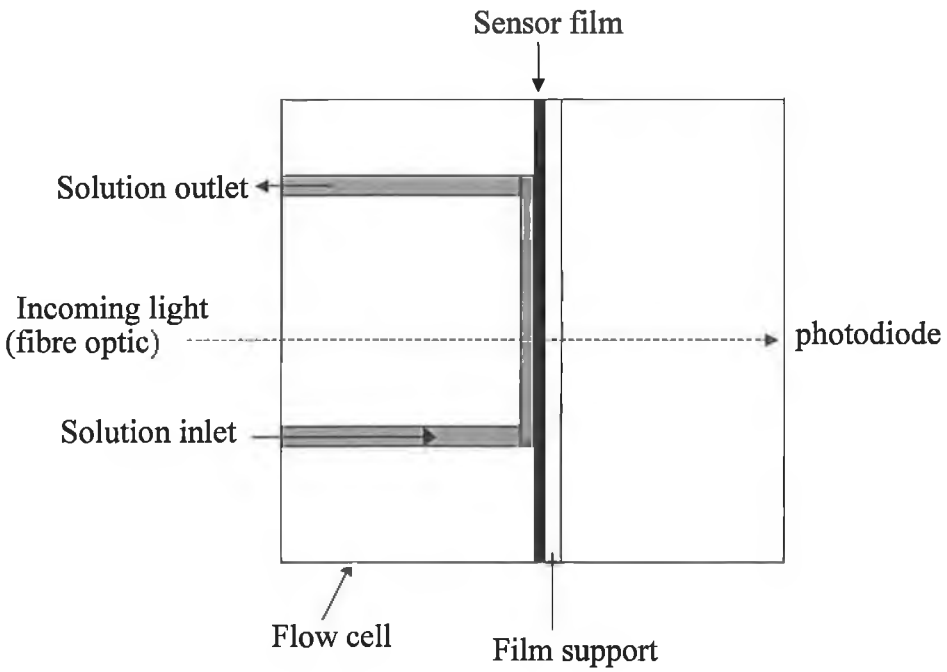

Figure 7: A simplified schematic diagram showing the flow cell set up for the thin film [17].

The thickness of the film was 2.9 ± 0.1 μm. A solution was pumped through the solution inlet of the flow cell. Its pH was varied by injection of buffered solutions. The response time was found to be less then 1.5 s as shown in as shown in Figure 8.

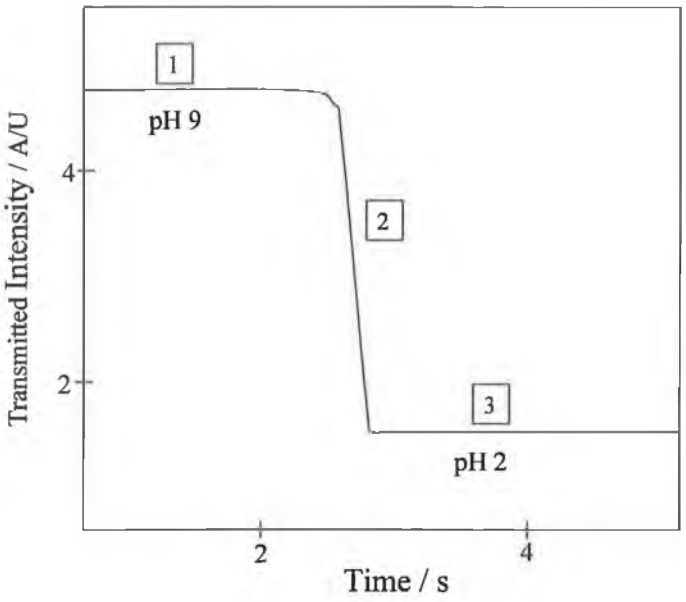

Figure 8: Response time of pH sensor constructed by the immobilisation of Congo red at hydrolysed cellulose acetate. (1) equilibrated response at pH 10.9 solution, (2) injection of pH 2 solution, (3) equilibrated response at a pH of 2.0 [17].

Due to the fast diffusion through miniaturised channels this particular set up design was found to be 10 times faster than various other optical methods reported [25, 26].

Bruno *et al.* [27] criticised the use of the membrane deposition method and the use of bright LEDs (laser diodes) with pH indicators due to their poor reproducibility. They suggested that fluorescence is a better method of optical sensing for pH because of the higher selectivity, lower volume requirements and increased sensitivity. A six channel, solid state, miniaturised fluorescence sensor using a blue LED as the excitation source and a photodiode as the detector was constructed. However, due to the poor reproducibility of the dye immobilisation, leading to different thickness of dye, the use of this device was limited.

More recently, a submersible autonomous pH sensor for natural waters was developed (SAMI –pH instrument) by Martz *et al.* [28]. They used a sulfonenphthalein dye (cresol red) as an indicator. The system used a small, low power, solenoid pump and a 3-way valve to control the amount of sample and

indicator dye. A gas impermeable reagent bag that contained cresol red was enclosed in a PVC box. This was attached to the side of the main housing. The light source used was a tungsten lamp. A photodiode was used as a detector. A schematic of the set up used is shown in Figure 9.

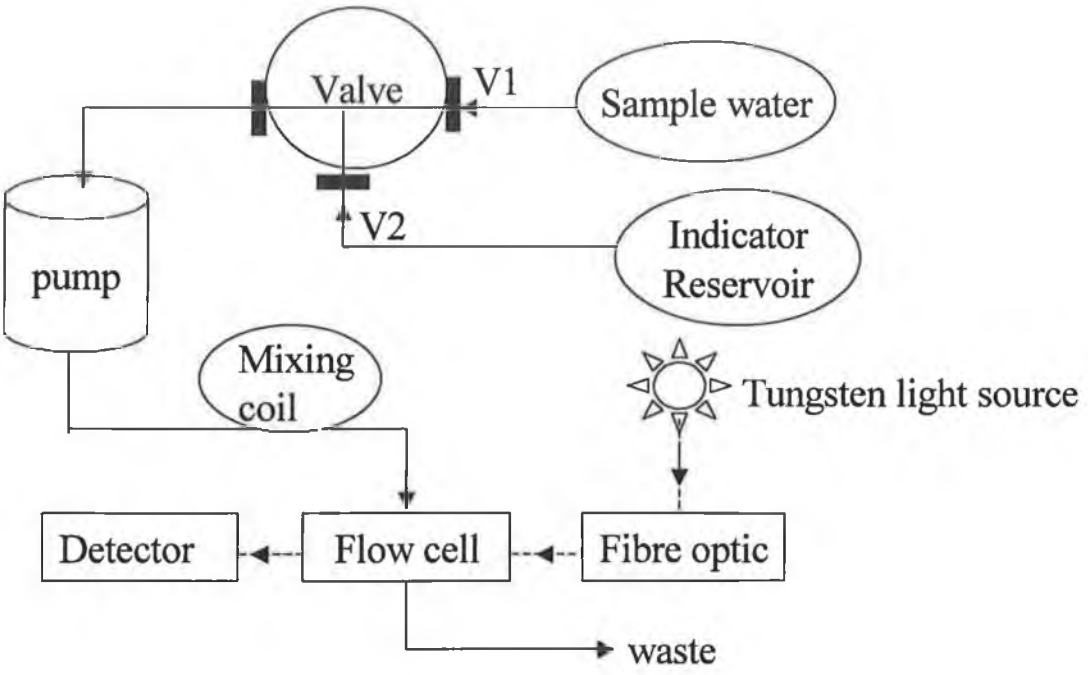

Figure 9: schematic diagram of submersible pH measuring instrument [28].

The instrument was programmed to monitor the pH of a water sample every 15 min. By switching the valve to V_2 and activating the pump the measurement was taken. The 3-way valve was switched between the water sample and the indicator reservoir. The pump pulled approximately 50 μL of indicator into the flow line. Pulses of the water sample followed this. The indicator and the water sample were driven towards the mixing coil where efficient mixing occurred. Table 1 shows a summary of the performance of the instrument.

Table 1: Specification of SAMI pH instrument [28]

Performance Criteria	Description	Result
Relative accuracy	Agreement between the UV –Vis and SAMI-pH	-0.003 ±0.004 pH unit
Dynamic range	Working range of the indicator	7.61 – 8.73 pH units
Response time	Time required to detect 99% of a pH change	~5 min.
Flush time	Time required to completely flush the indicator from the line	~6 min.
Indicator consumption	Assuming 48 measurements per day at 50μL per pH measuring cycle	~ 1 L per year

Ammonia Determination

Fibre optic NH_3 sensors based on the changes in absorbance of *p*-nitrophenol [29] and the changes in fluorescence of several pH indicators [30] have been described for the determination of NH_3 in aqueous solutions.

Caglar *et al.* [31] described a fibre optic probe used for the determination of NH_3 vapour. It was based on the changes of a pH indicator dye (bromothymol blue, BTB), which was immobilised onto a hydrophilic polymer support and attached to the end of an optical fibre, when it comes in contact with an atmosphere containing NH_3 vapour. For the measurement a three-necked vessel was used, for injecting the NH_3 vapour, the optical probe and the introduction of air or other vapours when required. The probe was constructed by positioning the optical fibres against a polymer support, which is held in position by a porous Millipore

PTFE membrane. After the probe was constructed the BTB was immobilised onto the probe by immersing the probe in a solution of BTB and methanol for 6 hours. A schematic of the optical system used for the detection of NH_3 is shown in Figure 10.

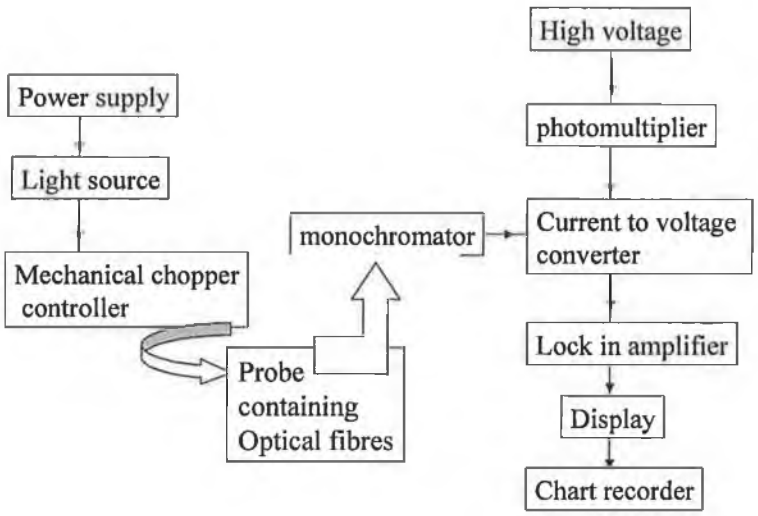

Figure 10: Schematic of fibre optical based system used for the detection of ammonia [31].

The limit of detection was 1.5 x 10^{-3} mol / L or 25.5 ppm. This is not a very low detection limit and is in fact higher then that of the threshold limit of NH_3 in water stated by the EPA (0.3 ppm) [32]. Vapours of hydrazine hydrate; trimethylamine and dimethylamine were all found to interfere with the measurement causing a decrease in the reflectance values.

Lead Detection

Yusof *et al.* [33] developed a novel flow through optical fibre reflectance sensor based on immobilised gallocynine for the detection of lead ions. The fibre optic based probe was built using two Teflon tubes. Figure 11 shows a schematic of the probe.

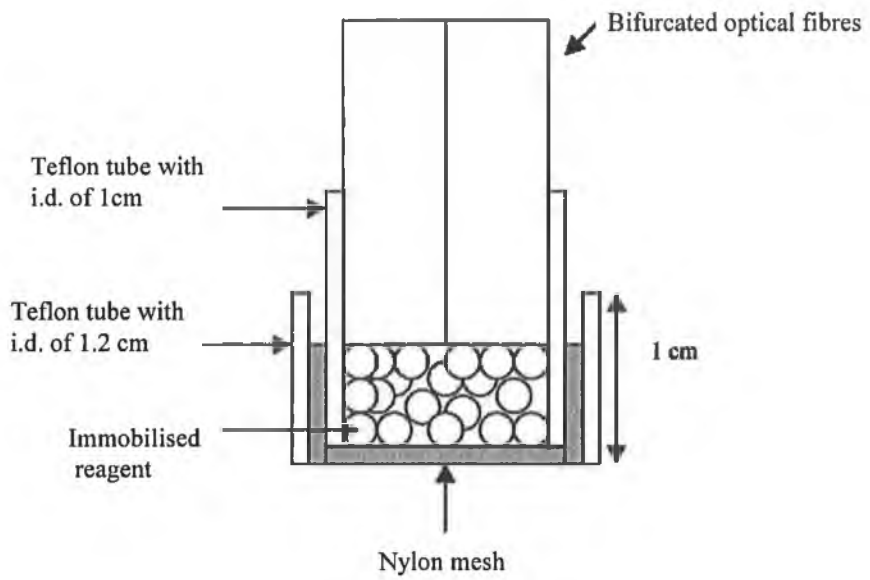

Figure 11: Schematic of fibre optic based probe for the detection of lead [33].

This probe was then incorporated into a flow cell system. A schematic of the instrumentation set up is shown in Figure 12. The lead was introduced to the carrier line through an injection port with a sample loop of 500 μL.

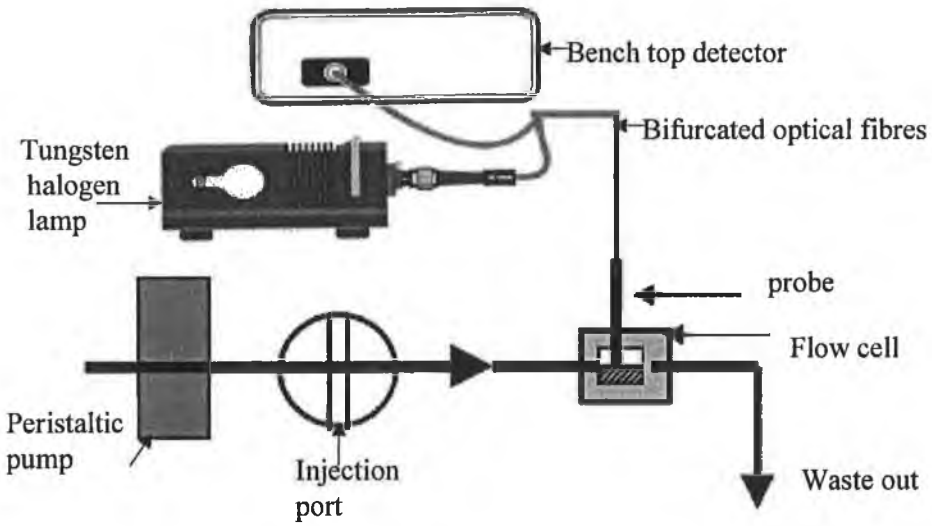

Figure 12: Schematic of instrumentation used for the detection of lead [33].

This configuration resulted in a linear correlation over the concentration range of 0.1 - 100 ppm lead with a limit of detection of 0.06 ppm. The reaction was reversible when acidified potassium nitrate (KNO_3) was used as the regenerating solution. This device provided a good broad linear range for the detection of lead, however, the response time of the device was relatively slow (5 min.) and Al (III), Ag (I), Cu (III) and Hg (II) were all found to interfere when present at 10ppm.

Optical Waveguides

A waveguide can be defined as any structure capable of guiding the flow of electromagnetic energy in a direction parallel to its axis, while substantially confining it to a region either within or adjacent to its surfaces [34]. This waveguide usually consists of a core (Si) surrounded by a cladding (SiO_2) with a lower refractive index than that of the core [35]. Light travels by total internal refraction at a critical angle that can be calculated using equation 1.

$$Sin\ \vartheta_{critical} = \frac{\eta_2}{\eta_1} \qquad \textbf{Equation 1}$$

The actual value of the critical angle is dependent upon the two materials on either side of the boundary. Where η_1 is the refractive index of the first material, η_2 that of the second, $\theta_{critical}$ is the angle at which total internal reflection will occur.

When a ray of light passes through the core of an optical waveguide and if no light escapes to the cladding then this is known as a bound ray. This results in the ray propagating indefinitely without any loss of power. A schematic diagram showing the pathway taken by a bound ray is shown in Figure 13.

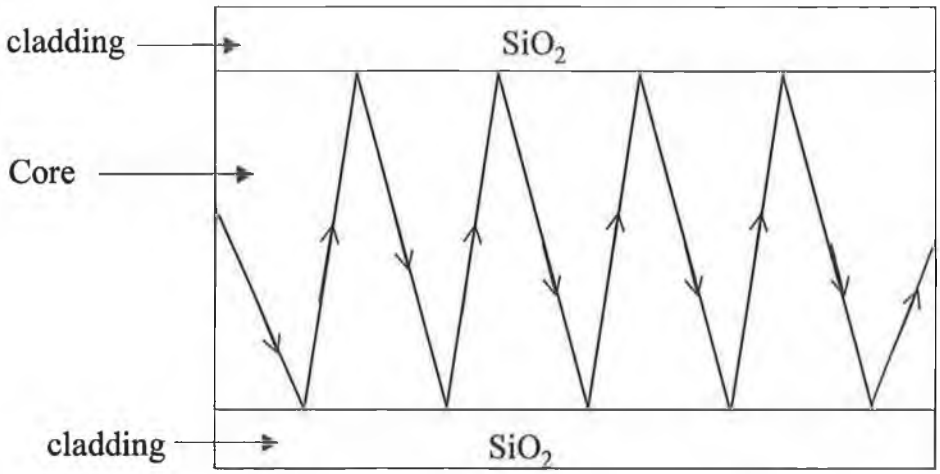

Figure 13: Schematic of bound ray.

The ray is bifurcated if one part is reflected and the other is transmitted to the cladding. Some of the energy is lost to the cladding as is schematically shown in Figure 14.

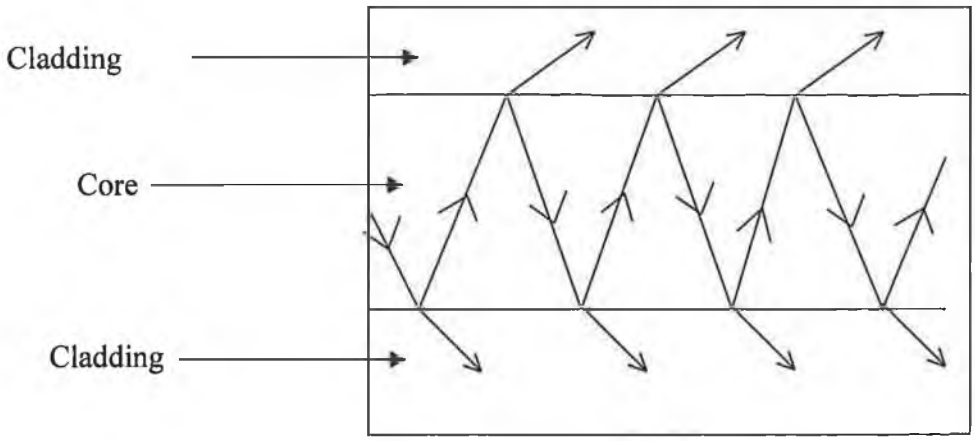

Figure 14: Schematic of bifurcating ray.

Optical waveguides have been used in the fabricating optical devices in various fields. For example, optical waveguides used for biological or chemical sensing have several advantages over other forms of sensors, such as the potential for high

sensitivity [36, 37] and low cost [38,39]. The use of an optical waveguide to detect ammonia gas is commonly based on evanescent field or guided wave absorption (guided waves occur when light propagates along or is constrained by the physical boundaries of a waveguide) and often involves pH sensing dyes for transduction [40, 41].

Optical waveguides have been used in the fabrication of optical devices in various fields. Optical waveguides that have been used for biological or chemical sensing have several advantages over other forms of sensors, such as their potential for high sensitivity [42, 43] and low cost [44,45]. The use of an optical waveguide to detect NH_3 gas in usually based on evanescent field or guided wave absorption (guided waves occur when light propagates along or is constrained by the physical boundaries of a waveguide) by pH sensing dyes [46, 47].

Yumit *et al.* [48] fabricated an optical waveguide that has been used in the detection of NH_3 based on a composite titanium dioxide film with K^+. The sensing device consisted of three major components; a substrate, a waveguide layer and a sensing layer. Bromothymol Blue (BTB) was used as the sensing layer. Figure 15 shows a schematic of the composite optical waveguide (OWG) sensor. A titanium dioxide film was chosen as the thin film layer due to the fact that it is optically transparent, stable and has a high refractive index. This results in a very sensitive system. The TiO_2 that is sputtered on to the OWG is chemically passive so this cannot be used as a sensing layer. Therefore the bromothymol blue (BTB) sensing layer was necessary and therefore coated onto the TiO_2 film.

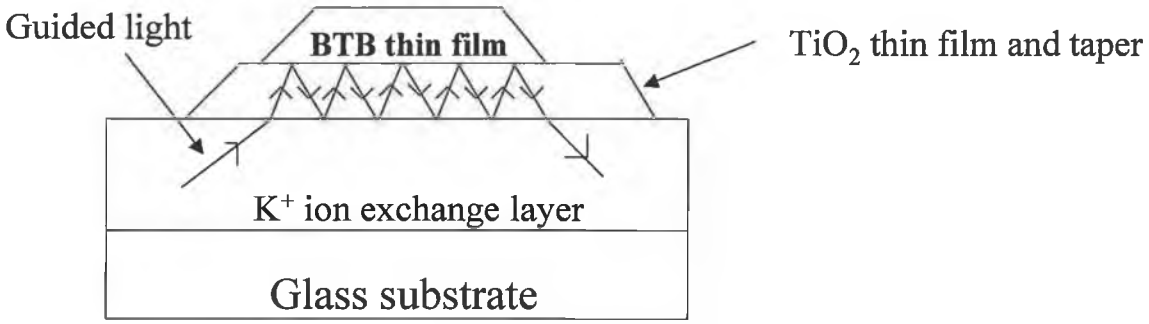

Figure 15: Schematic of modified optical waveguide using BTB film [48].

The sensitivity of the optical waveguide critically depends on the thickness of the sensing layer. Thick films result in low sensitivity. Very thin films (<46 nm) result in no measurable interaction observed between the light wave and the film. The set up used by Yumit for the sensing of NH_3 gas is shown in Figure 16.

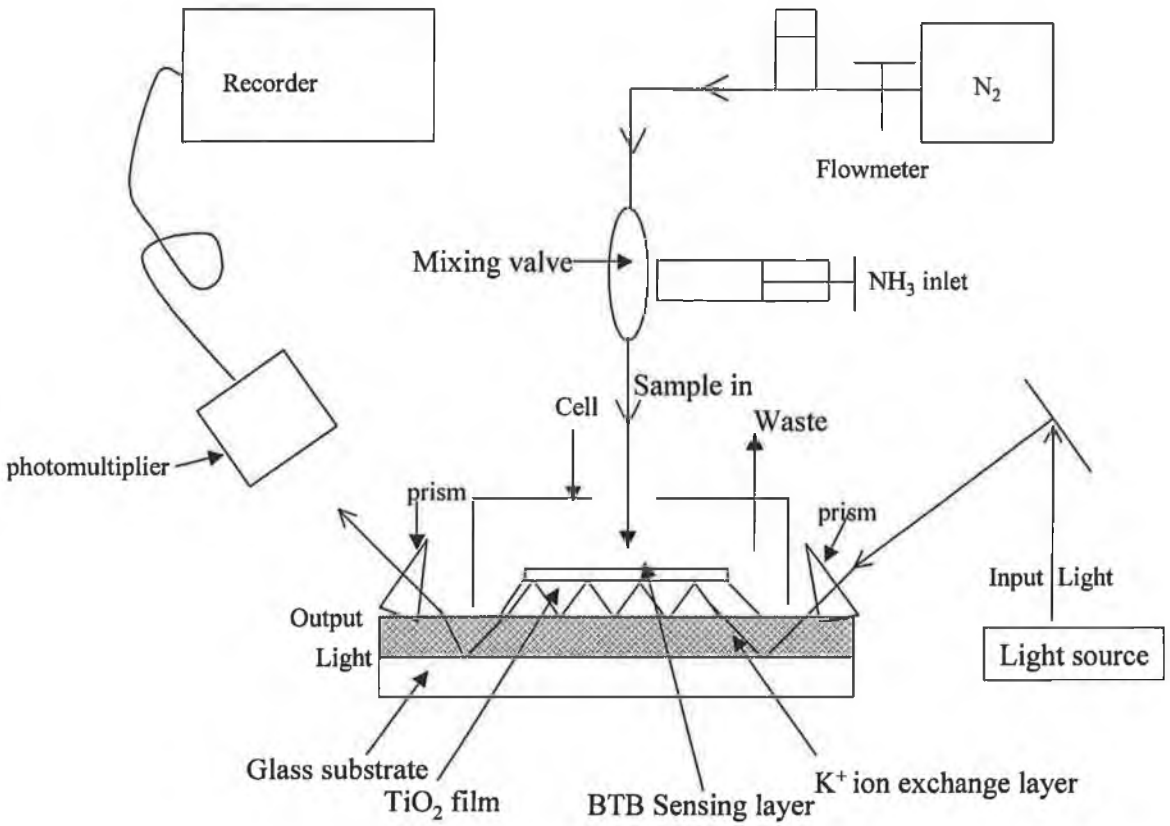

Figure 16: Schematic of gas sensing system [48].

A gas syringe was used to inject constant volumes of NH_3 into the flow cell. Standard NH_3 gas was obtained by vaporising a given amount of a 28 % NH_3 solution inside a 1000 cm^3 standard vessel, which was filled with pure N_2. Different amounts of the desired concentration of NH_3 gas were obtained by diluting the standard NH_3 gas with pure N_2 in a second vessel. This optical method for the detection of NH_3 gas was reversible. The response and recovery time were dependent on the flow rate of the carrier gas and were estimated to be between 1 and 30 s. The system can detect sub- ppm levels of NH_3.

Optical Devices using LEDs

Basic Colorimeters

As part of a cost effective teaching project a low cost, microwell colorimeter was designed and developed [49]. This device was used for the determination of Cu^{2+}. The instrument comprised an LED (green) as the light source (due to its inherent long life, low cost and low operating expense) and a photo resistor as the light detector. A schematic of the microwell colorimeter is shown in Figure 17. This device operated in transmittance mode.

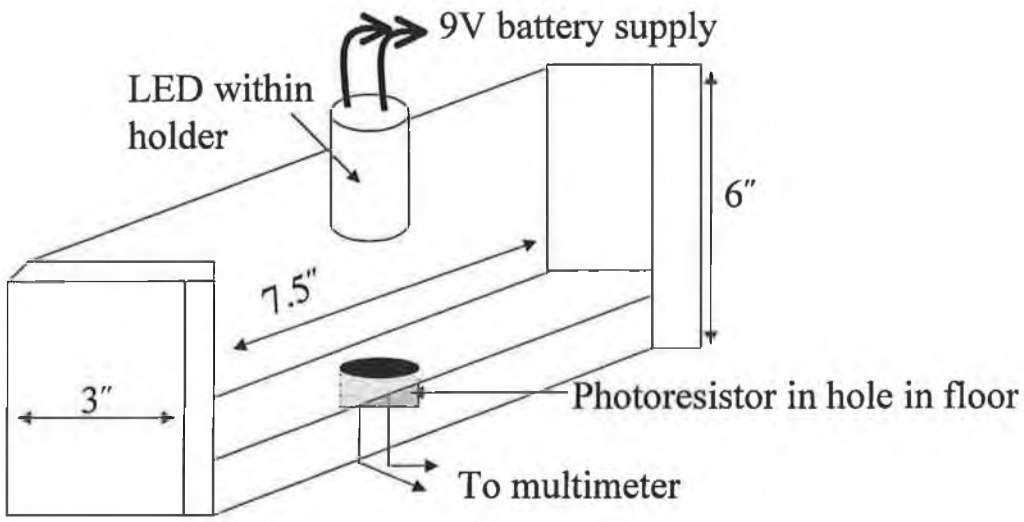

Figure 17: Schematic of microwell colorimeter [49].

A concentration range of 0.005 - 0.03 M Cu^{2+} was found for this device. This was not a very wide working range. More recently (2002) [50] another LED based device was developed to determine the molar absorbtivity of permanganate. This colorimeter was also based on the use of an LED as the light source and a photo resistor as the light detector but operated in transmission mode. A schematic of the film canister colorimeter is shown in Figure 18.

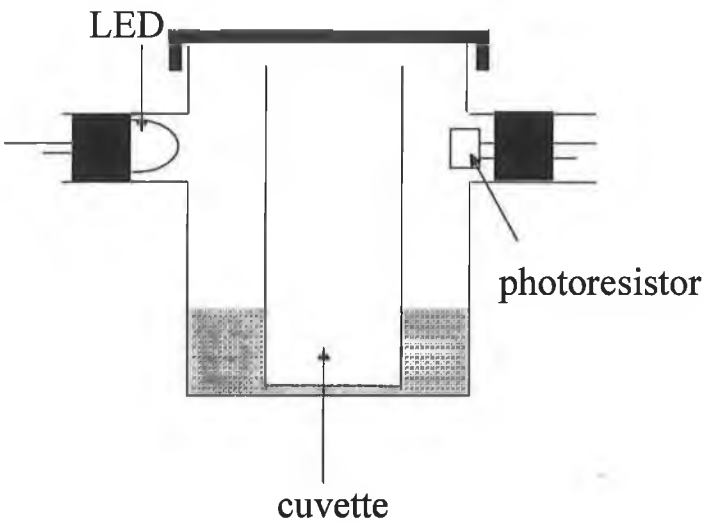

Figure 18: Schematic of film canister colorimeter [50].

A 1 KΩ resistor was placed in line with the LED to function as a voltage circuit divider. A 9 V battery powered the LED. As light struck the photo resistor its resistance decreased, which led to an increase in the voltage across the fixed resistor. The measured voltage mimicked changes in the cuvette. This change in voltage across the fixed resistor was recorded using a multimeter.

The optimum wavelength of the LED was 565 nm with the λ_{max} for a 3 x 10^{-4} M permanganate solution of approximately 540 nm but this solution had a broad absorption wavelength (490 nm – 570 nm). The molar absorbtivity found for the permanganate solution using the LED based device was found to be 1010 ± 71 M^{-1} cm^{-1}. The actual molar absorbtivity for this solution is 1328 M^{-1} cm^{-1} at 540 nm. There is a 32 % error present in the calculation of the molar absorbtivity of the

permanganate using the LED based device. The reason for this may be due to the difference in the dominant wavelength of the LED and the maximum absorbance of the solution. Also the difference in the molar absorbtivity value may be due to the polychromatic nature of the LED.

Use of LED as a Light Source For the Detection of Ammonia.

Radislav *et al.* [51] carried out a study with pH indicator dyes based on NH_3 gas sensors. They varied the conditions of temperature and humidity and observed the effects that these conditions had on a polymer film. The sensing system used is shown in Figure 19. The light from the LED was passed through a sample chamber containing the polymer dye film in a gas cell, and the emerging radiation was detected by the photodiode.

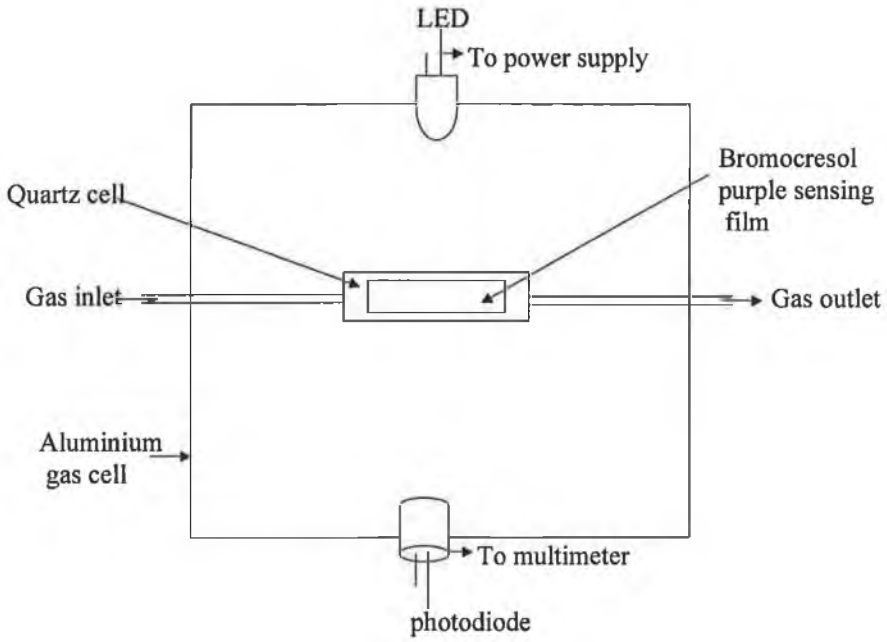

Figure 19: Schematic of ammonia sensing device [51].

The difference in the absorption spectra for bromocresol purple dissolved in water and immobilised on poly (methylphenylsiloxane), PMPS, film was also discussed. The results showed that the immobilisation of the indicator dye modified the

spectral properties of the dye, in particular the shape and position of the absorption band. It was found that temperature variations in the range of 20 – 40°C did not influence the absorption band and humidity changes produced a distortion of the peak profile. The peak position shifted towards a shorter wavelength with an increase in humidity.

Optical Device using Light Dependant Resistor (LDR) as Detector with LED as Light Source

Matias *et al.* [52] developed a very simple and low cost reflectometer for diffuse reflectance measurements. They used LDR as the detector and an LED as a light source. A schematic diagram of the diffuse reflectometer is shown in Figure 20.

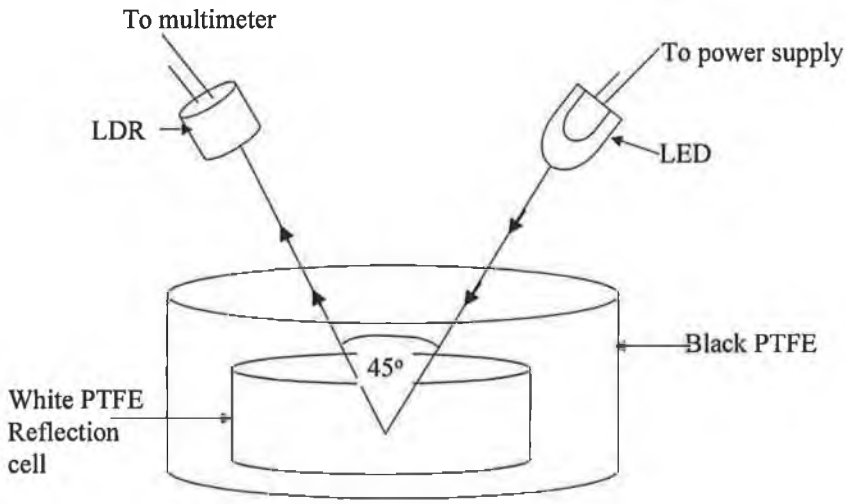

Figure 20: Schematic diagram of diffuse reflectometer [52].

The outer shell of the device was fabricated in black PTFE while the reaction and reflection cell were made from white PTFE. The LED and LDR were fixed with silicone glue to eliminate any movement. The results obtained from the device showed a very good level of accuracy and precision. Quantitative analysis of

nickel was carried out using dimethylgloxime as the colorimetric reagent. A set of standard nickel solutions was prepared ranging in concentration from 5.0×10^{-5} - 1.25×10^{-3} mol l^{-1}. The reflectance was measured for scarlet nickel dimethylglyoxime (Ni $(DMG)_2$) precipitate. The device gave an RSD of 6 %. This device was inexpensive to produce and because it is portable in-situ measurements were achievable.

Optical Devices using Multi Channel LEDs as Light Source

Aluminium Detection

Hauser *et al.* [53] used a device, which consisted of several LEDs to function as a spectrometer (Figure 21). A fibre optic coupler guides the light emitted from all seven LEDs into a single measuring cell.

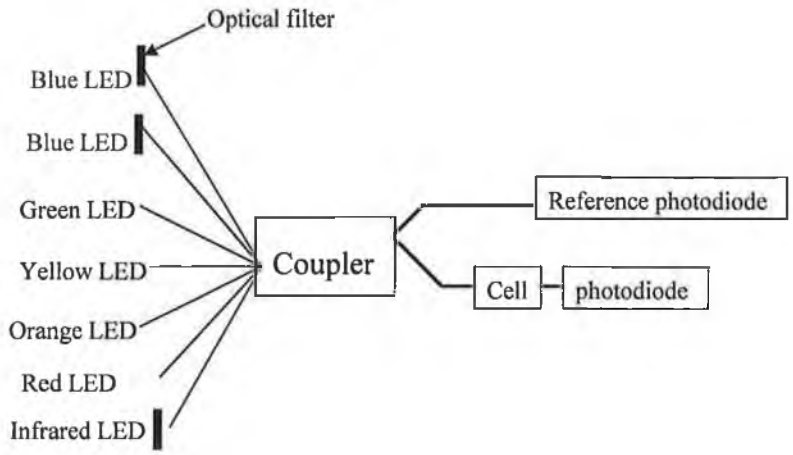

Figure 21: Simplified schematic diagram of electronic circuit of the instrument [53].

The LEDs ranged from, dominant λ_{max} of emission band of approximately 380 – 780 nm. Optical filters were used to narrow the emission band of some of the

LEDs. A rotary switch selected one of the seven LEDs. The system used azurol S for the detection of aluminium. The complex absorbed at 546 nm and the emission, dominant λ_{max} of the LED was found at 563 nm. The advantage of using seven LEDs over one or two is that depending on the colour of the complex to be detected the appropriate LED can be selected.

Thionine Detection

Cantrell *et al.* [54] developed a new type of spectrometer known as the "SLIM" spectrometer. SLIM stands for simple, low power, inexpensive, microcontroller – based spectrometer. In this paper a discussion of the design and fabrication of a miniature spectrometer based on modern semiconductor technology is given. The SLIM used three LEDs as light sources, a photodiode as a detector, a flow cell, a battery, a programmable microprocessor, a clock, a data logger to record information, a computer and a user interface. All of the components listed were integrated on one circuit board. The analyte used in the flow cell was thionine. The device measured the change in the light intensity as a sample passed through the flow cell. The device operated unattended in data logging mode. The microcontroller turned on the light source LED and the intensity was measured as the frequency output from a photo detector chip. The sample solution was held between two sheets of acrylic in a defined space between two O-rings. A schematic of the SLIM device is shown in Figure 22.

A

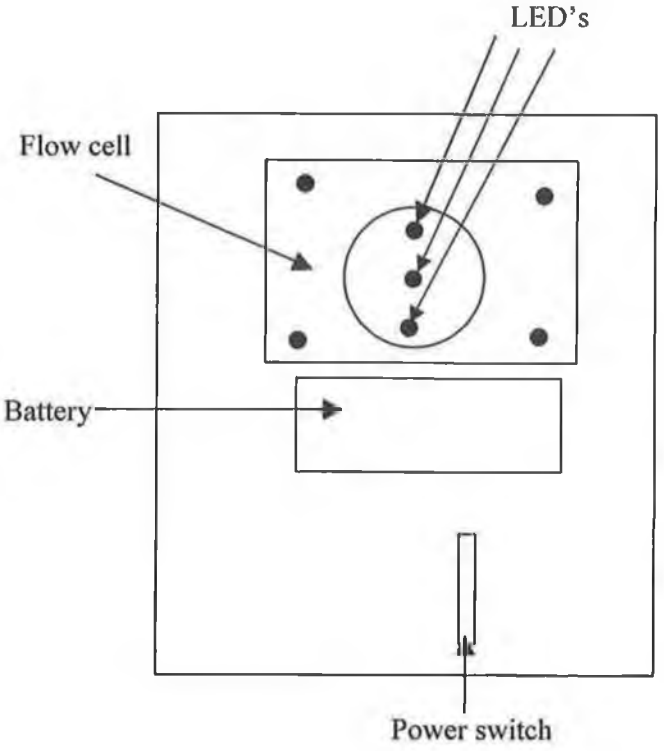

B

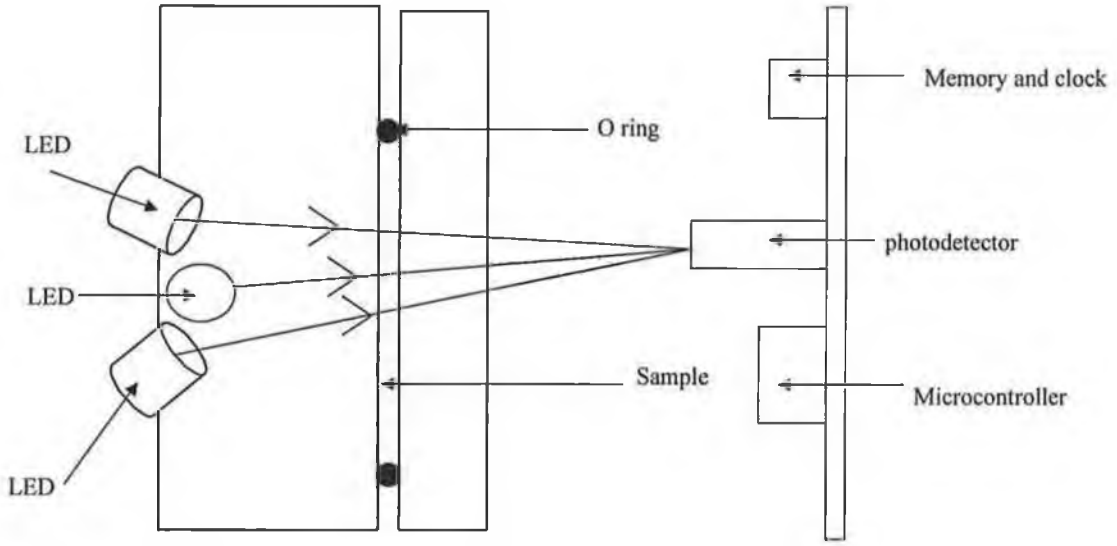

Figure 22: Schematic diagrams of the instrumental diagram indicating the layout of the basic components of the solid-state spectrometer. A = top view, B = side view [54].

The internal volume is circa 500 μL. There were inlets / outlet holes to facilitate for fluidic movement of the sample onto and around the chip. One side of the flow cell was thicker than the other. The thicker side contained three holes for the LEDs. The centre LED was at 90° from the opposite side of the cell while the other two LEDs were at 30° angles. The photo detector was placed opposite the centre LED so it received light from all 3 LEDs. The LEDs used for this experiment were red, yellow-orange and blue. The total cost of this integrated circuit and LEDs came to $25. The spectrometer did not collect data as an absorbance measurement but as an intensity signal proportional to the transmission. The spectrometer was covered in black felt to minimise the noise associated with ambient light. Thionine solutions were used to calibrate the system. The system was capable of detecting down to 0.2 μM of thionine with a 1.5 cm optical path length.

Aluminium, Zinc and Iron Detection

Trojanowicz *et al.* [55] have developed a flow photometer incorporating an LED as a light source for the simultaneous determination of Al (III), Zn (II) and Fe (II) using xylenol orange as the colorimetric reagent. A schematic of the optical device is shown in Figure 23.

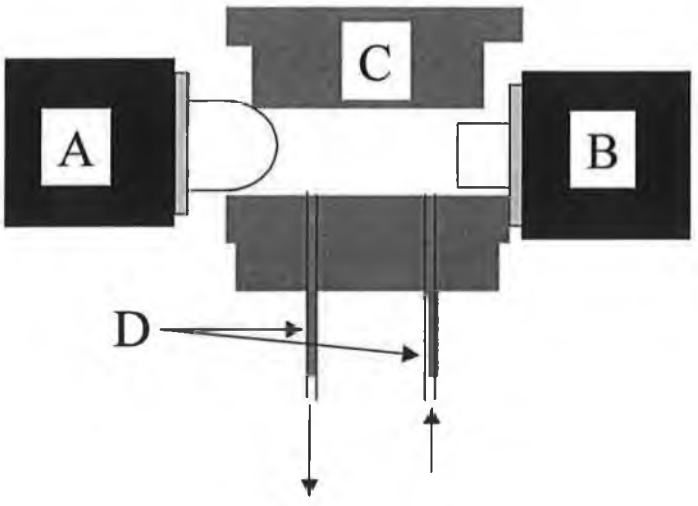

Figure 23: Schematic of flow through cell, (A) LED, (B) photodiode, (C) stainless steel body, (D) 1.5cm light path (1.5mm diameter) [55].

The principle operation of the LED photometer is based on the sequential switching of three diodes with emission wavelength maxima at 563, 580 and 638 nm. The operation was software controlled by generation of an appropriate voltage. The switching frequency was limited by the amount of time necessary for the diode, once switched on, to reach its maximum light intensity. It was found that the red diode takes the longest to reach its maximum light intensity (8 min.). The device was found to have a linear range of 0.25 – 25 ppm (Al (III)) and 0.2 – 30 ppm (Zn (II)). However, the optical device failed to determine the presence of iron in a mixture containing Al (III), Zn (II) and Fe (II).

LED Based Phase Fluorimetric Oxygen Sensor.

Phase fluorimetry is a method of measuring the luminescence lifetime of a fluorophore. When a fluorescent material is excited by light the resulting fluorescence is phase shifted relative to the excitation signal. This phase shift is dependant on the luminescence lifetime of the fluorescent material. Keefe *et al.* [56] developed a LED based fluorimetric oxygen sensor where oxygen was used as a quencher material and the concentration of oxygen was determined by measuring the phase shift of the emission relative to the excitation signal in the presence of the oxygen. Ru^{II}-tris (4,7-diphenyl-1, 10-phenanthroline) is used as the colorimetric reagent due to its long excited lifetime obtained with a ruthenium polypyridyl complex. A schematic of the experimental set up is shown in Figure 24

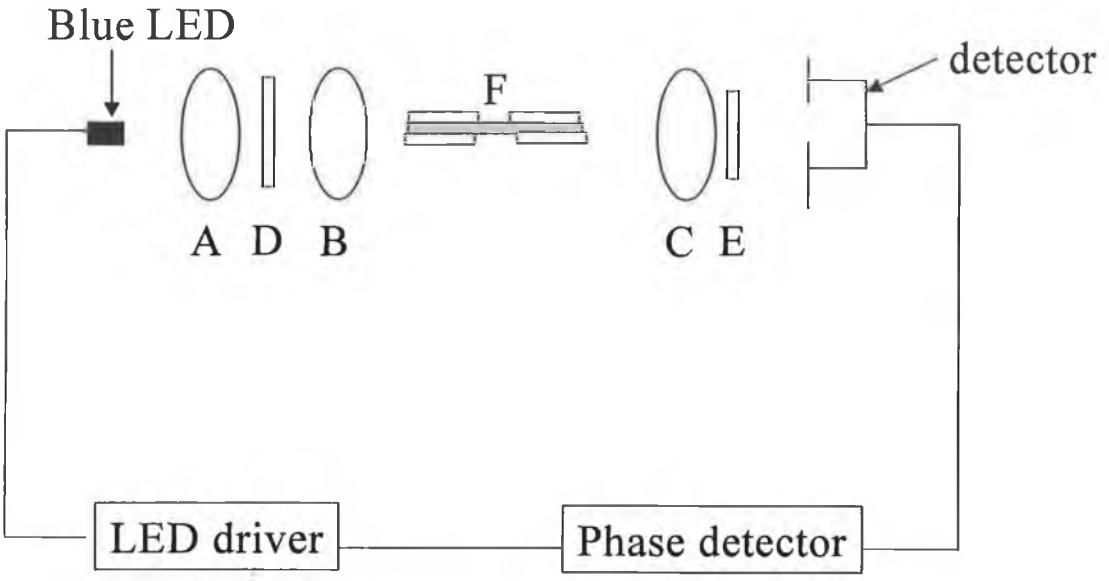

Figure 24: LED based phase fluorimetric measurement (A) collimating lens, (B) launching lens, (C) collecting lens, (D) short wave pass filter, (E) long wave pass filter and (F) sensing optical fibre in glass cell [56].

The sensing fibre is coated with a sol-gel derivative silica containing Ru $(Ph_2phen)_3^{2+}$. The λ_{max} of the ruthenium complex is 450nm with an emission λ_{max} of 610 nm. The LED used was a blue LED, which has a dominant wavelength of 470 nm (resulting in significant overlap with the absorption spectrum of the complex). The light emitted from the LED was passed through a short wavelength filter ($\lambda_{cut\ off}$ = 505 nm) and then launched into the optical fibre (F in Figure 24). A fraction of the excited fluorescence was coupled back into the detector by passing through a different filter ($\lambda_{cut\ off}$ = 550 nm) and was detected by the detector (photomultiplier tube). The concentration of oxygen was varied by diluting the oxygen with nitrogen. The optical device has proved to be successful in the determination of oxygen. Studies were carried out, by subjecting the system to 100% oxygen, then replacing the oxygen with 100 % nitrogen. The response time found for the system (when all adjustments of mass flow controllers were accounted for) was 5 s. The sensor exhibited greatest sensitivity at the lower oxygen concentration ranges (0 – 10 %). This could lead to problems when high oxygen levels are present.

From the research carried out on the use of LEDs integrated into an optical sensing device it can be concluded that these devices offer an attractive alternative method to optical sensing. They have proven to result in accurate and sensitive data in relatively short response times (in the order of s.) while significantly reducing the overall cost of the device

References

[1] A. A. Ensafi, A. Kazemzadeh, M*icrochemical Journal*, 1999, **63**, 381.

[2] Chan.M. Chan, C.S. Fung, K.Y. Wong, W. Lo, *Analyst*, 1998, **123**, 1843.

[3] W. E. Morf, K. Seiler, B. Lehmann, c. Behringer, S. Tan, K. Hartman, P.R. Sorensen, W. Simon, *Ion selective electrodes*, Pergamon Press, 1989, **5**, 115.

[4] T.J. Cardwell, R.W. Cattrall, L. W. Deady, M. Dorkos, G. R. O'Connell, *Talanta*, 1993, **40**, 765.

[5] Z. Liu, F. Luo, T. Chen, *Anal. Chim. Acta*, 2004, **510**, 189.

[6] A. Safavi, M. Bagheri, *Sens. Actuatos B*, 2003, **1**, 6889,

[7] M.Trinkel, W. Trettnak, F. Reininger, R. Benes, P. O'Leary, O.S. Wolfbeis, *Anal. Chim. Acta,* 1996, **320**, 235.

[8] S. Simhoney, A. Katzir, *App. Phys. Letters*, 1985, **47**, 1241.

[9] M. Snels, G. Baldacchini, *App. Phys. Letters*, 1988, **47**, 277.

[10] M.E. Meyerhoff, R.E. Robins, *Anal. Chem.* 1985, **52**, 2383.

[11] D.J. David, M.C. Willson, D.S. Ruffin, *Anal. Letters*, 1976, **9**, 389.

[12] T. Werner, I. Klimant, O.S. Wolfbeis, *Analyst*, 1995, **120**, 1627.

[13] A. Mills, Q. Chang, *Sens. and Actuators B*, 1994, **21**, 83.

[14] Y. Amao, N. Nakamura, *Sens and Actuators B*, 2004, **100**, 347.

[15] Z. Shakhsher, W.R. Seltz, *Anal. Chemistry*, 1994, **66**, 1731.

[16] R.A. Portrailo, S.P. Golubkov, P.S. Borsuk, P.M. Talanchuk, *Analyst,* 1994, **119**, 443.

[17] T.P. Jones, M.D. porter, *Anal. Chemistry*, 1988, **60**, 404.

[18] V.i. Agayn, D. R. Walt, *Bio/technology*, 1993, **11**, 726.

[19] S.T. Lee, B. Aneeshkumar, P. Radhakrishnan, C.P.G. Vallabhan, V.P.N. Nampoori, *Optics Co*MM., 2002, **205**, 253.

[20] A.Safavi, H. Abdollahi, *Anal. Chim. Acta,* 1998, **367**, 167.

[21] J.I. Peterson, S.R. Goldstein, R.V. Fitzergerald, D.K. Buckhold, *Anal. Chem.*, 1980, **52**, 864.

[22] S.A. Grant, K. Bettencourt, P. Krulevitch, J. Hamilon, R. Glass, *Sens. and Actuators B*, 2001, **72**, 174

[23] M. Ghanhehari, C.S. Vimer, *NDT&E International*, 2004, **37**, 611.

[24] M.D. P. Sotomayor, M. De Paoli, W.A. De Oliveira, *Anal. Chim. Acta,* 1997, **353,** 275.

[25] Z. Zhujun, W.R. Seitz, *Anal. Chim. Acta,* 1985, **171**, 45.

[26] D.M. Jordan, D. Walt, D.R. Milanovich, *Anal. Chem.*, 1987, **59**, 437.

[27] E. Bruno, S. Barnard, M. Rouilly, A. Waldner, J. Berger, P Ehrat, Anal. Chem., 1997, **69**, 507.

[28] T.R. Martz, J.J. Carr, C.R. French, M.D. DeGrandpre, *Anal. Che*m., 2003, **75**, 1844.

[29] M.A. Arnold, T.J. Ostler, *Anal. Che*m. 1986, **58**,1137.

[30] O.S. Wolfbeis, H.E. Posche, *Anal. Chi*m. *Acta,* 1986, **185**, 321.

[31] P. Caglar, R. Narayanaswamy, *Analyst*, 1987, **112**, 1285.

[32] http://www.epa.ie/
[Last accessed 03/02/05]

[33] N.A. Yusof, M. Ahmad, *Sens. And Actuators B*, 2003, **94**, 201.

[34] N.S. Kapany, J.J. Burke, *Optical Waveguide*, Academic Press, 1979, 7.

[35] A.W. Snyder, J.D. love, *Optical Waveguide Theory*, Chapman and Hall, 1983, 7.

[36] R.G. heideman, P.V. Lamberck, *Sens. and Actuators B*, 1999, **61**,100.

[37] W. Lukosz, *Sens. and actuators B*, 1995, **29**, 37.

[38] N.J. Goddard, K. Singh, J.P. Hulume, C.H. malins, R.J. Holmes, *Sens. and Actuators A,* 2002, **1**, 3354.

[39] R.Slavik, J.Homols, J. Ctryroky, E. Brynda, *Sens. and Actuators B*, 2001, **74**, 106.

[40] C.R. lavers, K. Itoh, S.C. Wu, M. Murabayashi, I. Mauchline, G. Stewart, T. Stout, *Sens. and Actuator B*, **69**, 200, 85.

[41] X.M. Chen, K. Itoh, M. Murabayashi, C. Igarashi, *Chem. Letters*, 1996,103.

[42] R.G. heideman, P.V. Lamberck, *Sens. and Actuators B*, 1999, **61**,100.

[43] W. Lukosz, *Sens. and actuators B*, 1995, **29**, 37.

[44] N.J. Goddard, K. Singh, J.P. Hulume, C.H. malins, R.J. Holmes, *Sens. and Actuators A,* 2002, **1**, 3354.

[45] R.Slavik, J.Homols, J. Ctryroky, E. Brynda, *Sens. and Actuators B*, 2001, **74**, 106.

[46] C.R. lavers, K. Itoh, S.C. Wu, M. Murabayashi, I. Mauchline, G. Stewart, T. Stout, *Sens. and Actuator B*, **69**, 200, 85.

[47] X.M. Chen, K. Itoh, M. Murabayashi, C. Igarashi, *Chem. Letters*, 1996,103.

[48] A. Yimit, K. Itoh, M. Murabayashi, *Sens. And Actuators B,* 2003, **88**, 239.

[49] J. Crump, R.K. Sandwick, *Jchemed*, 1994, **71**, 199.

[50] J. Gordon, A. James, S. Harman,K. Weiss, *Jchemed*, 2002, **79**, 8.

[51] R.A. Potyrailo, S.P. Golubkov, P.S. Borsuk, P.M. Talanchuk, *Analyst*, 1994, **119**, 443.

[52] F.A.A. Matias, M.M.D.C. Vila, M. Tubino, *Sens Actuators B*, 2003, **88**, 60.

[53] P.C. Hauser, T.W.T. Rupasinghe, N. E. Cates, *Talanta*, 1995, **42**, 605.

[54] K.M. Cantrell, J.D. Ingle, *Anal. Chem.*, 2003, **75**, 27.

[55] M. trojanowicz, J.S. Lobinska, *Anal. Chim. Acta*, 1990, **230**, 125.

[56] G.O'Keeffe, B.D. Mac Craith, A.K. McEvoy, C.M. McDonagh, J.F. McGilp, *Sens. and Actuators B*, 1995, **29**, 226.